A Study on Network Planning in Space-division Multiplexing based Elastic Optical Networks and Spatial Channel Networks

2021 年 3 月

呉　謙

A Study on Network Planning in Space-division Multiplexing based Elastic Optical Networks and Spatial Channel Networks

呉　謙

システム情報工学研究科

筑波大学

2021 年 3 月

Contents

List of Figures

List of Tables

List of Abbreviations

16-QAM 16-ary quadrature amplitude modulation

8-QAM 8-ary quadrature amplitude modulation

ADC Analog-to-digital converter

AGCA Automatic gain-controlled amplifier

B&S Broadcast-and-select

BP Blocking probability

BPSK Binary phase-shift keying

BV-OXC Bandwidth-variable optical cross-connect

BVT Bandwidth-variable optical transceiver

CDC Colorless, directionless, and contentionless

CSS Core-selective switch

DAC Digital-to-analog converter

DMUX Demultiplexer

DP Dual-polarization

DP-PSK Dual-polarization phase-shift keying

DSP Digital signal processor

EON Elastic optical network

FIFO Fan-in/fan-out

FM-MCF Few-mode multi-core fiber

FMF Few-mode fiber

FrJ-Sw Fractional joint switching

FS Frequency slice

GB guard-band

Gbps Giga bits per second

GHz gigahertz

HOXC Hierarchical optical cross-connect

ILP Integer linear programming

Ind-Sw Independent switching

IQ In-phase and quadrature

ITU-T International Telecommunication Union Telecommunication Standardization Sector

J-Sw Joint switching

LCoS Liquid crystal on silicon

LCSA Low-cost single-stage amplifier

LO Local oscillator

LPF Low-pass filter

LS Laser source

MCF Multi-core fiber

MCS Multicast switch

MIMO Multi-input-multi-output

MMF Multi-mode fiber

MS Matrix switch

MUX Multiplexer

MZM Mach-Zehnder modulator

OC Optical carrier

OCh Optical channel

OSNR Optical signal-to-noise ratio

OXC Optical cross-connect

PBC Polarization beam combiner

Pbps Peta bits per second

PBS Polarization beam splitter

QPSK Quadrature phase-shift keying

R&S Route-and-select module

RCSA Routing, core, and spectrum assignment

RMCSA Routing, modulation format, core, and spectrum assignment

RMSA Routing, modulation, and spectrum assignment

ROADM Reconfigurable optical add/drop multiplexer

RSA Routing and spectrum assignment

RSCSA Routing, spatial channel, and spectrum assignment

RSSA Routing, space, and spectrum assignment

RWA Routing and wavelength assignment

SCh Spatial channel

SCN Spatial channel network

SDM Space-division multiplexing

SL Space lane

SLC Space lane change

SMF Single-mode fiber

SMFB Bundle of single-mode fiber

Spa & Spe SpCh Spatial and spectral super-channel

Spa SpCh Spatial super-channel

SpCh Super-channel

Spe SpCh Spectral super-channel

SXC Spatial cross-connect

Tbps Tera bits per second

VGDA Variable-gain dual-stage amplifiers

WDM Wavelength-division multiplexing

WSS Wavelength selective switch

WXC Wavelength cross-connect

XT Intercore crosstalk

Acknowledgments

First, I would like to thank my advisor, professor Maiko Shigeno, for all her theoretical support and guidance in completing the thesis. Her dedication and patience not only inspired my academic research but also inspired my daily life.

I would like to thank Professor Akiko Yoshise and Professor Yongbing Zhang. They gave me many insightful and valuable suggestions to greatly improve my research.

My sincere thanks to my friends who helped me a lot in academic research and my daily life during my Ph.D. course.

I am appreciated for the *Super Global University* scholarship from the Ministry of Education, Culture, Sports, Science, and Technology - Japan for their economical support.

Finally, I am grateful to my parents for their comprehension, love, and spiritual support in my study abroad life.

Abstract

In this work, we introduced the evolution history of optical network architectures. Via reviewing the previous works focusing on the network planning, we clarified our contributions in network planning in space-division multiplexing based elastic optical networks and spatial channel networks. For better understanding of the readers, we discussed the related technologies on optical networks in detail for each network architecture. Then, we focused on the static routing, space, and spectrum assignment problem and proposed a novel channel-based integer linear programming model to solve it. We showed that our model has a overwhelming advantages over that of the previous work by simulation experiments. Moreover, we comprehensively evaluated the device costs, power consumption, and network performance of SDM transmission systems based on the application of various highly interrelated transmission technologies which can be referred to by the network operators in the network planning of space-division multiplexing based elastic optical networks. Finally, for the recently proposed new optical network architecture named spatial channel networks, we firstly focused on the resource allocation problem and defined it as routing, spatial channel, and spectrum assignment problem and proved its NP-hardness. For the proposed problem, we designed a integer linear programming model and a heuristic algorithm. Our approaches and the results of simulation experiments can be referred to by the network operators in the network planning of spatial channel networks.

Chapter 1

Introduction

Since the full commercialization of wavelength-division multiplexing (WDM) based optical networks in the early 21st century, WDM-based optical networks have remained able to essentially meet evolving traffic demands over time. However, with the development and increasing popularity of cloud computing, video-on-demand, the Internet of Things, 5G, and other emerging Internet applications and services, network traffic is now growing at an extremely rapid rate. Moreover, because of the lifetime limitation (generally 25 years) of older optical communication equipment deployed at the end of the last century, the deployment of next-generation ultra-large-capacity optical networks is imminent. Therefore, over the past decade, researchers have directed continuous effort toward next-generation optical networks, and consequently, the architecture of such optical networks has undergone several conceptual evolutions.

Thanks to the emergence of optical components such as bandwidth-variable optical transceivers and bandwidth-variable optical cross-connects as well as the transmission technologies of coherent optical orthogonal frequency-division multiplexing and Nyquist WDM technology, flexible optical transmission with variable bandwidth allocation and high spectrum efficiency has become possible. In 2009, M. Jinno et al. proposed the 'SLICE' architecture, driving the first evolution in optical network architecture from fixed-grid WDM-based optical networks to flexible-grid elastic optical networks (EONs). Compared with traditional WDM-based optical networks, more flexible spectrum divisions are possible in EONs, such as the 12.5 GHz frequency slices that conform to the G.694.1 standard recommended by the International Telecommunication Union Telecommunication Standardization Sector. Connection requests with different traffic volumes can be satisfied with varying bit rates, and lightpaths can be flexibly established by using different numbers of frequency slices and/or subcarriers without guard-band intervals as needed, thereby avoiding the wastage of spectrum resources to a certain extent and thus achieving higher spectrum efficiency.

Although EONs possess somewhat enhanced network capacity due to their high spectrum efficiency compared to traditional WDM-based optical networks, the growth in the transmission capacity of optical networks has dramatically slowed because the current transmission capacity per fiber is approaching the nonlinear Shannon limit of the existing single-mode fibers. However, Internet traffic is expected to continue to strongly increase, inexorably reaching this capacity limit. Thus, as a viable solution for overcoming this limit, space-division multiplexing technology has emerged, the basic concept of which is to expand the available spatial dimensions from the current single spatial dimension to multiple parallel spatial dimensions to increase the available spectrum resources. This technology has promoted a further evolution in optical network architecture from EONs to space-division multiplexing based EONs. Meanwhile, the emerging technologies for optical transmission and switching in space-division multiplexing based EONs – e.g., spectral & spatial super-channels, (fractional) joint switching, and space lane change (SLC) – are enabling flexible multidimensional optical transmission straddling both the spatial and spectral domains.

Considering the continuous growth in Internet traffic, the interconnections between adjacent backbone network nodes are expected to consist of dozens or even hundreds of spatial dimensions (fibers/cores) in the near future. The massive space-division multiplexing era is on the horizon. Moreover, the compound annual growth rates of the aggregate router blade interface rate have been approximately 40% in recent years. By 2024, the implementation of a commercial optical interface rate of up to 10 Tbps is anticipated to support Pbps-level optical networks. However, although a rate of 1.2 Tbps has been achieved in single-carrier 100 Gbaud DP-64-QAM transmission, the growth in the transmission rate of a single carrier has dramatically slowed in recent years. This is because the symbol rate is limited by the electronic/optoelectronic components, while the use of a higher-level modulation format will significantly restrict the reach of all-optical transmission. Therefore, considering the requirements of ultralong-haul and ultra-large-capacity all-optical transmission in backbone optical networks, the 10 Tbps optical interface that is predicted to be needed by 2024 will need to be implemented using various super-channels, for example, a super-channel consisting of one hundred 32 Gbaud DP-QPSK sub-channels. Such a super-channel will have enormous spectrum requirements, almost completely occupying the 4 THz spectrum of the entire C-band. This indicates that wavelength switching will no longer be necessary to transmit such an ultrahigh-capacity super-channel because it can be routed as an end-to-end entity through spatial bypass technology. Consequently, the space-division multiplexing based EON architecture, which requires a large number of wavelength cross-connects to support wavelength switching on each spatial dimension, will

no longer be applicable in future Pbps-level optical networks oriented toward the massive space-division multiplexing era.

In this context, the spatial channel network (SCN) architecture has been proposed recently as a promising optical network architecture to achieve Pbps-level optical transmission and switching. Hierarchical optical switching is the key concept underlying spatial channel networks. Specifically, in a spatial channel network, optical switching is supported by cooperation between spatial switching and wavelength switching, which requires fewer costly wavelength cross-connects than are required in the space-division multiplexing based EON architecture; thus, the deployment cost of the network nodes can be significantly reduced. Therefore, the spatial channel network architecture is a more economical and practical solution for the massive space-division multiplexing era.

In summary, over the past decade, the architecture of optical networks has been gradually evolving toward higher speed, larger capacity, higher flexibility, and lower cost. However, each evolution in the architecture of optical networks will pose challenges for network operators. Correspondingly, the network optimization problem is altering in consideration of the new network features introduced by each evolution. In this thesis, we discussed the network optimization problem from the network planning perspective and concluded our contribution to the research in this field.

1.1 Routing and wavelength assignment problem

Generally, the resource allocation problem in optical networks can be divided into two scenarios: the dynamic scenario and the static scenario. In the dynamic cases (also called real-time network planning), it is assumed that connection requests are unknown in advance, but they arrive and disappear stochastically (i.e., one-by-one). Algorithms are employed to assign resources dynamically required for the connection requests according to the current state of the network. It means that the assignment must be decided in an online manner, almost immediately, based on the current availability of network resources. Therefore, heuristic algorithms with quietly short execution time are ordinarily developed for dynamic problems.

In the static cases (also called long-term network planning), the network topology and all the connection requests are known in advance which need to be allocated in the network at the same time. Moreover, the decision of assignment is made in an off-line manner, without strict processing time constraints. Therefore, complex and time-consuming optimization methods, such as mathematical programming (e.g., integer linear programming : ILP), can be applied for static problems.

In WDM optical networks, the resource allocation problem is named the routing and wavelength assignment (RWA) problem. The objective of the RWA problem is to select an appropriate lightpath and a reasonable wavelength for each connection request. Addressing the dynamic RWA problem allows full use to be made of the available spectrum resources, enabling higher network throughput or a lower blocking probability, while the deployment cost can be reduced by addressing the static RWA problem in the network planning phase. A feasible solution to the RWA problem must satisfy the following constraints: 1) the selected lightpath should occupy the same wavelength on all links it passes through, which is referred to as the wavelength continuity constraint as shown in Fig. 1.1, and 2) each wavelength on a link can be assigned to at most one lightpath, which is referred to as the wavelength non-overlapping constraint. The RWA problem has been proven to be NP-hard [1, 2], and many related works have addressed it [2, 3].

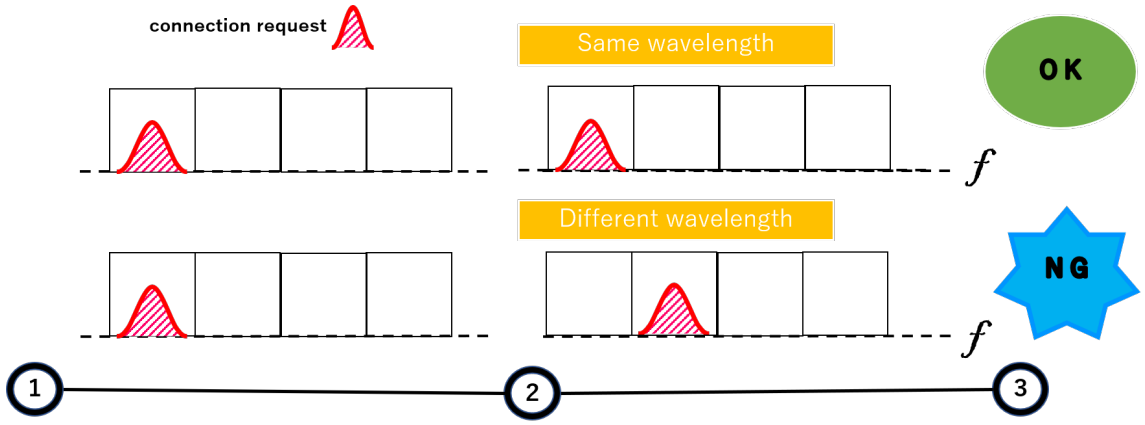

Figure 1.1: Illustration of wavelength continuity constraint in the RWA problem

1.2 Routing and spectrum assignment problem

With the emergency of various Internet services, network traffic is further increased [4]. In such a context, M. Jinno et al. proposed the so-called SLICE architecture, driving the first evolution in optical network architectures from WDM-based networks to EONs in 2009 [5]. In contrast to traditional WDM optical networks, flexible and variable spectrum allocation can be achieved in EONs. However, this new network feature also introduces an additional constraint called spectrum contiguity into the network optimization problem, that is, the FSs assigned to a connection request must be contiguous in the spectral domain as shown in Fig. 1.2 [6]. Thus, the network optimization problem for EONs is more complicated, evolving into the routing and spectrum assignment (RSA) problem [7]. Same with the

RWA problem, the RSA problem is NP-hard as well [6]. since 2009, the RSA problem and its derivative problems, such as the routing, modulation, and spectrum assignment (RMSA) problem, in which distance-adaptive modulation is considered, have been widely investigated [6–11].

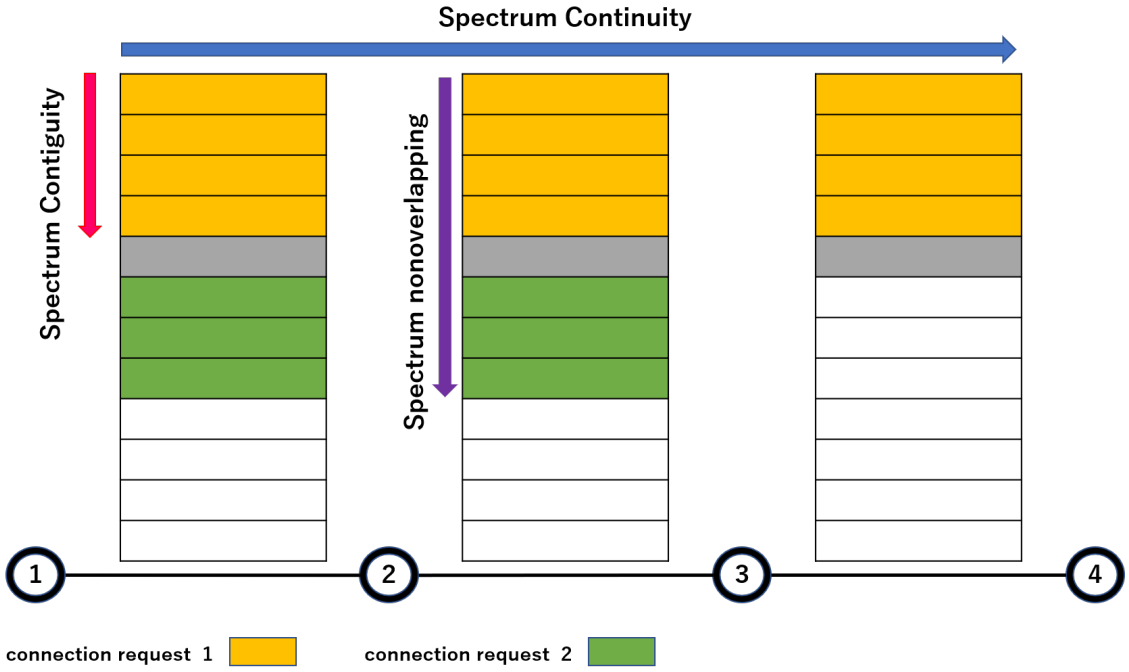

Figure 1.2: Illustration of spectrum continuity, spectrum contiguity, and non-overlapping constraints in the RSA problem

1.3 Routing, space, and spectrum assignment problem

The continuous increase in Internet traffic is inexorably pushing the capacity limits of standard single-mode fibers (SMFs) [12]. With the introduction of multiple spatial dimensions, space-division multiplexing (SDM) has emerged as a viable solution for overcoming this limitation [13,14]. Many new types of optical fibers with SDM technology have been developed as shown in Fig. 1.3. The simplest type of SDM fibers is a bundle of SMFs (SMFB), which employs several parallel SMFs. Another representative SDM fiber is MCF (multi-core fiber), which contains several cores with the same fiber [15–17]. The cores in the same fiber may be strongly-coupled or weakly-coupled with each other [18–20]. Moreover, SDM fibers with different modes in the same core, it is called multi-mode fiber (MMF) [21, 22]. If the number of modes is quite small, it is named few-mode fiber (FMF) [23, 24]. FMF with more than one core is called few-mode multi-core fiber (FM-MCF) [25, 26].

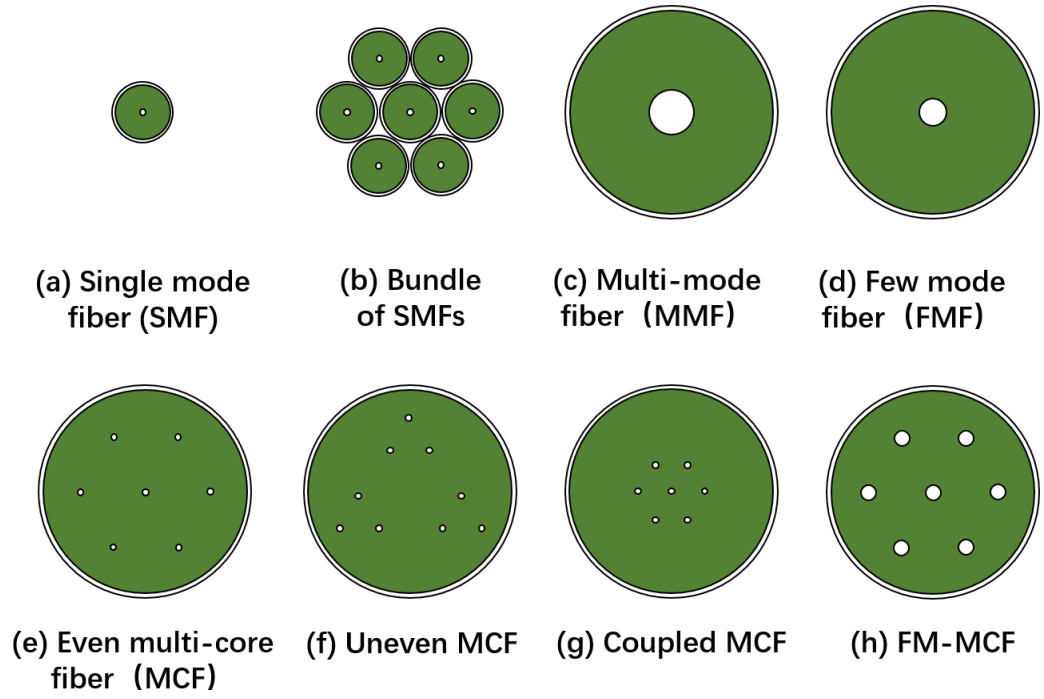

Figure 1.3: Different types of SDM fibers

Even there exist so many types of SDM fibers. In this work, we only consider the SMFB and/or MCF because of the following reasons: i) these two types of SDM fiber do not need to employ expensive multi-input-multi-output digital signal processor (MIMO-DSP) in the optical networks which will increase the network cost extremely with the number of strongly-coupled modes/cores [27, 28] ii) they have higher flexibility since optical signals in the SDM fibers with strongly-coupled modes/cores should be generated, routed, switched and received jointly [29]. iii) they can achieve better migration from existing optical networks to SDM-based ones.

As we stated above, new network features introduced by new network architectures will make the optimization problem in optical networks to evolve, just like the RWA problem in WDM-based networks to the RSA problem in EONs. Similarly, the expansion of spatial dimensions owing to SDM technology accomplished cross-dimensional transmission for connection requests, the assignment of SLs needs to be considered for the lightpath selection, which made the resource allocation problem more complicated. In SDM-based EON, the basic optimization problem is called routing, space, and spectrum assignment (RSSA) problem [30]. The name and meaning of the RSSA problem may change slightly with different factors considered. For instance, if the fiber type of network is MCF, it also called a routing, core, and spectrum assignment (RCSA) problem. Moreover, if the selection of

different modulation formats is considered, it may also extend to a problem usually called routing, modulation format, core, and spectrum assignment (RMCSA) problem. However, for simplicity, we collectively called them the RSSA problem in this paper. The RSSA problem is NP-hard which has been investigated in many previous works [29–34].

Table 1.1 listed the previous works on resource allocation in consideration of different SDM fiber types. We can observe that SMFB or MCF is the most frequently considered SDM fiber type, even there exist so many types of SDM fibers. The reasons are: i) these two types of SDM fiber do not need to employ expensive MIMO DSP in the optical networks which will increase the network cost extremely with the number of strongly-coupled modes/cores [27, 28] ii) they have higher flexibility since optical signals in the SDM fibers with strongly-coupled modes/cores should be generated, routed, switched and received jointly [29]. iii) they can achieve better migration from existing optical networks to SDM-based ones. Therefore, In this work, we only consider the SMFB and/or MCF. Moreover, the spatial dimension, namely, the fiber in the SMFB or the core in the MCF, we use the term 'space lane (SL)' for this concept instead.

Table 1.1: Previous works on resource allocation & SDM fiber type

SDM fiber type	References
SMFB	[32, 33, 35, 35–47]
MCF	[31, 36, 45–72]
MMF or FMF	[44, 46, 73–75]
FM-MCF	[31, 76, 77]

1.4 Our contribution to the RSSA problem

The RSSA problem is more challenging than the RWA and RSA problem because the decision of SL should be made which further increases the complexity to solve the resource allocation problem in optical networks. Generally, there are two kinds of approaches for dealing with the RSSA problem. The first one aims at determining all the network resources (routing path, space, and spectrum) jointly. In this case, the ILP model is applied for the static scenarios [53, 56, 57, 60, 64, 67, 73, 78–80]. Heuristic algorithms were usually developed for the dynamic scenarios [42, 59, 61, 62, 66, 81]. The second approach used by the remaining works divided the RSSA problem into two subproblems. Generally, there are two kinds of decomposition of the RSSA problem. It can be divide into a routing

subproblem and space and spectrum allocation problem (R + SSA). The two subproblems are solved separately. It firstly selected the routing path for the transmission of all the connection requests, then for the determined routing path, appropriate SL and spectrum are assigned. Another decomposition is a routing and SL subproblem and a spectrum allocation problem (RS + SA). Namely, it firstly selected routing path and SL for the transmission of all the connection requests, then the spectrum is assigned. Notably, since the second approach does not jointly optimize the RSSA problem, the optimality of the solution cannot be guaranteed.

The switching technologies considered in optical networks have a nonnegligible impact on the routing, space, and spectrum assignment for the transmission of connection requests. Namely, it has a considerable influence on the RSSA problem. In Table 1.2, we listed the switching paradigms considered in previous works. Moreover, as we mentioned above, in SDM-based EONs, the application of SLC technology will enhance the routing flexibility thereby affect the optimization of the RSSA problem. Table 1.3 classified previous works based on whether SLC technology is applied in resource allocation problems.

Table 1.2: Previous works on resource allocation in consideration of different switching paradigms

Switching paradigm	References
Ind-Sw	[31–33, 35–43, 46, 48–64, 66, 68–72]
J-Sw	[32, 33, 35, 38–46, 65]
FrJ-Sw	[32, 33, 35, 38–44]

Table 1.3: Previous works with or without space lane change technology

Space lane change	References
With	[31, 32, 36, 37, 42, 48, 51–58, 61–64, 66, 72]
Without	[31, 33, 36, 40, 43, 46, 49, 59, 60, 63, 68, 73–75]

For the static scenarios, only the ILP model proposed in previous work [47] can cope with the joint optimization of the RSSA problem which considered all the switching paradigms and SLC technology. In this paper, we proposed a novel ILP model for the RSSA problem in Chapter 3 which can also cope with considered all the switching paradigms and SLC

technology. Our simulation results verified the overwhelming performance over the ILP model in Ref. [47] on the RSSA problem.

Moreover, as we introduced above, the SDM transmission technologies (Spe SpCh, Spa SpCh, Spa & Spe SpCh) and the switching technologies (Ind-Sw, J-Sw, FrJ-Sw, and SLC) have a great influence on the architectures of optical nodes because the corresponding physical devices (i.e., SDM transceivers and ROADMs) should be deployed. Therefore, there is a need to simultaneously consider their impacts on device cost, power consumption, and network performance. To the best of our knowledge, there is no existing work focusing on this problem. In Chapter 4, we focus on filling this gap for reference in future research.

1.5 Routing, spatial channel, and spectrum assignment problem

As we stated above, network traffic has grown at an extremely rapid rate over the past few decades, which has inevitably compelled the development of optical transmission technologies, as well. As shown in the bottom left of Fig. 2.10, spectral super-channel transmission technology, which comprises several adjacent OCs without wavelength switching GBs between them, has been effectively applied in EONs, leading to higher spectrum efficiency. In addition, the expansion of the SLs in SDM-based EONs enhance the network capacity considerably. However, considering the aforementioned 10 Tbps client interface rate that is anticipated to be achieved by 2024, one hundred 32 Gbaud DP-QPSK OCs (each supporting 100 Gbps) will be required to establish such a connection request for long-haul transmission, or other combinations may be suitable for a shorter distance, such as twenty-five 64 Gbaud DP-16-QAM OCs [12, 28]. We can see that a total spectrum of 3.2 THz is required in the ideal case (i.e., with the ideal Nyquist shaping and a gridless spectrum) for a 10 Tbps DP-QPSK SpCh, and the entire C-band can accommodate only one such super-channel. This indicates that wavelength switching support will no longer be necessary for every SL, since, after a few more years, the spectral super-channel used to serve a single connection request may require the entire C-band spectrum. SCN with hierarchical optical cross-connects (HOXCs) have therefore been recently proposed [28, 82–86].

To the best of our knowledge, there exist no previous works aiming at the resource allocation problem in SCNs. Therefore, we clarified the resource allocation problem in SCNs and define it as the routing, spatial channel, and spectrum assignment (RSCSA) problem.

1.6 Our contribution to the resource allocation problem in SCNs

From the related research history introduced above, it is evident that with the various evolutions in the architecture of optical networks, from WDM optical networks to EONs and further to SDM-based EONs, to conform with the new network features introduced by each evolution, the basic resource allocation problem has accordingly evolved from RWA to RSA and then to RSSA. Accordingly, similar to what has occurred in the past, the resource allocation problem will also need to evolve to consider the newly introduced network features of hierarchical optical switching in the emerging SCN architecture. Dedicated algorithms considering the new features of SCNs will be essential to address the resource allocation problem in the newly proposed optical network architecture. Therefore, in this work, we clarified the resource allocation problem in SCNs and define it as the RSCSA problem. We proved the NP-hardness of the RSCSA problem. Considering the static scenarios, we proposed an ILP model to solve the RSCSA problem for small-scale instances and a heuristic algorithm for large-scale instances. To the best of our knowledge, this is the first work to focus on the resource allocation problem for SCNs, which can be referred to for the network planning of SCNs in the future.

Chapter 2

Technologies on Optical Networks

In the 1970s, the Corning Inc. of USA has succeeded in developing a practical silicon optical fiber in a world first. After that, the technology of using optical fibers for communication has been developing fast. The first optical fiber system is born in 1976 in Atlantic, USA [87]. Since then, the emergency of high bandwidth requirements for network applications promoted the development of optical networks.

An optical network consists of optical fibers carrying optical channels (OChs) and equipment deployed along the fibers to deal with light. It enables us to use light as media for transmission of large capacity, long-distance, and high reliability. The functionality of the optical network is closely related to the physics of light and the technologies of manipulating optical flow. In this way, with the development of breakthrough technologies, optical networks have been undergone several landmark evolutions. Correspondingly, the network optimization problem is altering with the evolution of optical networks.

In this chapter, we introduce the evolution history of the architectures of optical networks and the corresponding network feature. For each network architecture, we depict its network characteristics and the physical devices that support them. At the same time, we also explain the relationship between the above factors and the network optimization problem. Additionally, we discuss the related previous works and clarify the contribution of our work.

2.1 Wavelength-division multiplexing-based optical networks

In the early 1980s, network operators started to employ optical fibers in telecommunication networks. An optical fiber is a very light cable with a diameter almost as thin as a human hair [88].

However, compared to the electrical cable, it can provide large capacity and long-distance transmission with less loss [88]. The low fiber loss spectrum region is divided

into three wavelength bands: C-band (also called the conventional band) ranging from 1530 nm to 1565 nm, S-band (also called the short wavelength band) ranging from 1460 nm to 1530nm, L-band (also called the long-wavelength band) ranging from 1565 nm to 1625 nm. These three regions with low fiber loss are used for optical transmission in existing optical network systems. However, most systems are based on the C-band which is also considered in our work.

2.1.1 Wavelength-division multiplexing technology

As one of the earliest technological advances in optical networks, WDM technology enables a number of OChs to multiplex into a single fiber. At the beginning of the 2000s, up to 100 OChs per fiber have been achieved by WDM technology, which enhances the network capacity considerably.

An OCh is operating at a specific wavelength, in a nanometer (nm) unit, or equivalently at a specific optical frequency. The spectrum distance between adjacent OChs is expressed by the unit of gigahertz (GHz), which also called the spectrum grid. The spectrum carrying the data in an OCh is called an optical carrier (OC). The bandwidth of an OC should be less than the spectrum grid because a switching guard-band (GB) occupying a certain spectrum is necessary between two OCs for optical switching and routing. For a WDM-based optical network based on C-band, there are 40 OChs with a fixed spectrum grid 50GHz [89–91]. In such a case, the maximum bitrate carried by an OC is 40Gbps (or 100Gbps) [91, 92]. In Fig. 2.1, we illustrate three connection requests with 20 Gbps, 40 Gbps, and 50 Gbps traffic volume. For the transmission of these three connection requests, the total requirement of spectrum resources is 200 GHz. Actually, if the spectrum resource is fully utilized, the supportable traffic volume is 160 Gbps. However, in this example, the sum of the traffic volume is 110 Gbps. It is obvious that a waste of spectrum resources may occur in WDM-based systems.

2.1.2 Regeneration and distance-adaptive modulation

Various modulation formats have been developed for optical networks. Different levels of modulation formats (bits/s/Hz) own different transmission reaches (km), which also can be referred to as the level of spectral efficiency. If the distance between the source and destination exceeds the transmission reach of the selected modulation format for a connection request, regeneration performed by transceivers is necessary at intermediate nodes. It means that optical-electrical-optical (O-E-O) conversion should be performed, which raises the deployment cost of optical network nodes. Notably, when a connection request

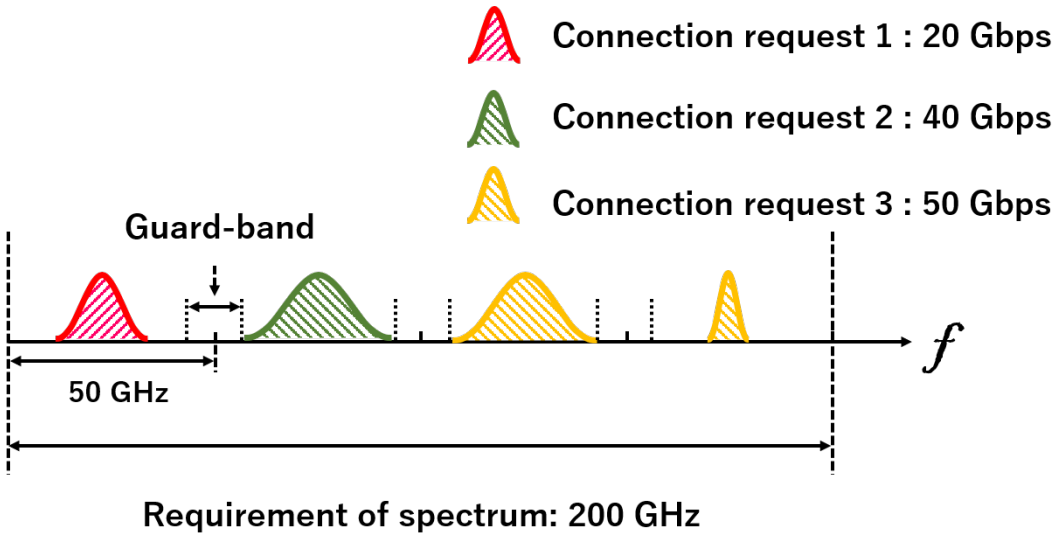

Figure 2.1: Transmission for connection requests with traffic volume of 20 Gbps, 40 Gbps, and 50 Gbps, respectively, in fixed 50 GHz grid WDM systems

passes through the intermediate node(s) remaining in the optical domain (without O-E-O conversion), it can be said that the connection request optically bypasses the intermediate node(s).

In our work, we consider the distance-adaptive modulation, that is, the highest feasible modulation level is automatically selected for each lightpath according to its path length. Moreover, four different modulation formats are considered: dual-polarization (DP) binary phase-shift keying (BPSK), quadrature phase-shift keying (QPSK), 8-ary quadrature amplitude modulation (8-QAM), and 16-ary quadrature amplitude modulation (16-QAM), respectively. Table 2.1 illustrates the corresponding transmission reach [km] and the modulation level of them.

Table 2.1: Transmission reach and modulation levels for different modulation formats considered in this work

Modulation formats	DP-BPSK	DP-QPSK	DP-8-QAM	DP-16-QAM
Transmission reach (km)	6300	3500	1200	600
Modulation level (bits/s/Hz)	2	4	6	8

2.2 Elastic optical networks

As we stated above, fixed grid WDM-based networks waste spectrum resources to a certain degree leading to a low spectral efficiency as shown in Fig. 2.1. EONs enabled narrower spectrum grid, such as the 12.5 GHz grid conforming to the G.694.1 standard recommended by the International Telecommunication Union Telecommunication Standardization Sector (ITU-T) [93]. In this context, 4 THz spectrum resources (C-band) can be divided into 320 numbers of 12.5 GHz frequency slices (FSs).

2.2.1 Super-channel in EONs

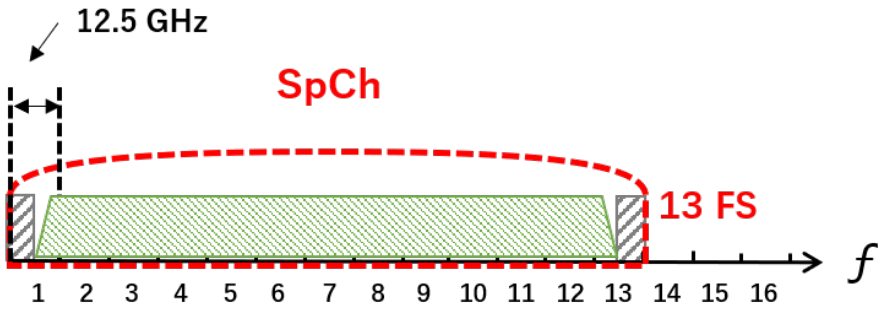

Figure 2.2: An example of super-channel in EONs

Thanks to the employment of bandwidth-variable optical transceivers (BVTs) and bandwidth-variable optical cross-connects (BV-OXCs), lightpaths can be flexibly established using super-channel (SpCh) which composed of different numbers of FSs without switching GB intervals according to the traffic volume needed by the connection request. Switching GBs (6.25GHz) is necessary on both sides for each SpCh (connection request). In Fig. 2.2, we showed a simple example of SpCh.

In an EON with a 12.5 GHz grid, we consider the transmission for the same connection requests with Section 2.1.1. The assignment is shown in Fig. 2.3. Compared with the result of the WDM-based systems, we can see that considerable spectrum resources can be saved in an EON due to a more flexible grid and the technology of SpCh.

2.3 Space-division multiplexing based elastic optical network

As we have introduced in the introduction, SDM technology enhanced the transmission capacity of optical networks with the expansion of the spatial dimension. Moreover, thanks

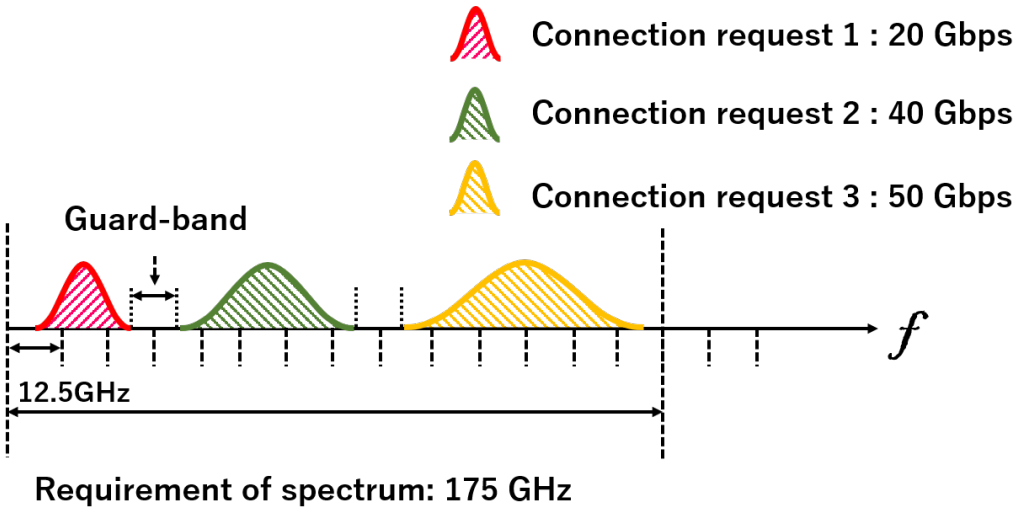

Figure 2.3: Transmission for connection requests with traffic volume of 20 Gbps, 40 Gbps, and 50 Gbps, respectively, in 12.5 GHz grid EON

to the SDM technology, there also emerges a lot of transmission technologies that further raise the transmission capacity of optical networks.

2.3.1 Spectrally & spatially flexible super-channel transmission

As a key transmission technology of SDM optical networks, a so-called spatial and spectral super-channel (Spa & Spe SpCh), which consists of several OCs allocated in the spatial and/or spectral domains, can provide excellent spectral efficiency [94]. In the spectral domain, continuous OCs are placed near the Nyquist condition without switching GBs between them. Moreover, in the spatial domain, such OCs can be distributed across numbers of spatial dimensions but within the same spectral range, meaning that they can share various components, such as the optical laser source and local oscillator in the transceiver [12, 29, 46, 95–97]. Therefore, Spa & Spe SpCh-based transmission can enable both higher spectral efficiency in the network layer and considerable cost savings (due to component sharing and dense electronic integration) compared to single-carrier-based transmission.

Recently, three types of Spa & Spe SpCh have been proposed for data transmission in spectrally and spatially flexible SDM optical networks [29,32,98]. These SpChs consist of multiple OCs distributed in the spectral and/or spatial domains.

A spectral super-channel (Spe SpCh), which is composed of several continuous OCs generated by the spectral transceiver, can offer high spectral efficiency for serving connec-

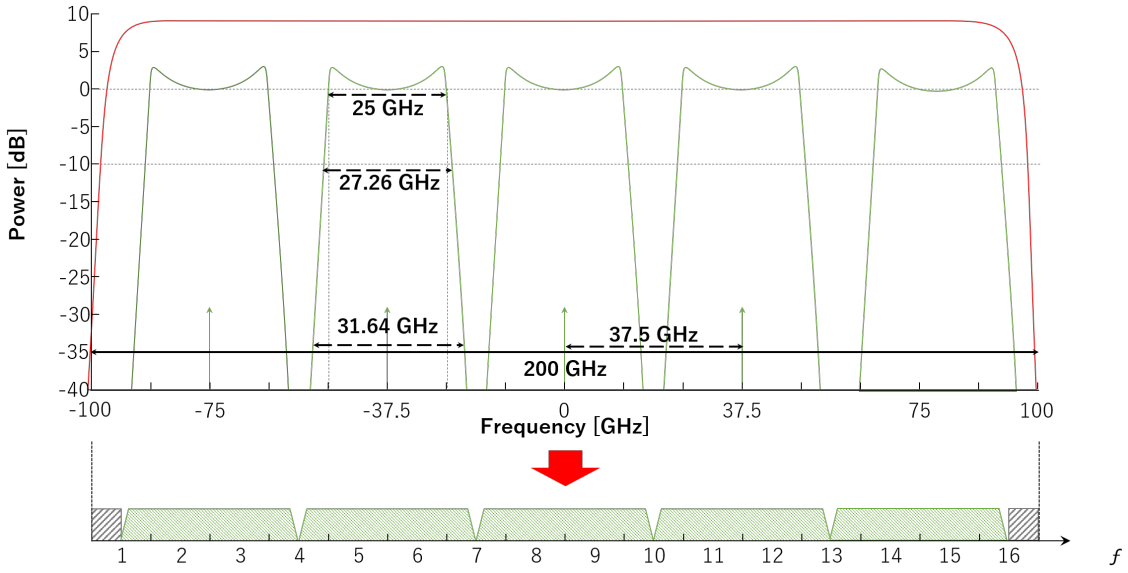

Figure 2.4: A Spe SpCh composed of 5 OCs spaced in accordance with the ITU-T 12.5 GHz grid

tion with flexible capacity. The OCs are placed near the Nyquist condition, that is, without switching GBs between them; GBs are necessary only between neighboring SpChs. Fig. 2.4 shows a Spe SpCh composed of 5 OCs with the following settings [99]:

- The OCs are dual-polarization phase-shift keying (DP-PSK) modulated by two in-phase and quadrature (IQ) Mach-Zehnder modulators (MZMs) driven by a 25 Gbaud square signal with a rise time of 0.32 ns, and they are Nyquist shaped by digital filters (integrated into the transceiver) with a resolution of 3.125 GHz. The corresponding spectral penalties incurred by the signal after Nyquist shaping are 2.26 GHz (at -10 dB) and 6.64 GHz (at -35 dB), respectively.

- At the intermediate nodes, the SpChs are routed by several flex-grid liquid crystal on silicon (LCoS)-based wavelength selective switches (WSSs) with a resolution of 7.5 GHz and a spectral addressability of 6.25 GHz. We assume that the maximum crosstalk of -35 dB is allowed. Consequently, a GB of 12.5 GHz (6.25 GHz on each side) between two Spe SpChs is considered sufficient to guarantee the effect of WSS cascading.

- The OCs are spaced in accordance with the ITU-T 12.5 GHz grid [93], and the total bandwidth (including the GB) of a SpCh should be a multiple of 12.5 GHz.

According to the above, we consider what is shown at the bottom of Fig. 2.4 to be equivalent

to what is shown at the top of Fig. 2.4 from the perspective of the network layer.

In contrast, a spatial super-channel (Spa SpCh) is an extension of the Spe SpCh concept to the spatial domain. The OCs generated by the spatial transceiver are arranged across numbers of or all of the spatial dimensions over the same spectral range. A key feature of Spa SpChs is that OCs at the same frequency but in different spatial dimensions can share a common laser source and local oscillator in the spatial transceiver. However, the disadvantage is that GBs are necessary for each of the spatial dimensions for a Spa SpCh.

Finally, a Spa & Spe SpCh is a hybrid of a Spe SpCh and a Spa SpCh generated by the spatial and spectral transceiver. In other words, a Spa & Spe SpCh can be created by combining multiple Spe SpChs in the same spectral range extending over multiple spatial dimensions. Thus, the assignment flexibility of a Spa & Spe SpCh spans both the spectral and spatial domains. Here, we assume that an $s \times o$ SpCh represents a Spa & Spe SpCh in which one Spe SpCh consisting of o contiguous OC(s) (i.e., o is the spectral span) is allocated to each of s spatial dimensions (i.e., s is the spatial span) in the same spectral range. Therefore, both Spe SpChs and Spa SpChs can be treated as special cases of Spa & Spe SpChs, where a Spa SpCh is an $s \times 1$ SpCh and a Spe SpCh is a $1 \times o$ SpCh.

Simple examples of these three types of $s \times o$ SpChs and the corresponding simple architecture of the transceivers are shown in Fig. 2.5, Fig. 2.6, and Fig. 2.7. For simplicity, we consider three 200 Gbps connections and one 150 Gbps connection to be transmitted in the DP-BPSK modulation format over 4 spatial dimensions. As in Fig. 2.4, the spectral grid size is set to 12.5 GHz (denoted by W_{FS}). Each OC occupies 37.5 GHz (denoted by W_{OC}), and a 6.25 GHz GB (denoted by W_{GB}) is allocated on each side of each occupied spatial dimension to separate adjacent SpChs. Therefore, in the case that a T Gbps connection is to be transmitted by an SpCh with a spatial span of s, the spectral span o of the SpCh (i.e., the number of required OCs in each of the s spatial dimensions) can be calculated using Eq. (2.1) [100]. In Eq. (2.1), BR_m represents the bit rate supported by an OC given a selected modulation format m. In the case of the DP-BPSK modulation format, BR_m is equal to 50 Gbps.

$$o = min\{i \in \mathbb{Z}^+ \mid T \leq BR_m \cdot s \cdot i\} \tag{2.1}$$

Based on Eq. (2.1), the number of required FSs in each spatial dimension (including the GBs) can be calculated using Eq. (2.2) [100, 101]:

$$n_{fs} = min\{i \in \mathbb{Z}^+ \mid (o \cdot W_{OC} + 2 \cdot W_{GB}) \leq W_{FS} \cdot i\} \tag{2.2}$$

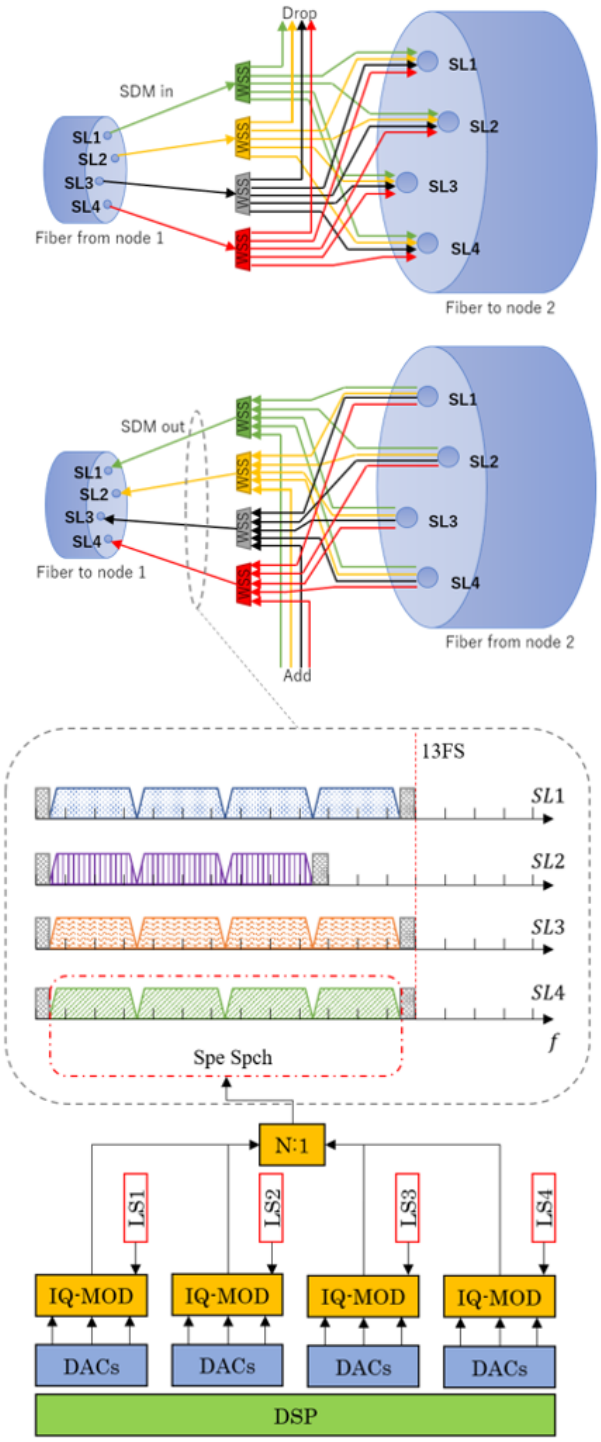

Figure 2.5: Illustration of ROADM architecture with independent switching, the corresponding spectral super-channel, and spectral transceiver. ROADM (reconfigurable optical add/drop multiplexer), WSS (wavelength selective switch), DSP (digital signal processor), IQ-MOD (modulator), LS (laser source), N:1 (coupler)

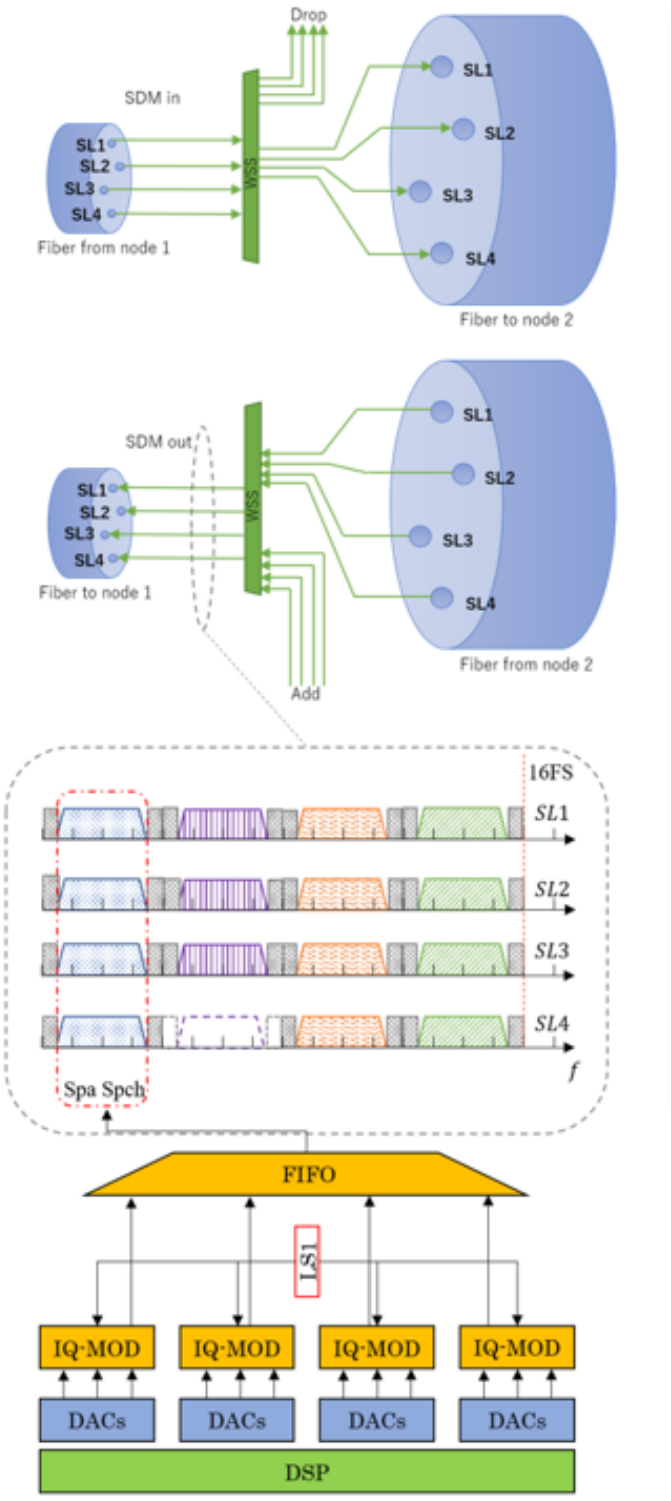

Figure 2.6: Illustration of ROADM architecture with joint switching, the corresponding spatial super-channel, and spatial transceiver. ROADM (reconfigurable optical add/drop multiplexer), WSS (wavelength selective switch), DSP (digital signal processor), IQ-MOD (modulator), LS (laser source), N:1 (coupler), FIFO (SDM fan-in/fan-out component)

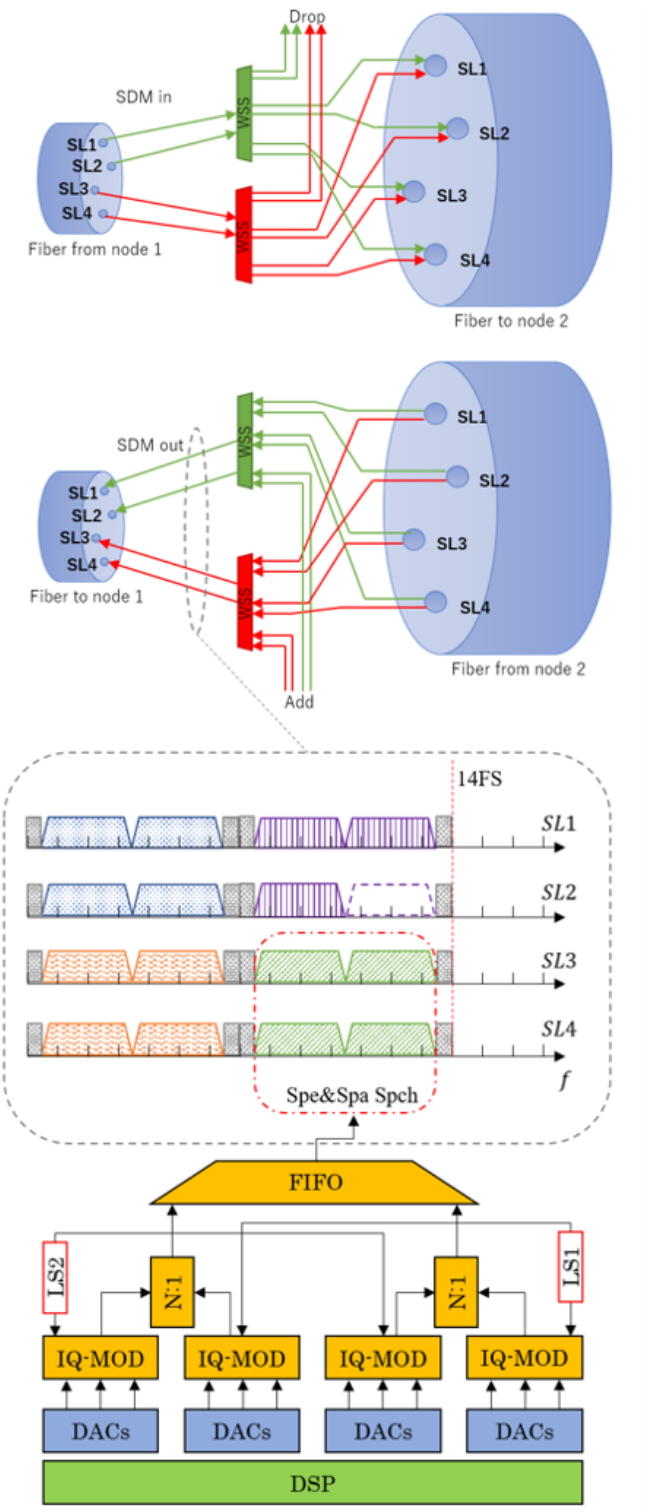

Figure 2.7: Illustration of ROADM architecture with fractional joint switching, the corresponding spatial spectral super-channel, and spatial spectral transceiver. ROADM (reconfigurable optical add/drop multiplexer), WSS (wavelength selective switch), DSP (digital signal processor), IQ-MOD (modulator), LS (laser source), N:1 (coupler), FIFO (fan-in & fan-out)

From the above, we can see that the SpChs shown in the middle place of Fig. 2.5 are actually Spe SpChs because their spatial span s is equal to 1. Similarly, the SpChs shown in the middle place of Fig. 2.6 are actually Spa SpChs because their spectral span o is equal to 1. Since GBs need to be placed in each spatial dimension to separate neighboring SpChs, an SpCh with a larger spatial span s is less spectrally efficient than one with a smaller s that can support an equivalent capacity. Moreover, as shown in Fig. 2.7, an SpCh with a larger s may result in resource wastage due to overprovisioning when serving a connection with a low traffic volume [29, 46]. However, as noted above, an SpCh with a larger s enables considerable savings in terms of device cost and power consumption. We will discuss these considerations in detail in Section 4.

2.3.2 Reconfigurable optical add/drop multiplexer

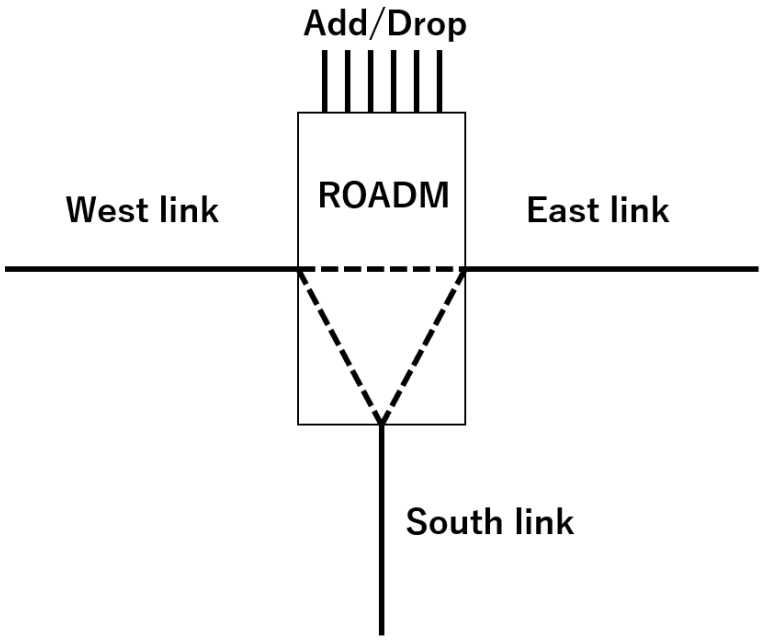

Figure 2.8: 3-degree reconfigurable optical add/drop multiplexer (ROADM)

A reconfigurable optical add/drop multiplexer (ROADM) is a kind of optical add/drop multiplexer employed at each node in optical networks, which increases the ability of remote switching in the wavelength layer. It is achieved by using the WSS. This allows single or multiple wavelengths carrying optical signals to be added to and/or dropped from the optical network without converting the optical signals into electronic signals and then back to optical signals. A 3-degree ROADM is shown in Fig. 2.8. In this ROADM architecture,

optical bypass is supportable for all three directions at the node. Transceivers are deployed only for the add/drop of the optical signal (connection request).

2.3.3 ROADM-based all-optical switching

With the development of switching equipment, complex optical switching can be achieved for the transmission of connection requests at intermediate nodes in SDM-based EONs. Definitely, the achievement of complex optical switching requires ROADMs with more complex architecture. In this section, we discuss the switching technologies applied in SDM-based EONs and their corresponding ROADM architectures.

2.3.4 Switching technologies

Two key factors have a considerable influence on the ROADM architecture: i) the spatial switching granularity and ii) the space lane change (SLC) technology.

Regarding spatial switching granularity (denoted by g throughout the rest of the paper), since the SpCh should be switched as a single entity when being routed along the lightpath, spatial switching granularity must be identical to the spatial span s of the SpChs. Moreover, the extra physical impairments introduced by SDM fibers will also affect g. For instance, an MCF is mostly affected by inter-core crosstalk, in which part of the signal traveling on one core leaks to adjacent cores, while an MMF is strongly impacted by mode coupling and/or differential mode delay [102]. The strongly coupled spatial dimensions in such fibers should be switched simultaneously. Therefore, the available g of the ROADM and s of the SpChs also differ depending on the SDM fiber type.

Depending on the difference of the spatial switching granularity, there are three proposed switching paradigms [103]. The first switching paradigm is called independent switching (Ind-Sw) and represents the case in which g is equal to 1. As shown in Fig. 2.5, in the absence of SLC support, each spatial dimension can be switched independently to any output port with the same spatial dimension index (i.e., conforming to the spatial continuity constraint). In contrast, the spatial continuity constraint is relaxed in the situation with SLC support, as shown in Fig. 2.5. Ind-Sw can offer high routing flexibility, especially when SLC is supported. However, it requires the largest number of WSSs/splitters (and a high port count per WSS/splitter when SLC is supported). Ind-Sw corresponds to SpChs with a spatial span s of 1 (i.e., Spe SpChs) and can be applied to uncoupled or weakly coupled SDM fibers, such as bundles of SMFs and uncoupled SM-MCFs.

SLC, as shown in Fig. 2.9, is a nonnegligible transmission technology in SDM-based EONs. For the same spatial switching granularity g, if the connection request can em-

ploy different spatial dimensions along the lightpath, it means that SLC is available during the transmission. Obviously, SLC can further increase the routing flexibility for the same spatial switching granularity g so that higher spectrum efficiency can be accomplished [29, 34, 104, 105]. As a negative effect, it consumes higher equipment costs due to the deployment of higher port-count WSSs.

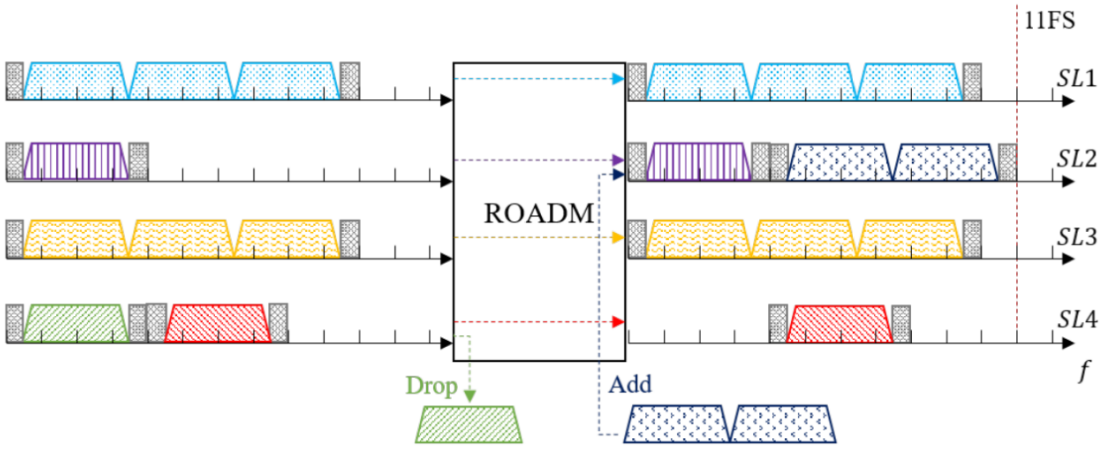

(a) Transmission without space lane change technology

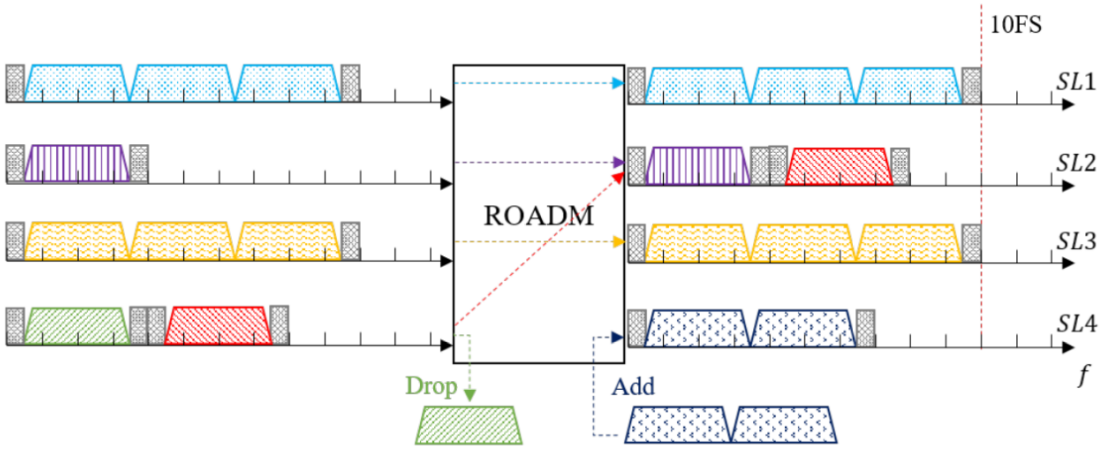

(b) Transmission with space lane change technology

Figure 2.9: Examples of spectrum assignments with and without SLC support.

The second switching paradigm is called joint switching (J-Sw) and represents the case in which g is equal to S. As shown in Fig. 2.6, all spatial dimensions are treated as a single entity. In this case, the switching architectures with and without SLC support are equivalent. J-Sw is a promising approach for achieving economical SDM optical networks since it requires the smallest number of WSSs/splitters [100, 106]. However, it offers the

lowest routing flexibility. J-Sw corresponds to SpChs with a spatial span equal to S and can be applied to all types of SDM fibers.

The last switching paradigm is called fractional joint switching (FrJ-Sw) and is a hybrid approach combining Ind-Sw and J-Sw. As shown in Figs. 2.7, the spatial dimensions are divided into several (i.e., S/g) groups such that the number of spatial dimensions in each group is equal to g. FrJ-Sw strikes a balance between Ind-Sw and J-Sw in terms of device cost and routing flexibility. Note that strong coupling between spatial dimensions in the same group is allowed for FrJ-Sw, while there should be either weak or no coupling between spatial dimensions belonging to different groups. Therefore, in addition to uncoupled or weakly coupled SDM fibers, FrJ-Sw is also suitable for bundles of FMFs and FM-MCFs.

2.4 Spatial channel network

As we introduced in our introduction, SCN is a new optical network architecture that is promising as the solution of the massive SDM era. In this section, we discuss the technologies related to SCN.

2.4.1 Spatial channels

First, we introduce the concept of spatial channels (SChs) in SCNs. It should be noted that in some previous works, the abbreviation 'SCh' has been used for the term 'super-channel'. In this paper, 'SpCh' is used instead as the abbreviation for 'super-channel' to avoid confusion. Moreover, in the physical domain, an SCh generally refers to an indivisible physical medium used to carry light, employing SL(s) in an optical fiber. In summary, in the context of SCNs, an SCh is a dedicated concept that is defined as an ultrahigh-capacity optical data stream that occupies a large amount of spectrum, and it can be optically routed in an end-to-end manner as a single entity through spatial cross-connects (SXCs) (called spatial bypass in SCNs) [28, 82–86]. As shown in Fig. 2.10, there are four types of SChs in SCNs, which are listed as follows:

- Type I: An SCh that carries a single high-capacity spectral SpCh (shown in red and yellow in Fig. 2.10). SChs of Type I can be routed in an end-to-end manner through spatial bypass without wavelength switching.

- Type II: An SCh that carries multiple spectral SpChs established between the same source-destination pair (shown in orange and green). SChs of Type II can also be

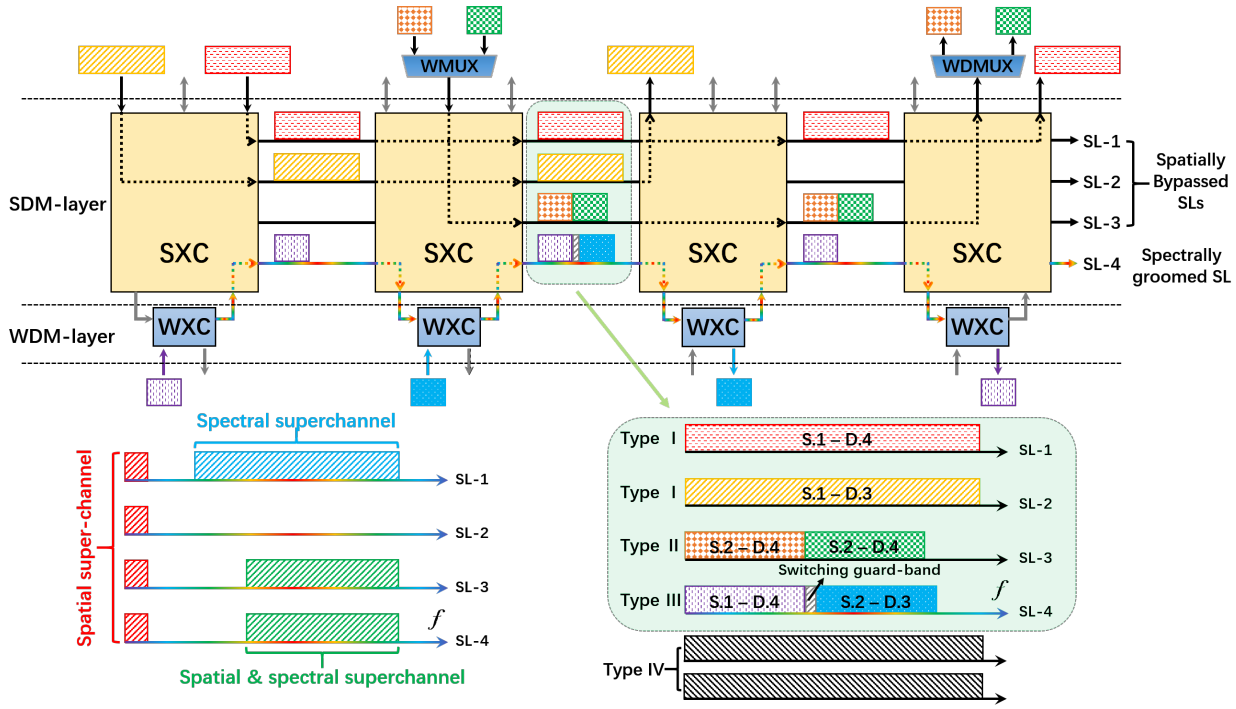

Figure 2.10: Illustration of the spectral and spatial SpChs in SDM-based EONs vs. the SChs in SCNs

end-to-end spatially bypassed, while multiple spectral SpChs belonging to such an SCh can be allocated without wavelength switching GBs.

- Type III: An SCh that carries multiple spectral SpChs established between different source-destination pairs (shown in purple and blue). These spectral SpChs are added/dropped by the wavelength cross-connect (WXCs) at intermediate node(s), and thus, wavelength switching GBs are required between them.

- Type IV: An SCh that carries a single ultrahigh-capacity spatial and spectral SpCh (shown in black), which occupies multiple SLs.

In this paper, we consider the SDM links of SCNs to comprise multiple SLs whose corresponding physical entities are single-mode cores in parallel SMFs or MCFs. Although other SDM fibers also exist, such as FMFs, strongly coupled MCFs, and FM-MCFs, we do not discuss them in this paper for the following reasons: i) poor compatibility with conventional SMF systems in terms of requiring costly and complex MIMO-DSPs and ii) a relatively short transmission reach due to the strong crosstalk caused by the inter-mode/inter-core coupling and the intermodal dispersion resulting from the propagation delay differences between modes. Therefore, in this case, an SCh of Type IV can be routed

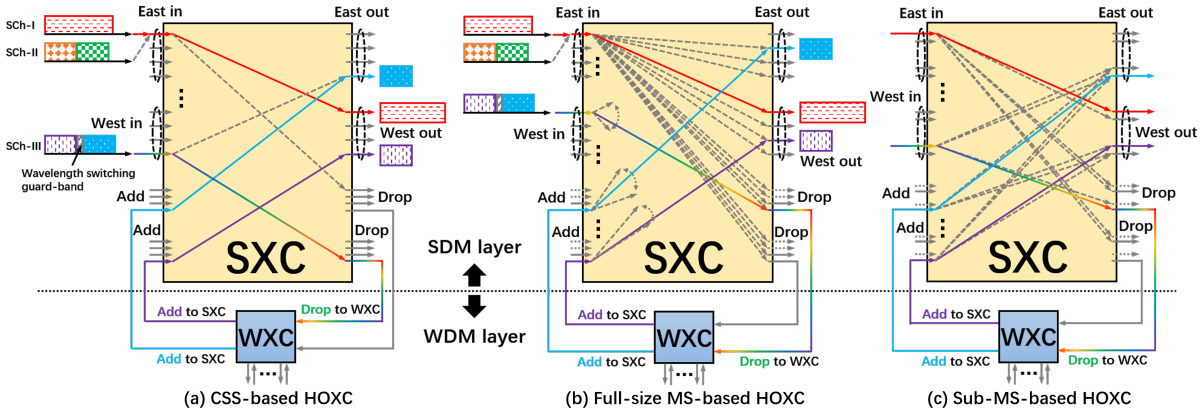

Figure 2.11: Illustration of three HOXCs proposed for use in SCNs from the networking perspective: (a) CSS-based HOXC; (b) Full-size MS-based HOXC; (c) Sub-size MS-based HOXC. Solid arrow: active switching; dotted arrow: possible switching.

as multiple independent SChs of Type I.

2.4.2 Hierarchical optical cross-connects

As shown in Fig. 2.10, in an SCN, the optical switching process is implemented by hierarchical SDM and WDM layers to achieve higher cost efficiency. SChs of Type I, Type II, and Type IV are spatially bypassed without passing through the WDM layer. In Ref. [28], four different types of HOXCs, which support different degrees of cost efficiency, routing flexibility, and scalability, have been proposed to achieve this functionality. In fact, the concept of HOXCs was first proposed in the late 1990s [107, 108], and some efforts were made in this direction before the concept of SDM-based EONs began to gain in popularity [109, 110]. This paper aims to identify the distinctive features of SCNs from the networking perspective but does not focus on explaining the detailed architectures of HOXCs for SCNs or comparing them with previous architectures. Readers can refer to Ref. [28] for more detailed related information.

Fig. 2.11 illustrates the HOXCs proposed for use in SCNs, which are implemented on the basis of full-size core-selective switches (CSSs) [111], sub-CSSs, full-size matrix switches (MSs) [112], and sub-MSs.

- Full-size CSS-based HOXC: The full-size CSS-based HOXC is the most cost-efficient solution among the four HOXCs. It also supports the scaling up of the nodal degree. However, SLC is not supported by this HOXC. For example, as shown in Fig. 2.11. (a), if we assume that the logical indices of the SLs (fibers/cores) are the same on

each link, then an SCh that enters an intermediate node can be switched only to output ports (including drop ports) with the same index.

- Sub-CSS-based HOXC: The sub-CSS-based HOXC is also a cost-efficient solution but costs more than the full-size CSS-based HOXC. However, it supports the scaling up of not only the nodal degree but also the number of SLs per degree in compensation for its additional cost. In addition, it has the same features as the full-size CSS-based HOXC from the networking perspective, as shown in Fig. 2.11.(a).

- Full-size MS-based HOXC: The full-size MS-based HOXC is the solution that provides the highest routing flexibility among the four HOXCs. As shown in Fig. 2.11. (b), this HOXC allows an SCh to be switched to any output port (including drop ports). However, it is also the costliest solution and does not support the scalability of the nodal degree and the number of SLs (per degree). It is worth noting that since the full-size MS-based HOXC supports full SLC, an add/drop port can be used to add/drop SChs to/from SLs with different indices (at different time points). Therefore, the add/drop port counts can be reduced to some extent (an example is illustrated by the gray dotted arrow).

- Sub-MS-based HOXC: The sub MS-based HOXC is a compromise solution relative to the full-size MS-based HOXC. In this case, the SLs are divided into multiple groups (e.g., two groups in the example shown in Fig. 2.11. (c)), and SLC is available within each group. Compared to the full-size MS-based HOXC, this solution sacrifices some routing flexibility in exchange for support for the scalability of the number of SLs per degree and considerable cost savings. Nevertheless, it is still much costlier than either of the two CSS-based HOXCs.

In summary, the above four HOXCs show various differences in cost efficiency, routing flexibility, and scalability. However, all of them cost less than conventional optical cross-connects (OXCs), which require wavelength switching support on each SL in SDM-based EONs. In this paper, we consider only SCNs implemented on the basis of full-size/sub-CSS-based HOXCs (as shown in Fig. 2.11. (a)) and defer the consideration of applications of the two MS-based HOXCs to future research. This is because the two CSS-based HOXCs offer significantly higher cost efficiency – readers can refer to the cost assessments in Refs. [113] and [28] for more details – and scalability than the two MS-based HOXCs do and thus are considered more suitable for use in future commercial SCNs.

Chapter 3

A Novel Channel-based Model for the Routing, Space, and Spectrum Assignment Problem

As we discussed in Section 1.3, the RSSA problem has been investigated by a lot of works. For the static scenario, mathematical models are generally applied, such as the ILP model. Moreover, different switching technologies will make the RSSA problem different. In this chapter, we propose a novel channel-based ILP model that can solve the static RSSA problem in consideration of all the above switching technologies (Ind-SW, J-Sw, FrJ-SW, and SLC) and give a detailed account of it. To the best of our knowledge, there is no existing channel-based ILP model that can be applied to solve the static RSSA problem in the same consideration of switching technologies with ours. To evaluate the performance of our proposed ILP model, we compare it with the previous slot-based model which considered the same switching technologies as ours in Ref. [47] via simulation experiments.

This chapter is laid out as follows. In Section 3.1, we depict our channel-based ILP model for solving the RSSA problem with the objective of minimizing the maximum FS index. In Section 3.2, we propose decomposed ILP models that help us to solve the RSSA problem. In Section 3.3, we compare our model with the previous slot-based model in Ref. [47] via simulation experiments and analyze the numerical results.

3.1 Channel-based ILP model

3.1.1 Parameters

E: the set of network links.
R: the set of connection requests.

t^r: the traffic volume [Gbps] of connection request r.

P^r: the set of candidate physical paths for serving connection request r.

g: the spatial switching granularity of the network.

G_g: the set of switching group a of spatial switching granularity g.

m_p: the level of the most efficient modulation format that can be applied for path p depending on its length [km].

t_{OC}: the traffic volume [Gbps] that a single OC can support. It depends on the symbol-rate of the transceiver and the selected modulation format.

n_p^r: the number of FSs for serving connection request r by path p.

C_p^r: the set of available channels for connection request r on path p.

δ_{cf}: a binary constant that is equal to 1 if channel c containing FS f is assigned to connection request r on path p, 0 otherwise.

Notably, parameter n_p^r is calculated by Eq. (2.2) if a connection request r with traffic volume t^r [Gbps] is transmitted by a path p in a network with spatial switching granularity g.

Moreover, C_p^r is a pre-computed set obtained by n_p^r. We illustrate Fig. 3.1 to make it clearer. Fig. 3.1 shows three types of channels. For a connection request requiring 2 FSs (i.e., n_p^r=2), 5 channels shown in yellow should be created (assuming the maximum FS index is 6). Similarly, for a connection request requiring 4 FSs, 3 channels shown in blue should be created. The channel marked in green is created for a connection request that requires 6 FSs. It is obvious that such a pre-created channel is kind of a container that satisfied the spectrum contiguity constraint. Moreover, it is worth noting that the size of the pre-computed set C_p^r is determined by both n_p^r and the maximum FS index we set. If the maximum FS index is set as 320 FSs (i.e., the numbers of FSs on C-band for 12.5GHz standard), 320 - n_p^r + 1 channels should be created beforehand for each given n_p^r. Therefore, For a given set of connection requests, according to the number of FSs for serving each connection request (i.e., n_p^r), we create the set of available channels (i.e., C_p^r) in advance. Notably, the computing time of C_p^r can be ignored compared to the optimization time of the ILP model. In this way, connection requests can be assigned without considering the spectrum contiguity constraint during the process of optimization, which can reduce the optimization time of the ILP model.

3.1.2 Variables

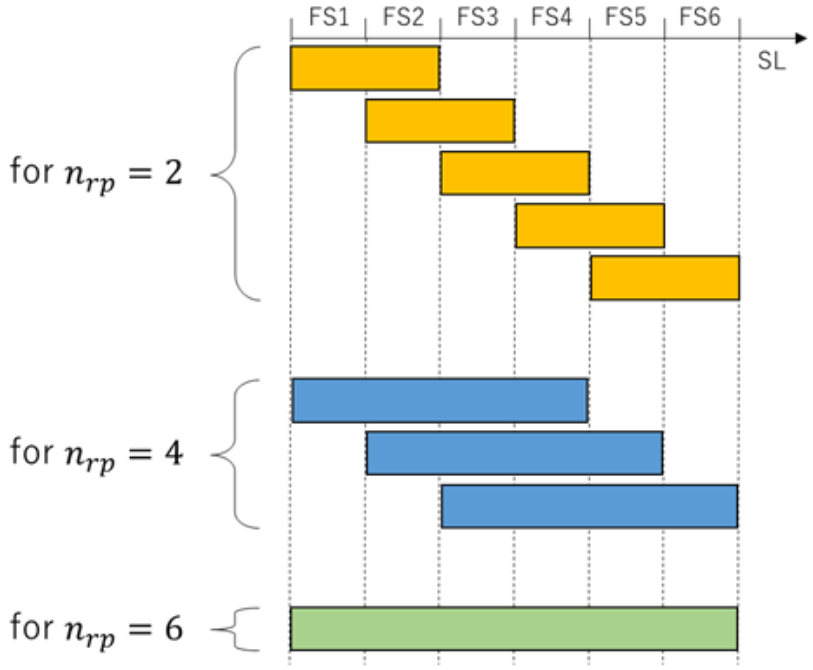

Figure 3.1: Examples of channels created for connection requests requiring different number of FSs

$x_c \in \{0, 1\}$: a binary variable that is equal to 1 if channel c on path p is used to serve connection request r, and 0 otherwise.

$y_{eac} \in \{0, 1\}$ a binary variable that is equal to 1 if path p passing switching group a on link e selected channel c to serve a connection request r, and 0 otherwise.

$F_{max} \in \mathbb{Z}^+$: an integer variable that indicates the maximum index of required FSs in the network.

3.1.3 Objective function

$$\text{Minimize} \quad F_{max} \tag{3.1}$$

As shown in Eq. (3.1), our objective is to minimize the the maximum index of required FSs in the network (i.e., F_{max}).

3.1.4 Constraints

Constraint for Spectrum Continuity

$$\sum_{p \in P^r} \sum_{c \in C_p^r} x_c = 1 \quad \forall r \in R \tag{3.2}$$

Constraint (3.2) represents that only one physical path p and one channel c on such physical path p can be selected for each connection request. It means that the FS(s) used for serving a connection request r is on the same position in the spectrum domain on each link traversed by the selected path p, which ensures spectrum continuity.

Constraint for the Decision of Switching Group

$$\sum_{a \in G_g} y_{eac} = x_c \quad \forall r \in R, p \in P^r, e \in p, c \in C_p^r \tag{3.3}$$

For Constraint (3.3), if x_c is equal to 1, it means that channel c on path p is selected for connection request r. At this time, only one switching group a can be selected by such a path p on each link e of this path. If x_c is equal to 0, it is obvious that none of all the switching groups can be chosen.

Constraint for Spectrum Non-overlapping

$$\sum_{r \in R} \sum_{p \in P^r : e \in p} \sum_{c \in C_p^r} \delta_{cf} \cdot y_{eac} \leq 1 \quad \forall e \in E, a \in G_g, f \in F \tag{3.4}$$

In Constraint (3.4), if δ_{cf} is equal to 1, it ensures that each FS f can only be used at most once to form channel c for each switching group a on each link e, i.e., spectrum non-overlapping. If δ_{cf} is equal to 1, it is satisfied automatically.

Constraints for the Maximum Index of Required FSs

$$\sum_{p \in P} \sum_{c \in C_p^r} (c + n_p^r) \cdot y_{eac} - 1 \leq F_{max} \quad \forall r \in R, e \in E, a \in G_g \tag{3.5}$$

For each connection request r, its ending FS index (left part of Constraint (3.5)) is no more than the maximum index of required FSs in the network (i.e., F_{max}) for each switching group a on each link e.

3.2 Decomposed ILP models for RSSA problem

Since the RSSA problem is well-known as NP-hard. It becomes difficult to solve ILP models completely in a reasonable time for large-scale instances. However, with a decomposition of the problem, the computational time may be extremely reduced. Therefore, we divide the RSSA problem into two subproblems: i) routing and SL problem, and ii) spectrum assignment problem. For the first subproblem, we propose an ILP model named ILP-RS model. For the second one, we propose an ILP model named the ILP-SA problem.

In the ILP-RS model, we only determine a path and the switching group traversed by such a path. We do not consider specific spectrum allocation. It means that the spectrum continuity constraint is relaxed because it is the main reason that limits the convergence efficiency of the RSSA problem. The objective is to minimize the maximum number of required FSs in each switching group of all the links in the network. Strictly speaking, the solution to such an objective is the lower-bound of the RSSA problem. Sometimes it may be an infeasible solution because the spectrum continuity constraint is ignored.

3.2.1 ILP-RS model

Parameters

In the ILP-RS model, the parameters are the same as those in the channel-based ILP model (refer to Section 3.1.1).

Variables

$x_p \in \{0, 1\}$: a binary variable that is equal to 1 if path p is selected to serve a connection request r, and 0 otherwise.

$y_{pea} \in \{0, 1\}$: a binary variable that is equal to 1 if switching group a on link e is traversed by path p.

$F_{use} \in \mathbb{Z}^+$: an integer variable that indicates the maximum number of required FSs in each switching group of all the links in the network.

Objective Function

$$\text{Minimize} \quad F_{use} \tag{3.6}$$

As Eq. (3.6) shown, we aim at minimizing the maximum number of required FSs in each switching group of all the links in the network (i.e., F_{use}) regardless of how these FSs

are assigned. That is, we do not consider the spectrum continuity constraint in the ILP-RS model.

Constraints

Constraint for the Decision of Path and Switching Group

$$\sum_{p \in P^r} x_p = 1 \quad \forall r \in R \tag{3.7}$$

Constraint (3.7) ensures that only one path p can be selected for each connection request r.

Constraint for the Decision of Switching Group

$$\sum_{a \in G_g} y_{pea} = x_p \quad \forall r \in R, p \in P^r : e \in p \tag{3.8}$$

Constraint (3.8) ensures that for each path p serving a connection request, only one switching group a can be selected for each link e on it.

Constraint for the Maximum Number of Required FSs

$$\sum_{r \in R} \sum_{p \in P^r : e \in p} n_p^r \cdot y_{pea} - 1 \leq F_{use} \quad \forall e \in E, a \in G_g \tag{3.9}$$

For each switching group a on each link e, the sum of the number of FSs required by connection requests whose path passed that switching group a on link e (i.e., the left part of Constraint (3.8)) should be bound by F_{use}.

3.2.2 ILP-SA model

Parameters

After the ILP-RS model is solved, we applied the ILP-SA model for spectrum assignment. We employ the outputs of the ILP-RS model as the input of the ILP-SA model.

Parameters

$a_{p_{out}}, p^r_{out}$: $a_{p_{out}}, p^r_{out} = \{p \in P^r : e \in p, a \in G | y_{pea} = 1\}$, the selected path p^r_{out} and the switching group $a_{p_{out}}$ used to serve the connection request r.

N_{fs}: the number of FSs on C-band (320 in our work).

Variables

f^r_{start}: an integer variable that indicates the starting FS index of connection request r.

$\delta^{rr'} \in \{0, 1\}$: a binary variable equals 0 if the ending FS index of r' (i.e., $f^{r'}_{start} + n^{r'}_{p^r_{out}}$) is smaller than the starting FS index of r (i.e., f^r_{start}) and 0 otherwise.

F_{max}: the same with F_{max} in the channel-based model.

Objective Function

$$\text{Minimize} \quad F_{max} \tag{3.10}$$

As Eq. (3.10) shown, the objective of the ILP-SA model is the same as that of the channel-based model.

Constraints

Constraint for Spectrum Assignment

$$F_{max} \geq F_{use} \tag{3.11}$$

$$F_{max} \geq f^r_{start} + n^r_{p^r_{out}} - 1 \quad \forall r \in R \tag{3.12}$$

$$\delta_{rr'} + \delta_{r'r} = 1 \quad \forall r, r' \in R \tag{3.13}$$

$$f^r_{start} \geq f^{r'}_{start} + n^{r'}_{p^{r'}_{out}} - N_{fs} \cdot (1 - \delta^{rr'}) - 1$$
$$\forall r, r' \in R : r \neq r', p^r_{out} \cap p^{r'}_{out} \neq \emptyset, a_{p_{out}} = a_{p'_{out}} \tag{3.14}$$

Constraint (3.11) indicates that the maximum index of required FSs must not be less than the maximum number of required FSs in each switching group of all the links in the network because the spectrum continuity is considered in the ILP-SA model. Constraint (3.12) ensures that the maximum index of required FSs must be larger than the

ending FS index of each connection request. Constraint ensures the position order for any two different connection requests. For Constraint , if $\delta^{rr'} = 1$, it indicates that the starting FS index of r should be greater than the ending FS index of r'. This constraint is deactivated due to the larger value of N_{fs} on the right-hand side of the constraint. The outputs of the ILP-SA model can be used as the initial solution when solving the proposed channel-based ILP model. In some cases, the initial solution is the optimal solution which can be returned by the solver immediately so that greatly saved the optimization time. In other cases, the channel-based ILP model needs to be further optimized. The initial solution can reduce the optimization time to a certain extent.

3.3 Simulation and numerical results

In this section, we apply the previous slot-based model in Ref. [47] (hereinafter referred to as the slot-based ILP model) whose numerical results are used as the benchmark to evaluate our channel-based ILP model via simulation experiments. Both of them are optimized in consideration of different spatial switching granularities. A simple 6 nodes 18 directed links n6s9 network interconnected by 4-core MCF [114] is considered shown in Fig. 3.2. The available spatial switching granularities g are 1, 2, and 4, corresponding to the cases of Ind-Sw, FrJ-Sw, and J-Sw, respectively.

We assume that the spectrum gird (i.e., W_{FS}) is 12.5 GHz based on the ITU-T standard G.694.1 [93]. The transceiver is operating at a fixed 32 Gbaud transmitting/receiving an OC with 37.5GHz (i.e., W_{OC}) bandwidth. The switching GB (i.e., W_{GB}) is 12.5GHz (6.25GHz on each side of an SpCh).

Four modulation formats DP-BPSK, DP-QPSK, DP-8QAM, and DP-16QAM can be selected for serving each connection request. We consider distance-adaptive modulation. That is, the modulation format with the highest spectral efficiency depending on its length is selected for each connection request [115]. The corresponding transmission reaches of the above modulation formats are 6300km, 3500km, 1200km, and 600km, respectively [116–118].

The traffic volume (Gbps) of each connection request is generated ranging from 100 Gbps to 1 Tbps in accordance with a uniform distribution. We consider different traffic loads by increasing the number of connection requests – from 100 to 300, 50 per step. The source node and target node of each connection request are randomly selected. 50 traffic matrices are generated randomly for each traffic load.

Gurobi optimizer v9.0.1 [119] is the solver software used for the optimization of the channel-based ILP model proposed, the decomposed ILP models proposed, and the slot-

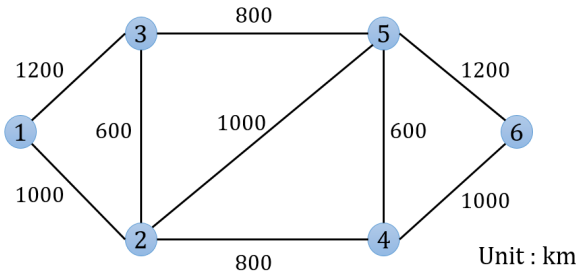

(a) N6S9 network

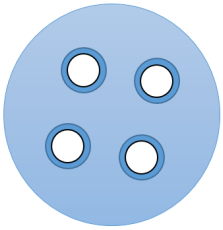

(b) 4-core MCF

Figure 3.2: Network topology and fiber considered in the simulation experiment: (a) 6-node 18-directed links N6S9 network topology; (b) 4-core MCF

based ILP model. We set the running time limit to 3600 seconds of these three models for each traffic matrix. Notably, the output of the ILP-SA model is used as the initial solution of both the channel-based ILP model and the slot-based ILP model. The simulation experiments were executed under Microsoft Windows 10 by a computer with Intel 6-core 12 thread 3.7 GHz CPU and 32 GB memory. The detailed numerical results are shown in Table 3.1.

Table 3.1: Performance evaluations of two ILP models for different spatial switching granularities in the n6s9 network

Traffic load $\|R\|$		100			150			200			250			300		
spatial switching granularity i		1	2	4	1	2	4	1	2	4	1	2	4	1	2	4
Lower-bound		48.43	54.63	68.93	70.03	79.73	101.13	93.20	106.37	135.80	115.27	131.30	167.33	138.87	158.17	200.83
ILP-RS	Done(%)	96.67	96.67	100.00	76.67	100.00	100.00	90.00	100.00	100.00	93.33	100.00	100.00	93.33	100.00	100.00
	FS index	48.47	54.67	68.93	70.27	79.73	101.13	93.30	106.37	135.80	115.33	131.30	167.33	138.93	158.17	200.83
	Gap(%)	0.07	0.07	0.00	0.34	0.00	0.00	0.11	0.00	0.00	0.06	0.00	0.00	0.05	0.00	0.00
	Runtime(s)	26.33	20.66	0.07	156.87	1.07	0.05	76.07	0.20	0.04	54.75	0.25	0.07	54.65	0.26	0.06
ILP-SA	Done(%)	100.00	100.00	76.67	100.00	66.67	20.00	63.33	30.00	43.33	10.00	6.67	26.67	0.00	0.00	33.33
	FS index	51.30	54.73	69.17	73.70	80.10	102.27	94.63	107.37	143.93	117.10	133.07	186.43	141.50	162.73	239.13
	Gap(%)	0.00	0.00	0.32	0.00	0.45	1.08	0.39	0.94	1.70	1.35	1.34	6.16	1.85	2.80	9.76
	Runtime(s)	0.07	0.57	151.86	0.77	208.96	513.52	238.90	444.36	412.63	550.77	565.74	535.85	600.00	600.00	585.20
Slot-based ILP	Done(%)	70.00	93.30	83.33	13.33	70.00	23.33	20.00	30.00	0.00	6.67	6.67	0.00	0.00	0.00	0.00
	FS index	49.50	54.73	69.10	73.13	80.07	102.17	94.63	107.37	142.83	117.10	133.07	179.17	141.50	162.73	222.87
	Gap(%)	2.00	0.18	0.23	4.15	0.41	0.99	1.53	0.94	4.77	1.55	1.34	6.55	1.85	2.80	9.74
	Runtime(s)	1114.03	240.81	608.15	3120.79	1082.07	2760.87	2881.42	2520.93	3600.00	3363.58	3362.33	3600.00	3600.00	3600.00	3600.00
Channel-based ILP	Done(%)	100.00	100.00	100.00	33.33	80.00	100.00	26.67	30.00	100.00	6.67	6.67	100.00	0.00	0.00	100.00
	FS index	48.43	54.67	68.93	72.70	79.97	101.13	94.57	107.37	135.80	117.10	133.07	167.33	141.50	162.73	200.83
	Gap(%)	0.00	0.00	0.00	3.38	0.27	0.00	1.46	0.94	0.00	1.55	1.34	0.00	1.85	2.80	0.00
	Runtime(s)	283.72	33.23	2.68	2553.83	1002.41	37.60	2853.23	2524.20	96.10	3363.68	3361.95	209.99	3600.00	3600.00	616.23

In Table 3.1, 'Done' represents the percentage of the number of times that model com-

pletely solved in the 50 traffic matrices. 'FS index' is the result of optimal solutions. If the optimal was not found within the running time limit, the current obtained solution was used. 'Gap' is the ratio of 'FS index' and lower-bound which are given by the parameter 'Objbound' of GUROBI. 'Runtime' is the execution time of GUROBI. Notably, all values in Table 3.1 are the average of the results for 50 traffic matrices.

From Table 3.1, we can see that when the number of connection requests is 100, the channel-based ILP model can always obtain the optimal for 50 traffic matrices ('Done' = 100%) regardless of the spatial switching granularity g. In contrast, the slot-based ILP model may not obtain the optimal for some traffic matrices regardless of the spatial switching granularity g. Moreover, from the rows of 'FS index' and 'Gap', it is obvious that the channel-based ILP model can get a better solution than the slot-based one for all the spatial switching granularities. The optimization time of the channel-based ILP model is quietly less than that of the slot-based one from the rows of 'Runtime'. Similar behaviors can be observed when the number of connection requests increased to 150. From the results that the number of connection requests is 200 and 250, the two models are hardly solved and the 'Runtime' and solutions of them do not show a significant difference when spatial switching granularity g are 1 and 2. However, for the case that spatial switching granularity g is 4, the slot-based ILP model cannot be solved once while the channel-based one can always get optimal within the running time limit for all the traffic matrices. When the number of connection requests is 300, for the cases that spatial switching granularity g are 1 and 2, the solution of the two models is the same and both of them cannot obtain the optimal within the running time limit. For the case that spatial switching granularity g is 4, two models perform the same behavior with that of when the number of connection requests is 300. Consequently, there is no doubt that the proposed channel-based ILP model has an overwhelming advantage over the slot-based one from the comparison between the numerical results.

Chapter 4

Evaluation of Device Cost, Power Consumption and Network Performance in Spatially and Spectrally Flexible SDM Optical Networks

As we discussed in Section 1.3, newly designed Spa & Spe SpCh transceivers can support the high-speed transmission with excellent spectral efficiency by allowing the optical carriers to be flexibly distributed in both the spatial and spectral domains without GBs. In addition, SDM-based ROADMs with varying spatial switching granularities and add/drop ports have been developed to support super-channel transmission. Moreover, ROADMs with SLC support can further improve the routing flexibility in the network layer. Different considerations of the aforementioned technologies have distinct advantages and disadvantages. These technologies can be combined in various ways to support different types of SDM transmission, leading to different network performance. Therefore, in this chapter, we evaluate the device cost, power consumption, and network performance of SDM transmission systems based on different implementations of these technologies to serve as a reference for future research. Notably, in this chapter, we named the SDM-based EON with the spatially and spectrally flexible transmission as the spatially and spectrally flexible SDM optical networks.

The remainder of this chapter is organized as follows. In Section 4.1, we introduce the architecture of single-carrier transceiver and Spa & Spe SpCh transceiver. We also propose cost and power consumption models for the Spa & Spe SpCh transceiver. In Section 4.3, we consider the ROADM architecture and propose corresponding cost and power consumption models. In Section 4.4, we evaluate the differences in device cost, power consumption, and network performance via simulation experiments.

4.1 Single-carrier transceiver architecture

As a promising advanced technique, Nyquist-shaped signal transmission enables the data transmission rates to be maximized with a rectangular spectrum while the bandwidth usage is minimized. Digital filtering, which is performed in the DSP of the transceiver, is usually employed to shape the signal spectrum [94, 99, 120]. Recently, an advanced high-spectral-resolution optical Nyquist-shaping filter has been reported that can achieve a resolution of 0.8 GHz and a spectral addressability of 400 MHz/pixel [121]. However, the use of such an optical filter might not be profitable due to the high associated device cost [120]. Therefore, in this paper, we assume that digital filtering is applied. Fig. 4.1 depicts a single-carrier DP-PSK transceiver architecture relying on digital filters [99, 120, 122, 123].

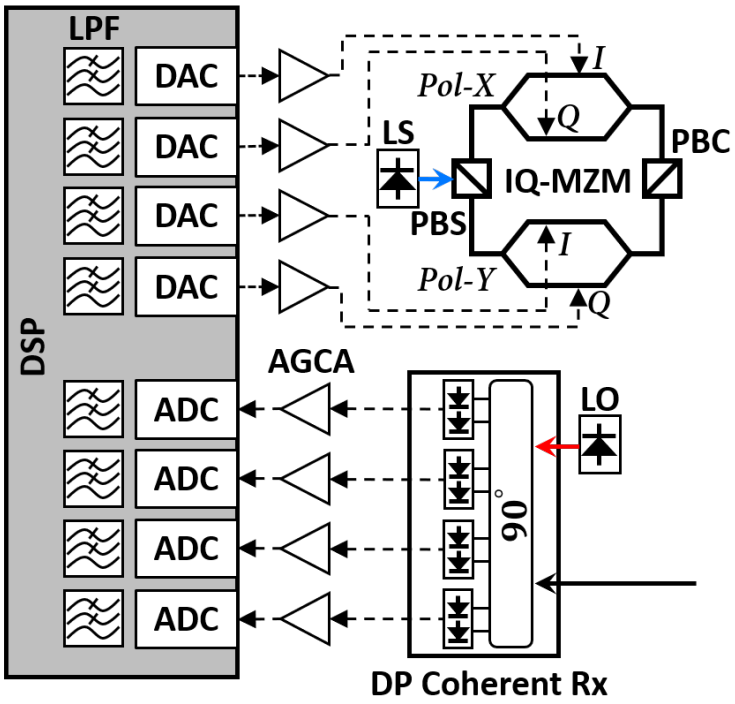

Figure 4.1: Architecture of a single-carrier DP-PSK transceiver relying on digital filters for Nyquist-shaped signal transmission. DAC: Digital-to-analog converter. ADC: Analog-to-digital converter. LS/LO: Laser source/local oscillator. PBS/PBC: Polarization beam splitter/combiner. LPF: Digital low-pass filter. AGCA: Automatic gain-controlled amplifier.

Table 4.1 shows the relative costs and power consumption values (in watts) of the components depicted in Fig. 4.1; the listed values are drawn from the data presented in Ref. [120]. In Table 4.1, the cost of the DSP chip includes the analog front-end, i.e., the analog-to-digital/digital-to-analog converters (ADCs/DACs) and the automatic gain-

controlled amplifiers (AGCAs). The total relative cost of the illustrated single-carrier transceiver is normalized to 1 for use as a benchmark throughout the rest of the paper.

Table 4.1: Relative costs and power consumption values of the components of a single-carrier transceiver for Nyquist-shaped signal transmission

Component	Unit cost	Power (W)	Num.	Total cost	Total power (W)
DSP chip	0.36	38.5	1	0.36	38.5
PM IQ modulator	0.22	0.0	1	0.22	0.0
Modulator driver	0.07	6.0	1	0.07	6.0
LS\LO	0.05	1.5	2	0.10	3.0
RF LPF	0.004	0.0	8	0.03	0
DP coherent Rx	0.22	1.5	1	0.22	1.5
Transceiver				1	49

4.2 Spatial and spectral super-channel transceiver architecture and cost analysis

The architecture of a 3×2 SpCh transceiver is shown in Fig. 4.2 [99, 120, 122]. For SDM fibers with multiple coupled modes (e.g., FMF and MMF), an SDM (mode) multiplexer and demultiplexer are required. In this paper, we only consider the SDM fibers whose physical entities are single-mode cores in the parallel SMFB or MCF because they are more compatible with the existing SMF technologies [28, 124]. Although there exist other SDM fibers such as FMFs, strongly coupled MCFs, and FM-MCFs, we do not include them in the discussion because they require a complicated MIMO-DSP whose complexity increases nonlinearly with the increase of the number of coupled modes/cores [27] and may need a long time to be widely deployed [28].

From Fig. 4.2, it is obvious that the laser source (LS) and local oscillator (LO) can be shared in the spatial domain. As an alternative design, a comb generator modulator/driver (unit cost: 0.18/0.07; power: 0 W/2 W) and an arrayed waveguide grating (unit cost: 0.02) can be employed instead of multiple independent lasers [99, 120]; however, we do not consider this option in this paper. In addition, a joint DSP can be applied instead of multiple parallel DSPs [27, 122, 125–128]. In this paper, we assume a 20% reduction in the cost of a joint DSP due to the joint implementation of the decoder and carrier recovery [122, 128, 129], and we assume that a 40% reduction in the cost of all other components (except the lasers) can be achieved due to linecard integration (photonic, analog, and digital) [120,122].

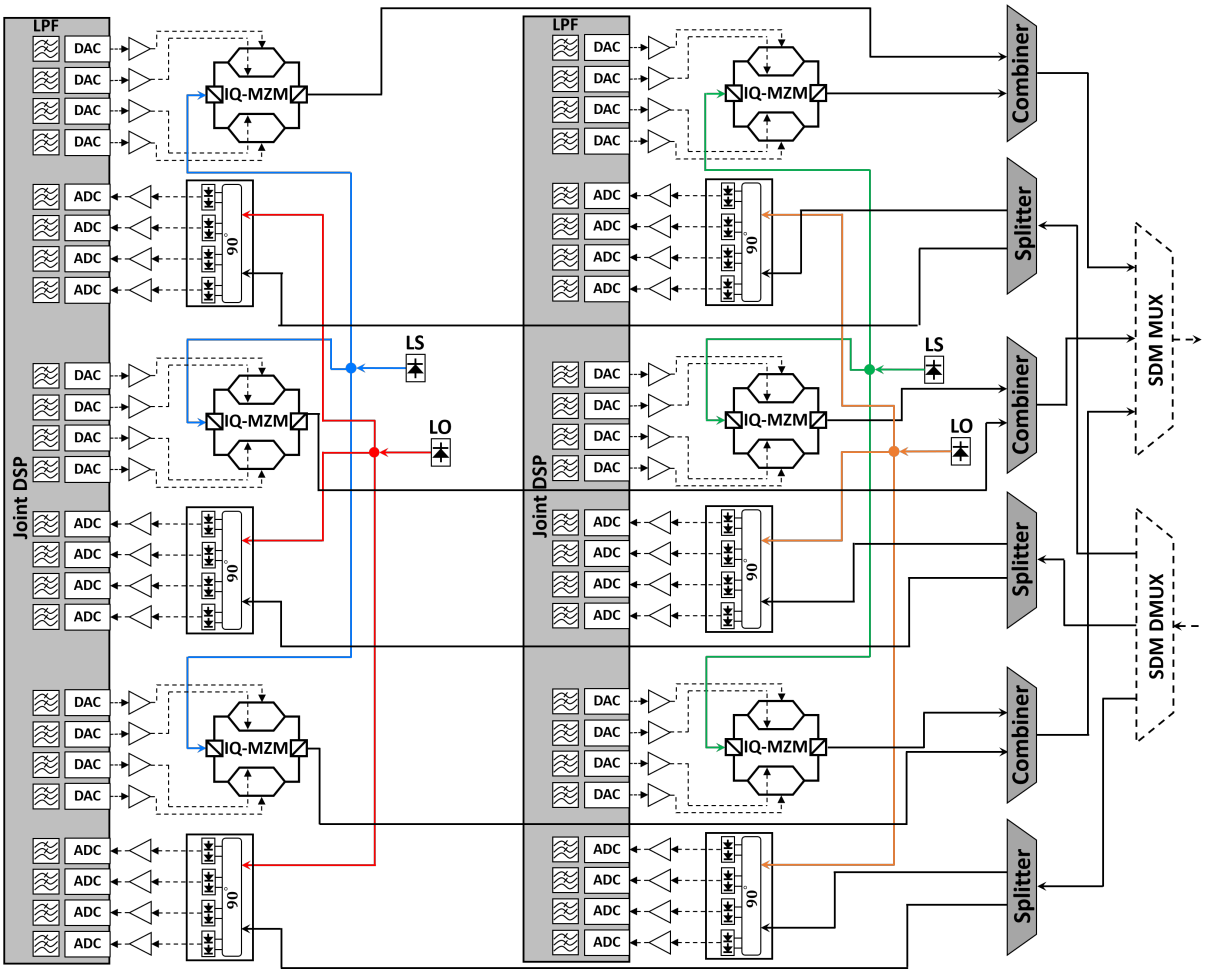

Figure 4.2: Architecture of a 3×2 SpCh transceiver. SDM MUX/DMUX: SDM multiplexer/demultiplexer (for MMF/FMF only).

Finally, we do not consider the cost of the splitter/combiner since it is negligible compared to the cost of the other components [120, 130, 131]. Consequently, we can calculate the relative cost of an $s \times o$ SpCh transceiver (C_{tc}), where s and o do not equal 1 simultaneously, as shown in Eq. (4.1):

$$C_{tc}(s,o) = \begin{cases} 0.1 \cdot o + 0.612 \cdot s \cdot o & \text{if } s > 1 \\ 0.1 \cdot o + 0.684 \cdot s \cdot o & \text{if } s = 1 \end{cases} \tag{4.1}$$

Similarly, the power consumption of an $s \times o$ SpCh transceiver (P_{tc}) can be calculated using Eq. (4.2):

$$P_{tc}(s,o) = 3 \cdot o + 46 \cdot s \cdot o \tag{4.2}$$

According to Eqs. (4.1) and (4.2), the relative cost and power consumption of the illustrated 3×2 SpCh transceiver are 3.872 and 282 W, respectively. These values correspond to a relative cost per OC of 0.645 and a power consumption per OC of 47 W. It is obvious that this SpCh transmission strategy achieves considerable savings in terms of device cost compared to single-carrier transmission (relative cost of 1) without significantly affecting the power consumption.

4.3 ROADM architecture and cost analysis

Fig. 4.3 illustrates the ROADM architecture at an intermediate node with 3 degrees (denoted by D throughout the rest of the paper) in the case of FrJ-Sw ($g = 2$) without SLC support for a 4-SMF bundle. For clarity, we consider the ROADM to be composed of two modules, namely, i) a route-and-select (R&S) module or a broadcast-and-select (B&S) module, and ii) an add/drop module, and explain these modules individually.

4.3.1 Route-and-select module

As shown in the top part of Fig. 4.3, the R&S module contains the WSSs and variable-gain dual-stage amplifiers (VGDAs) (unit cost: 0.18; power: 12 W). In addition, in the case of MCFs, a multi-core amplifier can be used instead of multiple VGDAs [42, 122, 124], and SDM fan-in/fan-out (FIFO) components should be deployed [96, 132]. The segment in the dotted green frame is actually identical to the ROADM architecture introduce in Section 2.3.4. From the top part of Fig. 4.3, it is obvious that the required number of VGDAs is

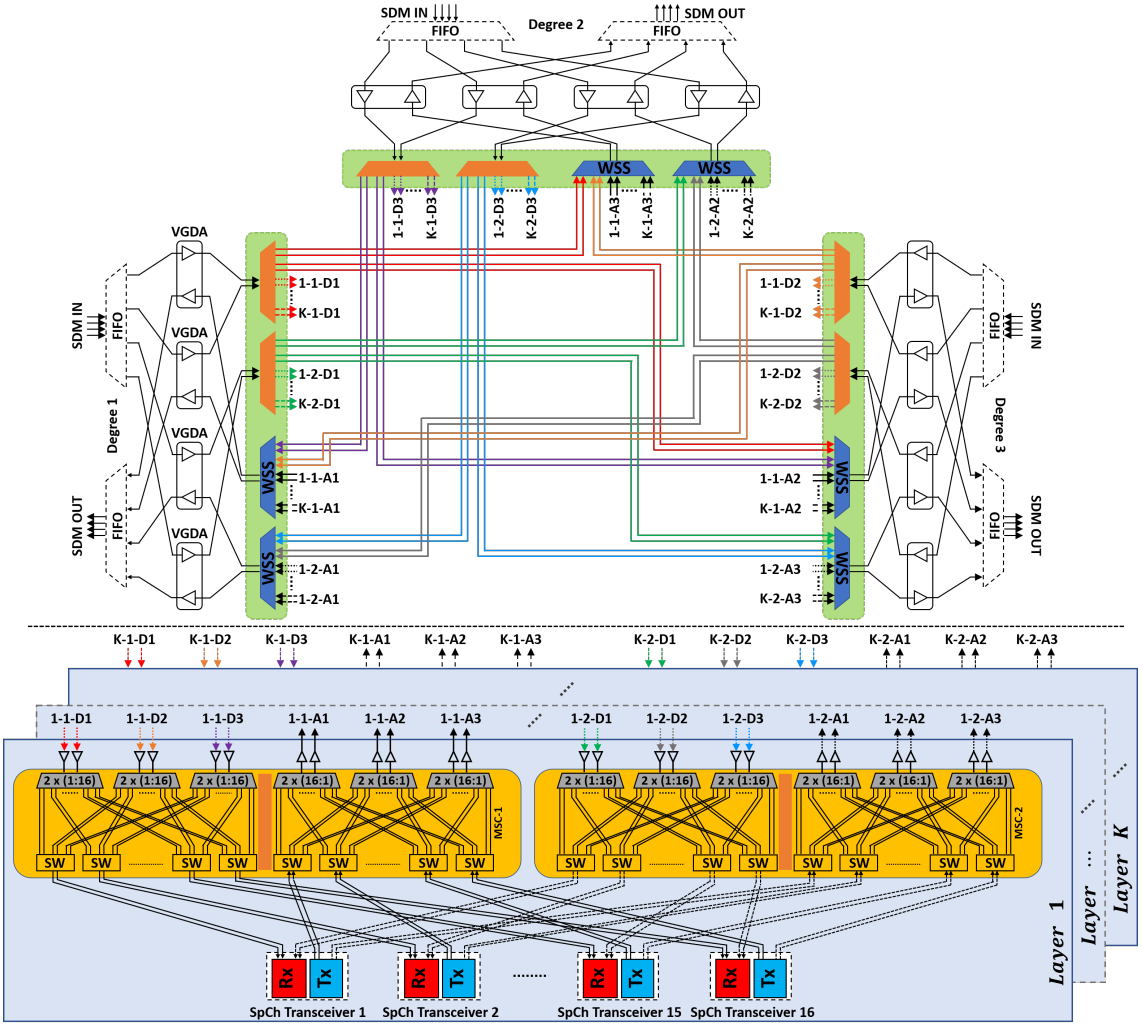

Figure 4.3: ROADM architecture in the case of FrJ-Sw ($g = 2$) without SLC support for bundles of 4-SMFs. FIFO: SDM fan-in/fan-out component (for MCF only); VGDA: variable-gain dual-stage amplifier; SW: optomechanical switch.

equal to $D \cdot S$. In addition, the number of required WSSs and the port count per WSS are listed in Table 4.2 [120, 124]. The value of K in Table 4.2 is the number of layers in the add/drop module, which determines the number of port groups used for add/drop.

Table 4.2: The number of required WSSs and port count per WSS

	Num. of WSSs / degree	Port count / WSS
With SLC	$2 \cdot D \cdot \frac{S}{g}$	$g \times \{1 \times [\frac{S}{g} \cdot (D-1) + K]\}$
Without SLC		$g \times [1 \times (D + K - 1)]$

Notably, a $1 \times N$ WSS can be reconfigured to implement a $G \times (I \times O)$ WSS with the total port count remaining the same [33, 133]. On this basis, in this paper, we use the relative costs of the WSSs with different port counts that are listed in Table 4.3 to calculate the cost of the WSSs (C_{WSS}) [103, 120].

Table 4.3: Relative costs of WSSs with different port counts

Port count	1×5	1×9	1×20	1×40	1×80	1×160	1×320
C_{WSS}	0.22	0.34	0.54	0.85	1.35	2.13	3.37

In accordance with the above discussion, the device cost of the R&S module (C_{rs}) can be calculated using Eq. (4.3):

$$C_{rs}(D, S, g) = C_{WSS} \cdot 2 \cdot D \cdot \frac{S}{g} + 0.18 \cdot D \cdot S \tag{4.3}$$

Regarding the power consumption of the WSSs (P_{WSS}), we assume that the power consumption per output/input port of a WSS at the ingress/egress is approximately 1 W [134, 135]. Thus, the power consumption of the R&S module (P_{rs}) can be calculated using Eq. (4.4):

$$P_{rs}(D, S, g) = P_{WSS} \cdot 2 \cdot D \cdot \frac{S}{g} + 12 \cdot D \cdot S \tag{4.4}$$

Finally, since the FIFO is an optomechanical component (power: 0 W) whose device cost is also negligibly small compared to those of other components [28], the proposed cost and power consumption models are not only applicable for SMFB but also for MCF.

4.3.2 Broadcast-and-select module

The key advantage of the R&S-based architecture is that it can provide superior isolation on the blocking ports and a low insertion loss regardless of the port count, making it more suitable for nodes with remarkably high degrees [136]. However, the B&S-based architecture [34, 105, 136, 137] can offer cost, power consumption, and optical/electronic complexity reductions by replacing the $G \times (1 \times O)$ WSSs at the ingress (i.e., the orange trapezoid) with $G \times (1 \times O)$ splitters. That is, in comparison to the R&S module, the B&S module reduces the number of WSSs by half. $G \times (1 \times O)$ splitters can be implemented by an array of G numbers of $1 \times O$ passive splitters.

Since the cost of the splitter is negligible compared to the costs of the other components [120, 130, 131], the device cost of the R&S module (C_{bs}) can be calculated using Eq. (4.5):

$$C_{bs}(D, S, g) = C_{WSS} \cdot D \cdot \frac{S}{g} + 0.18 \cdot D \cdot S \tag{4.5}$$

Moreover, the splitter is an optomechanical component whose power consumption equals 0W. Therefore, the power consumption of the B&S module (P_{bs}) can be calculated using Eq. (4.6):

$$P_{bs}(D, S, g) = P_{WSS} \cdot D \cdot \frac{S}{g} + 12 \cdot D \cdot S \tag{4.6}$$

4.3.3 Add/drop module

The colorless, directionless, and contentionless (CDC) add/drop module can be implemented with either multicast switches (MCSs) or $M \times N$ WSSs. In this paper, we consider the MCS-based implementation, as shown in the bottom part of Fig. 4.3 [103, 124], because the $M \times N$-WSS-based implementation results in a higher device cost [120]. To limit the cost and complexity of the CDC add/drop module, we assume that the complexity of the MCSs cannot increase without bound. Therefore, we consider that the CDC add/drop module is composed of K layers to support sufficient SpCh transceivers (add/drop ports). For clarity, we list the remarkable features of the CDC add/drop module architecture shown in the bottom part of Fig. 4.3 as follows:

- The number of SpCh transceivers that can be supported by each layer is T. Thus, the maximum number of SpCh transceivers that the ROADM can support is $T \cdot K$.
- The number of twin MCSs in each layer is equal to $\frac{S}{g}$.
- The numbers of input ports and output ports for each MCS are equal to $g \times D$ and $g \times T$, respectively. We refer to such an MCS as a $g \times (D \times T)$ MCS.
- The numbers of low-cost single-stage amplifiers (LCSAs) used to compensate for the splitter/combiner losses are as follows: $D \cdot g$ per MCS, $2 \cdot D \cdot g$ per twin MCS, $2 \cdot D \cdot S$ per layer, and $2 \cdot K \cdot D \cdot S$ in total.

In this paper, we consider the use of LCSAs (unit cost: 0.06; power: 6 W) with a gain of 17 dB, which limits the splitting ratio to approximately 1:16 [103,124,138,139]. Therefore, a commercial twin 4×16 MCS (cost: 0.49; driver power: 5 W) is chosen as the baseline and a 25% cost increase (toward to a twin 8×16 MCS) is assumed [124]. Moreover, to achieve a manufacturable product, we consider that a $g \times (D \times T)$ MCS is implemented by g individual $D \times T$ MCSs [103, 124].

Consequently, for a ROADM that supports a maximum of $16 \cdot K$ SpCh transceivers, the device cost of the add/drop module ($C_{A/D}$) can be calculated as shown in Eq. (4.7):

$$C_{A/D}(T, D, S) = K \cdot [S \cdot C_{MCS_{D\times 16}} + 0.12 \cdot D \cdot S] \tag{4.7}$$

Similarly, the power consumption of the add/drop module ($P_{A/D}$) can be calculated as shown in Eq. (4.8):

$$P_{A/D}(T, D, S) = K \cdot [5 \cdot S + 12 \cdot D \cdot S] \tag{4.8}$$

According to Eq. (4.3)~(4.8), we can summarize the total device cost and power consumption of a ROADM for various different designs as shown in Table 4.4.

Table 4.4 indicates that a larger g (corresponding to a larger spatial span s of SpChs) can reduce the device cost of the ROADM regardless of whether SLC is supported. Additionally, for all different g, both the device cost and power consumption of a ROADM without SLC support are significantly lower than those of a ROADM with SLC support. Moreover, both the device cost and power consumption of a B&S-based ROADM are significantly lower than those of the R&S-based ROADM.

Finally, it is worth noting that there is no uniform standard for the device cost and power consumption of the components because of the differences among products made by

Table 4.4: Device cost and power consumption for different ROADM architectures

Spatial switching granularity g	SLC	R&S-based		B&S-based	
		Cost	Power	Cost	Power
1	With	35.68	1552	27.04	1296
	Without	29.28	1264	23.84	1152
2	With	32.00	1360	25.20	1200
	Without	27.04	1264	22.72	1152
4	With	25.20	1264	21.80	1152

Nodal degree $D = 4$; the number of SLs $S = 4$; the number of SpCh transceivers $T = 60$.

different manufacturers. Moreover, for certain components that are still under development, no commercial products are yet available. The values used in our work are taken from previous publications and/or commercial products. The reader can use various alternative values depending on the specific situation of interest based on the proposed architectures (and their alternatives) because the architectures will be essentially the same.

4.4 Simulation and numerical results

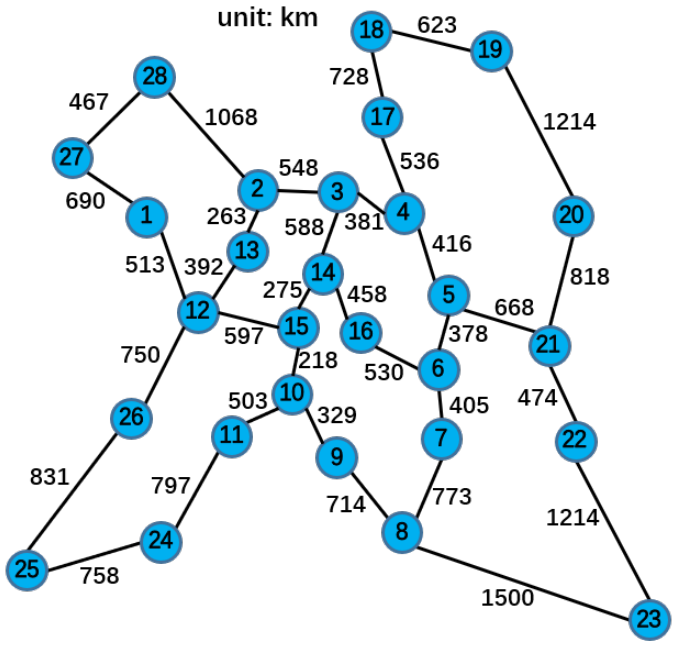

Figure 4.4: The 28-node EON topology with 68 directed links considered in the simulation experiments

In this section, we evaluate the device cost, power consumption, and network performance of SDM transmission systems via simulation experiments executed using the 28-node European Optical Network (EON) topology with 68 directed links (average nodal degree: 2.43), as shown in Fig. 4.4. The following assumptions are adopted in the simulation experiments:

- A bundle of 12 independent SMFs is assumed for each link in the network, which enables us to fairly compare the considered SDM technologies regardless of performance constraints due to different transmission media.

- The total optical spectrum per SMF is considered to be 4 THz (C-band), that is, 320 FSs on the ITU-T 12.5 GHz grid [93].

- The DP-BPSK, DP-QPSK, DP-8QAM, and DP-16QAM modulation formats can be selected in the simulation experiments. The selection of the modulation format should consider the required quality of transmission (QoT) of the connection. A common assumption in the optical transmission is that the transmission distance of the optical path is the sole QoT factor of interest [8,116,140]. Under this assumption, to ensure the QoT of the connections, the maximum transmission distances will be different for different modulation formats. In this paper, we assume that the maximum transmission distances for DP-BPSK, DP-QPSK, DP-8QAM, and DP-16QAM are 6300, 3500, 1200, and 600 km [29, 32, 100], respectively. For a given lightpath, we will select the modulation format with the highest spectral efficiency depending on its length. It is worth noting that the maximum transmission distance for each modulation format above can only be applied for the case of SMFB because the distance will be shorter due to the impact of the inter-core crosstalk in the case of MCF [58].

- The available spatial spans s for $s \times o$ SpChs are considered to be 1, 2, 3, 4, 6 and 12.

- The connections are assumed to arrive at each source node one by one following a Poisson-distributed process with an average arrival rate of λ, and their average holding time is assumed to follow a negative exponential distribution with parameter μ. Therefore, the average offered load (the number of connections loaded at points in time) per node follows an Erlang($\frac{\lambda}{\mu}$) distribution. Moreover, each connection between a pair of source and destination nodes is considered to be unidirectional due to the asymmetric nature of current Internet traffic, and the destination node is randomly selected in the network. The traffic volume for each connection is generated from the range of 0.1 Tbps to 1 Tbps with uniform distribution.

- We assume that several SpCh transceivers with maximum support of n numbers of OCs are deployed at each node. It is worth noting that since the connections that arrive and disappear stochastically are not known in advance, an SpCh transceiver will support connections with different traffic volumes at different points in time. Therefore, an appropriate setting of n is very important. If n is too large, a waste of device expenditure will occur when supporting a connection with a small traffic volume. In contrast, if n is too small, multiple SpCh transceivers should be employed to support a connection with large traffic volume, which results in low spectral efficiency because of the additional requirement of GBs between the SpChs. In our simulation experiments, to ensure a fair comparison between the different SpCh transceivers with different s, n is set as 12 for all of them.

- The basic k-shortest-path algorithm (k = 3) and the first-fit spectrum allocation policy [6] are applied to assign the FSs for each connection.

4.4.1 Results for network performance

In this part, we evaluate the network performance in terms of the maximum average network throughput [Tbps] within a reasonable blocking probability (BP) 1% for different transmission systems [34, 45, 65, 141–143]. The differences among these transmission systems are due to i) the different spatial spans s of the applied Spa & Spe SpCh and the corresponding SpCh transceivers, ii) the different switching granularities g of the ROADMs, and iii) whether the SLC is supported at the ROADM. Notably, the switching granularities g of the ROADMs should be always identical with the spatial spans s of the applied Spa & Spe SpChs to achieve all-optical switching, as we have discussed in Section 2.3.4.

A set of offered loads ($\frac{\lambda}{\mu}$) from light to heavy achieved by fixing the average arrival rate λ and gradually increasing the average holding time $1/u$ (a general method that has been widely applied in previous works [34, 45, 65, 141–143]) are simulated until we obtain a BP close to 1%. The average network throughput is the average carried traffic per second along with the entire simulation. Therefore, the maximum average network throughput can be obtained from the process of incrementing the offered loads; 10^6 bidirectional connections are generated to obtain reliable results.

Fig. 4.5 shows the (maximum average) network throughput for different transmission systems against the number of installed SpCh transceivers at nodes (recorded as T in the rest of the paper). It is worth noting that the network throughput will be bounded by the inadequacy of both the spectrum resource (320 FSs on C-band) and T. As shown in Fig. 4.5, the network throughput for all transmission systems is the same when we limit T

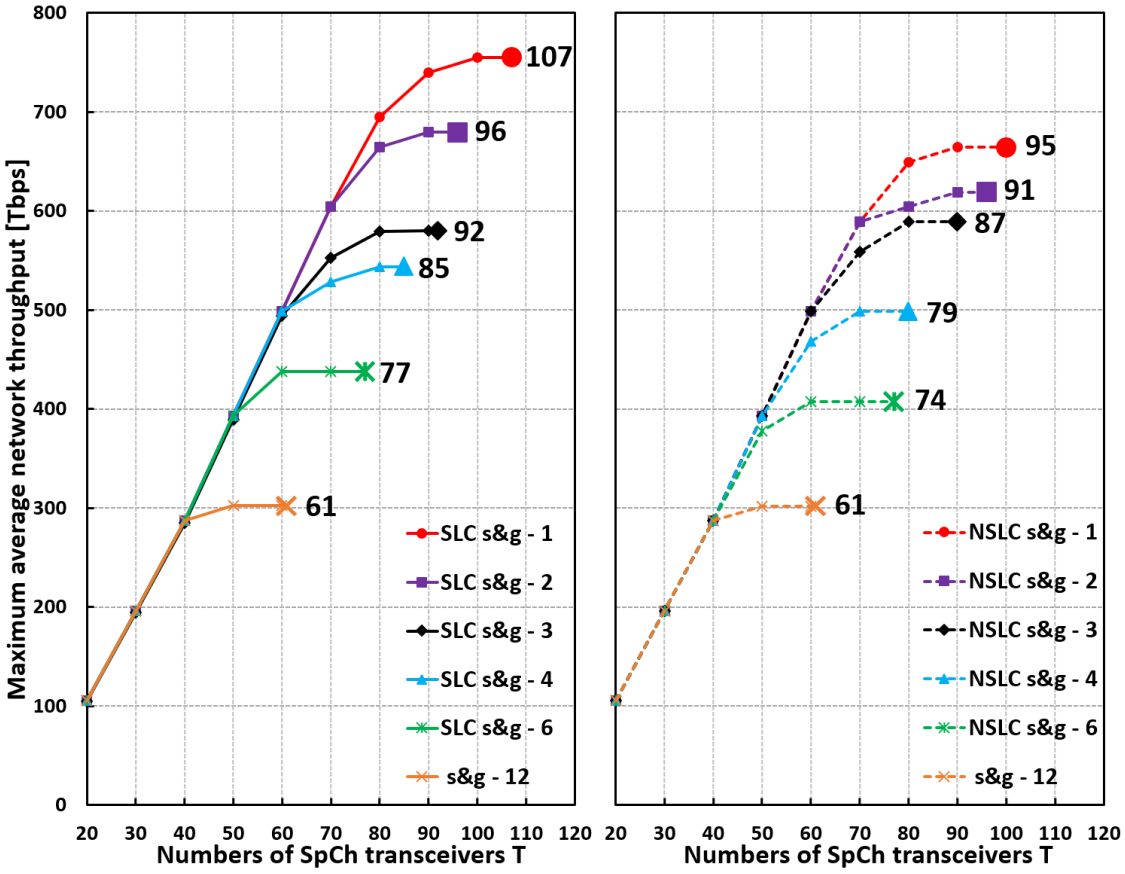

Figure 4.5: The maximum average network throughput [Tbps] vs. the number of installed SpCh transceivers at nodes T for different transmission systems

to small values. In this case, the primary factor that restricts the network throughput for all transmission systems is the inadequacy of the installed SpCh transceivers. Then, we can see that the network throughput for each transmission system increases with the growth of T until it reaches a certain value (i.e., the large mark shown in Fig. 4.5). The number on the right of each large mark is actually the number of the maximum required SpCh transceivers per node in the network (record as T_{max}) for the corresponding transmission system, which is calculated by allowing the installation of the SpCh transceivers as needed. For each transmission system, it is pointless to further install additional SpCh transceivers that exceed its corresponding T_{max} because in this case, the only reason that the network throughput is restricted is the insufficiency of the spectrum resource.

From Fig. 4.5, it is obvious that i) the transmission system with smaller $s\&g$ achieves larger network throughput regardless of whether SLC is supported and ii) for transmission systems with the same $s\&g$, the one with SLC support (the left part) provides larger network throughput than the one without SLC support (the right part). One reason for these behaviors is that the spectral efficiency decreases as s increases (due to resource wastage caused by the GBs and over-provisioning). Another reason is that the application of ROADMs with smaller g, as well as the means of SLC technology, can offer higher routing flexibility (as shown in Fig. 2.9), leading to less generation of spectrum fragments. In other words, higher spectral efficiency and/or routing flexibility indicates the ability to establish more connections within the limited spectrum resource, and of course, a higher requirement for the number of SpCh transceivers. This is also the reason that the transmission system with smaller $s\&g$ and/or SLC support will have a larger T_{max}.

Moreover, we can see that the increase of the network throughput slows down with the growth of T for each transmission system, which means that the gain of the network throughput brought by additional SpCh transceiver declines. Particularly, in the case of T close to T_{max}, the gain is almost negligible due to the lack of spectrum resource. Therefore, to strike a balance between the network performance and CAPEX, an appropriate T is important in network planning.

4.4.2 Results for device cost and power consumption

In this part, we investigate the effects of different transmission systems in terms of network CAPEX containing device cost and power consumption. The number of connections loaded to each node at different points in time fluctuates along the simulation process, which follows the Erlang distribution with an average of $\frac{\lambda}{\mu}$. Certain installed SpCh transceivers may be activated at a certain point in time and deactivated at another point in time. To conform to the real world case, we do not consider the power consumption of these deactivated

Table 4.5: Device cost (in thousand-unit) vs. the number of installed SpCh transceivers per node T for different transmission systems

SLC sup.		With SLC					Without SLC					12
$s\&g$		1	2	3	4	6	1	2	3	4	6	
T	20	6.5	5.4	5.2	5.1	5.0	6.1	5.3	5.2	5.1	5.0	4.9
	30	9.1	7.6	7.4	7.3	7.2	8.8	7.5	7.3	7.2	7.1	7.0
	40	12.0	10.1	9.8	9.7	9.5	11.7	10.0	9.8	9.6	9.5	9.4
	50	14.9	12.7	12.3	12.1	11.9	14.6	12.5	12.2	12.1	11.9	11.7
	60	17.6	14.9	14.9	14.3	14.1	17.2	14.8	14.4	14.2	14.0	13.8
	70	20.5	17.4	16.9	16.7	16.4	20.2	17.3	16.8	16.6	16.4	
	80	23.1	19.6	19.1	18.8		22.8	19.5	19.0			
	90	26.0	22.1	21.5			25.7	22.0				
	100	28.9										
T_{max}		30.8 (107)	23.4 (96)	22.0 (92)	20.1 (85)	17.9 (77)	27.0 (95)	22.2 (91)	20.8 (87)	18.5 (79)	17.3 (74)	14.0 (61)

SpCh transceivers. Additionally, please note that an SpCh transceiver can maximally support 12 OCs, which indicates that it is composed of 12 single-OC transceivers (see Fig. 4.2). When it serves a connection that requires a small number of OCs, only a part of single-OC transceivers will be activated. Therefore, the power consumption of a transmission system at a point in time is strongly related to the number of activated SpCh transceivers as well as the number of activated single-OC transceivers in these SpCh transceivers. In this paper, the power consumption is calculated dynamically at each point in time, and the final results are averaged throughout the entire simulation. In contrast, the SpCh transceivers are installed in the deployment phase, which indicates that the architecture and the number (i.e., T) of transceivers do not change with time. Therefore, unlike power consumption, the device cost for each transmission system is calculated statically regardless of whether these SpCh/single-OC transceivers are activated or deactivated.

Moreover, as we discussed in Section 4.3, the ROADMs can be implemented by either R&S or B&S architecture. In our simulation experiments, the B&S-based ROADMs are considered because although the R&S architecture can achieve higher scalability due to its low insertion loss, the B&S architecture is the currently preferred option considering the scale of the current backbone networks due to its higher cost efficiency.

The network device costs (in thousand-unit) from the simulation experiments reported in Section 4.4.1 are shown in Table 4.5. We can see that the device cost is higher for a transmission system with a smaller $s\&g$. Additionally, for transmission systems with the same $s\&g$, the one with SLC support leads to higher device cost than the one without SLC support. The reason for these findings is that, as seen from Table 4.2, a ROADM

Table 4.6: The average network power consumption [KW] vs. the number of installed SpCh transceivers per node T for different transmission systems

SLC sup.		With SLC					Without SLC					12
$s\&g$		1	2	3	4	6	1	2	3	4	6	
T	20	172	160	157	155	153	158	154	153	152	152	151
	30	276	261	257	254	252	262	255	253	252	251	250
	40	393	375	370	367	364	379	369	366	364	363	359
	50	526	504	498	494	490	512	498	494	492	474	388
	60	647	622	622	607	535	633	616	608	573	504	387
	70	780	750	690	651	548	749	723	652	614	517	
	80	880	811	718	651		812	741	666			
	90	940	838	731			839	766				
	100	968										
T_{max}		967 (107)	839 (96)	731 (92)	663 (85)	548 (77)	840 (95)	766 (91)	678 (87)	614 (79)	517 (74)	387 (61)

with smaller g requires more WSSs/splitters, while a ROADM with SLC support requires more ports per WSS/splitter. However, compared to the device cost of the whole system (dozens of the deployed SpCh transceivers and ROADMs), these cost savings are not obvious (within 5%). Therefore, we have not illustrated the data with a figure because these differences are difficult to distinguish in a figure.

Nevertheless, there is an exception in which the device costs for the transmission systems with $s\&g$ equaling 1 are significantly higher than those of the other transmission systems. This is because of the 20% cost reduction due to the implementation of joint DSP in the spatial domain (if $s > 1$). Thus, it is evident that joint DSP is a critical technology that can enable remarkable cost savings for SDM transmission.

The (average) power consumption (in KW) from the simulation experiments reported in Section 4.4.1 is shown in Table 4.6. We can see that the transmission system with a smaller $s\&g$ consumes more power. This is because OCs in the same spectral region but distributed throughout the spatial domain can share a common LS and LO, meaning that the SpCh transceiver with larger s can achieve relatively greater savings in terms of power consumption according to Eq. (4.2). Additionally, due to the lower port-count requirement of the ROADM without SLC support (as shown in Table 4.2), we can see that the transmission system without SLC support leads to lower power consumption than does the transmission system with SLC support.

Additionally, for each transmission system, the changes in power consumption will slow down when T approaches the T_{max}. For instance, for a transmission system with $s\&g$ equaling 1 and SLC support (the 1st column), the gap between the cases of T=20 and T=30

is 104 KW, but the gap between the cases of T=90 and T=100 is reduced to 28 KW. This is because when T is close to the T_{max}, the additional installed SpCh transceivers will rarely be activated due to the lack of spectrum resource. Moreover, since different T_{max} values are held by the different transmission systems, the gap between them will become obvious with the increase of T, which can also be seen from the Table 4.6.

4.4.3 Results for cost efficiency and power efficiency

From the above results, it is obvious that the transmission system with smaller $s\&g$ and/or SLC support can provide higher network throughput due to its higher spectral efficiency and routing flexibility but also results in higher device cost and power consumption. Moreover, network throughput, device cost, and power consumption all increase with the growth of T. That is, a trade-off relationship exists between network throughput and device cost/power consumption. Therefore, to evaluate the cost efficiency of the different transmission systems, we introduce a new criterion recorded as CE [Gbps / unit cost], which equals the ratio of the network throughput in Fig. 4.5 to the device cost in Table 4.5. That is, the CE indicates the network throughput gain per unit cost. Fig. 4.6 shows the CE of different transmission systems against T.

From Fig. 4.6, we can see that the shape of CE for each transmission system is convex. With the increase of T, the CE increases first and then decreases. This observation shows that to achieve higher cost efficiency, a larger T is not necessarily better. This finding conforms to the results in Fig. 4.5 because the more closely the T approaches T_{max}, the slower the growth of the network throughput will be. However, the growth of the device cost remains almost stable; therefore, there must exist a T that achieves the highest CE (shown as the large mark in Fig. 4.6 and recorded as T_{CE} in the rest of the paper). We list the T_{CE} for each transmission system in Table 4.7.

Table 4.7: T_{CE} for each transmission system

SLC sup.	With SLC					Without SLC					12
$s\&g$	1	2	3	4	6	1	2	3	4	6	
CE	30.0	34.7	33.4	34.9	32.9	29.2	34.1	34.7	32.9	31.7	30.6
T_{CE}	80	70	60	60	50	70	70	60	60	50	40
T_{max}	107	96	92	85	77	95	91	87	79	74	61

From Table 4.7, we can see that the transmission system with smaller $s\&g$ and/or SLC support has higher T_{CE}. As we have discussed above, the transmission system with smaller $s\&g$ and/or SLC support can provide higher spectral efficiency and/or routing flexibil-

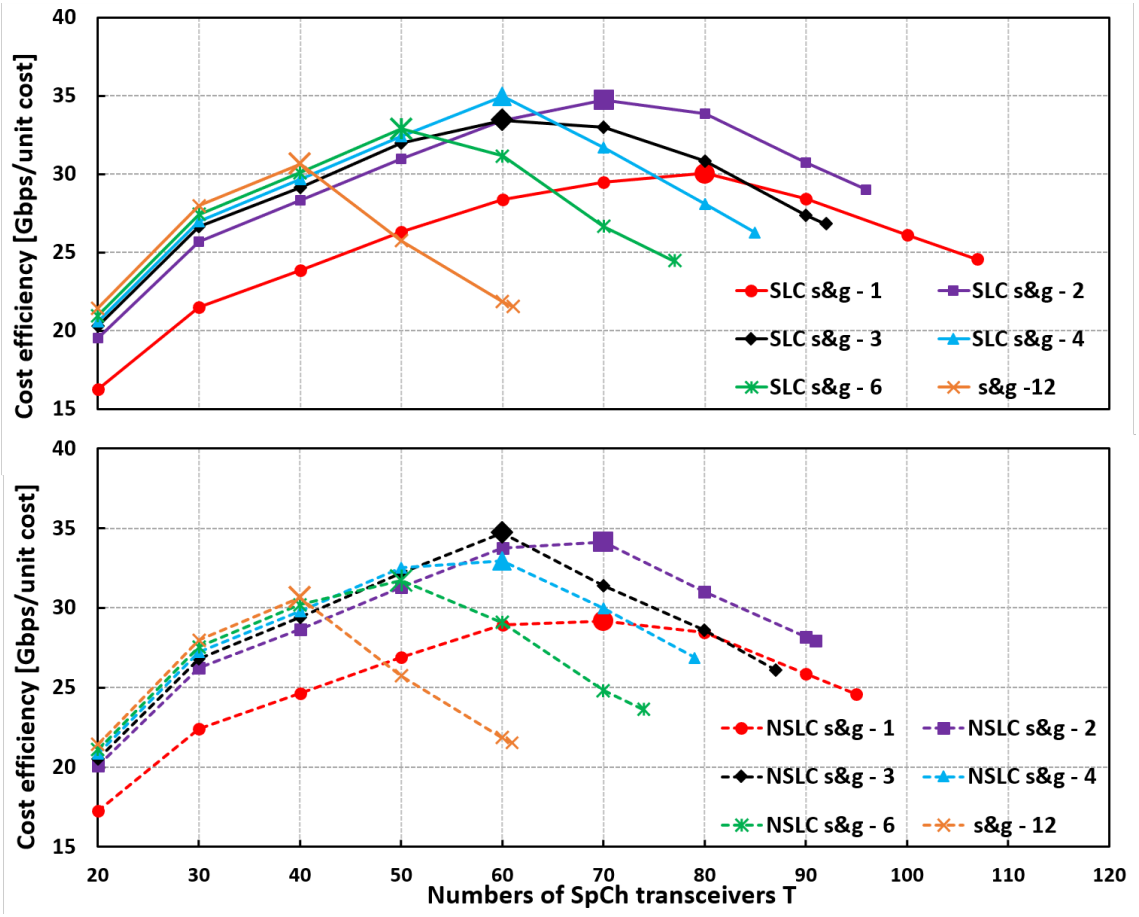

Figure 4.6: The cost efficiency CE vs. the number of installed SpCh transceivers per node T for different transmission systems

ity, leading to higher T_{max}. From Fig. 4.5, it is obvious that with the increase of T, the growth of network throughput is remarkable until T approaches T_{max}. Therefore, the transmission system with larger T_{max} exhibits larger T_{CE} as well. Among all the transmission systems, the one with $s\&g$ equaling 4 and SLC support achieves the highest cost efficiency (CE=34.9) in the case of T equaling 60. Moreover, we can observe that the transmission systems with s & g equaling 2~4 for both the cases with and without SLC support provide competitive cost efficiency. We consider that the reason is that these transmission systems strike a good balance between the network performance and device cost.

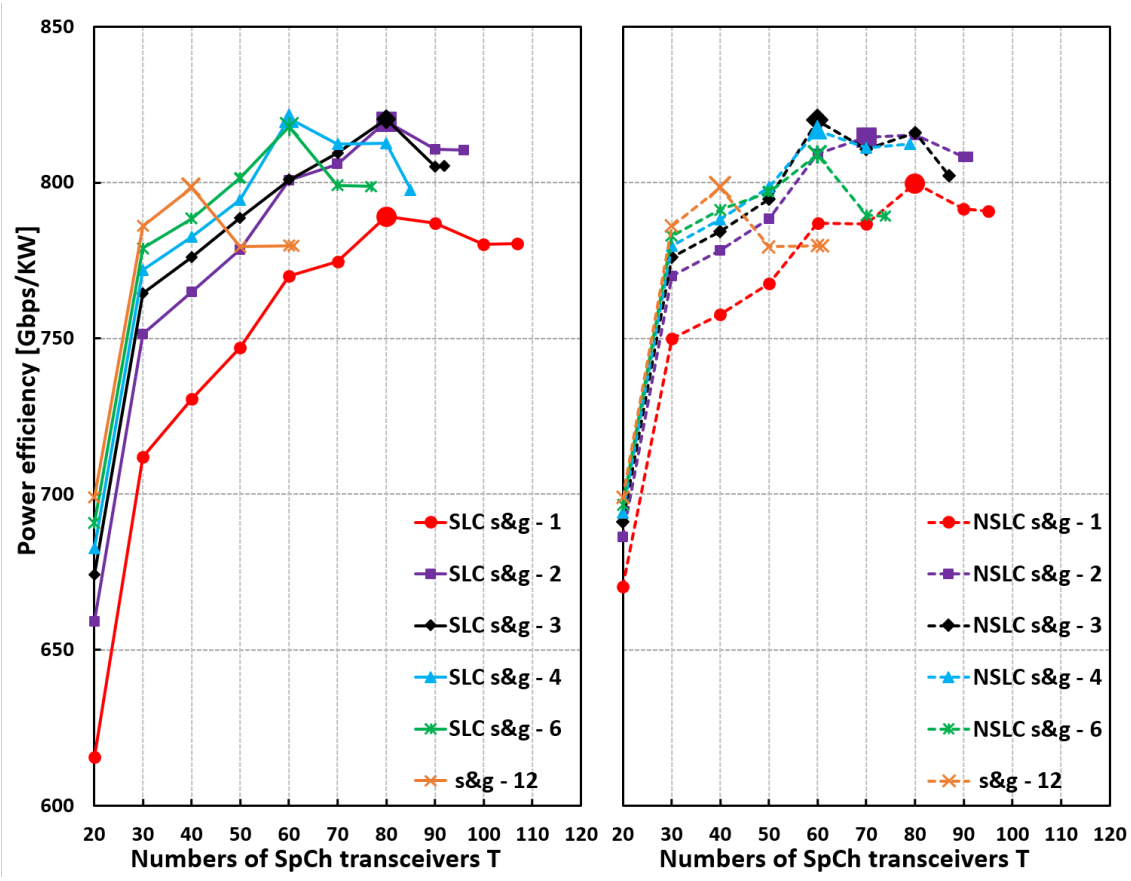

Figure 4.7: The power efficiency PE vs. the number of installed SpCh transceivers per node T for different transmission systems

As with the evaluation of cost efficiency, we introduce another criterion recorded as PE [Gbps / KW], which equals the ratio of the network throughput in Fig. 4.5 to the power consumption in Table 4.6, to evaluate the power efficiency for each transmission system. Fig. 4.7 shows the PE of the different transmission systems against T.

From Fig. 4.7, we can observe that PE has a similar trend to that of CE in Fig. 4.6. For each transmission system, the shape of PE is also convex and there exists a T that leads to

maximum PE (recorded as T_{PE}). Similarly, we list the T_{PE} for each transmission system in Table 4.7.

Table 4.8: T_{PE} for each transmission system

SLC sup.	With SLC					Without SLC					12
$s\&g$	1	2	3	4	6	1	2	3	4	6	
PE	789	820	820	821	818	800	815	820	817	809	798
T_{PE}	80	80	80	60	60	80	70	60	60	60	40
T_{max}	107	96	92	85	77	95	91	87	79	74	61

From Table 4.8, we can see a similar result to that of Table 4.7. The transmission system with $s\&g$ equaling 4 and SLC support (PE=821) is the best, and the transmission systems with s & g equaling 2∼4 are competitive.

Chapter 5

Hierarchical Routing and Resource Assignment in Spatial Channel Networks (SCNs): Oriented Toward the Massive SDM Era

As introduced in Section 1.6, the resource allocation problem in SCNs has been clarified. In this chapter, we consider the static scenario which mainly related to the network planning phase and hence is not subject to strict computational time constraints. We propose an ILP model for the static RSCSA problem.

This chapter is organized as follows. In Section 5.1, we discuss the RSCSA problem in detail. In Section 5.2, we prove the NP-hardness of the RSCSA problem. In Section 5.3, we propose and give a detailed demonstration of our ILP model and heuristic algorithm, for solving the RSCSA problem. In Section 5.5, we evaluate the performance of the two proposed approaches via simulation experiments. For small-scale instances, we compare the performance of both the ILP model and heuristic algorithm. For large-scale instances, we show the numerical results of the proposed heuristic algorithm.

5.1 Introduction to the RSCSA problem

Similar to the RWA problem in WDM optical networks, the RSA problem in EONs, and the RSSA problem in SDM-EONs, the RSCSA problem can be subdivided into two main cases: the dynamic case and the static case.

In the dynamic case, which emerges during network operation, it is assumed that the connection requests are unknown in advance and that they stochastically arrive and disappear one by one. The resources required to serve connection requests are assigned dynamically in accordance with the current state of the network. The objective of the dynamic

RSCSA problem is to minimize the network blocking probability (BP) or to maximize the network throughput while maintaining an acceptable BP (e.g., 1%) [34, 141], which is the same as the objectives of the previous dynamic RWA, RSA, and RSSA problems.

In the static case, which mainly relates to the network planning phase, a traffic matrix that contains a set of connection requests that must be served in the network is known in advance, and resources must be assigned to all of these connection requests simultaneously. In the static RSCSA problem, the main objective is to minimize the number of SLs that are used/required in the network, for the following three reasons:

- Minimizing the number of FSs that are used/required (or the maximum index of these FSs) in the network, as is done in the static RWA, RSA, and RSSA problems, is pointless in this case because in an SCN, each connection request is transmitted by an SCh, which may occupy the entire C-band spectrum.

- Minimizing the number of SLs used is equivalent to maximizing the number of SLs in the network that are not occupied and thus are available for future connection requests – assuming that the network scenario is semidynamic, we optimize the network by reassigning the currently established connections as a 'static' set, and any connection requests that subsequently arrive in the network are handled dynamically [144]. Therefore, minimizing the number of SLs used reduces the level of congestion in the network.

- The last reason is that there are many different possible types of SCN systems. Note that scalability of the SLs is not supported by all types of HOXCs, and in general, a system with 20 SLs is much cheaper than one with 40 SLs. Therefore, if we can reduce the number of SLs required to below 20 during the network planning phase, great cost savings can be achieved.

Another objective of the RSCSA problem, although with a lower priority, is to minimize the number of SLs with wavelength switching support that are used/required, for the following two reasons:

- As stated before, compared to SDM-EONs, the key feature of SCNs is that wavelength switching support is not necessary on every SL because some connection requests can be transmitted by SChs of Type I and Type II, which can be spatially bypassed at intermediate nodes. As shown in Fig. 2.11, the number of SLs with wavelength switching support has a one-to-one relationship with the number of deployed WXCs. Therefore, during the network planning phase, minimizing the number of required SLs with wavelength switching support is equivalent to minimizing

the number of required WXCs at HOXCs. Between two HOXCs that support the same number of SLs, the one with fewer WXCs will certainly cost less.

- As introduced in Section II-A, there are four types of SChs, and from the networking perspective, an SCh of Type IV can be routed as multiple independent SChs of Type I. SChs of Type I and Type II can be spatially bypassed at intermediate nodes using SLs without wavelength switching support. However, if the available SLs without wavelength switching support are inadequate, SLs with wavelength switching support can also be used. In contrast, SChs of Type III can pass only through SLs with wavelength switching support. Therefore, in the semidynamic scenario, for two solutions to the RSCSA problem that require an equal number of SLs, the one that uses fewer SLs that support wavelength switching is preferred – the more idle SLs with wavelength switching support there are, the higher the possibility of satisfying more subsequent connection requests.

In summary, the static RSCSA problem is a multiobjective problem in which the decision on how to allocate resources, such as routing paths, SLs, modulation formats, and spectrum, for each connection request should be jointly made in an offline manner.

5.2 NP-hardness of the RSCSA problem

In this section, we prove the NP-hardness of the RSCSA problem by reducing the RWA problem for traditional WDM optical networks to the related RSCSA problem.

The RWA problem is a well-known NP-hard problem [145]. An instance of the RWA problem includes a set of connection requests $r \in R$ and a set of wavelengths $\lambda \in \Lambda$. The objective is to assign a routing path p_r and a wavelength λ_r to each $r \in R$ while minimizing the number of wavelengths that are used/required in the network (λ_{max}). In addition, the assignments should comply with the wavelength continuity and nonoverlap constraints. To solve the RWA problem in a form that is equivalent to the RSCSA problem, we consider the network scenario shown in Fig. 5.1.

We assume that a set of connection requests $r \in R$ and a set of SLs $l \in L$ ($L \rightarrow \Lambda$) are given. Note that the two CSS-based HOXCs considered in this paper do not support SLC. Therefore, the wavelength continuity constraint is converted into an SL continuity constraint in the RSCSA problem, and a corresponding SL nonoverlap constraint should also be satisfied. Here, we simplify the RSCSA problem by ignoring the second (minor) objective and assume that each $r \in R$ exactly occupies the entire C-band of a single SL. Thus, we should assign a routing path p_r and an SL l_r ($l_r \rightarrow \lambda_r$) to each $r \in R$ while

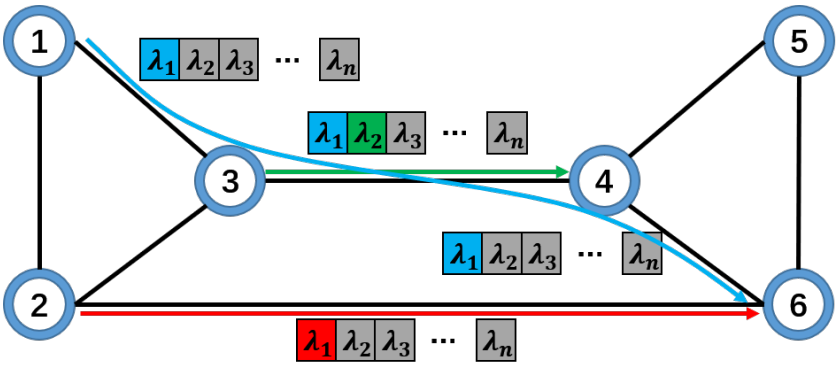

(a) Wavelength continuity and non-overlapping in RWA problem

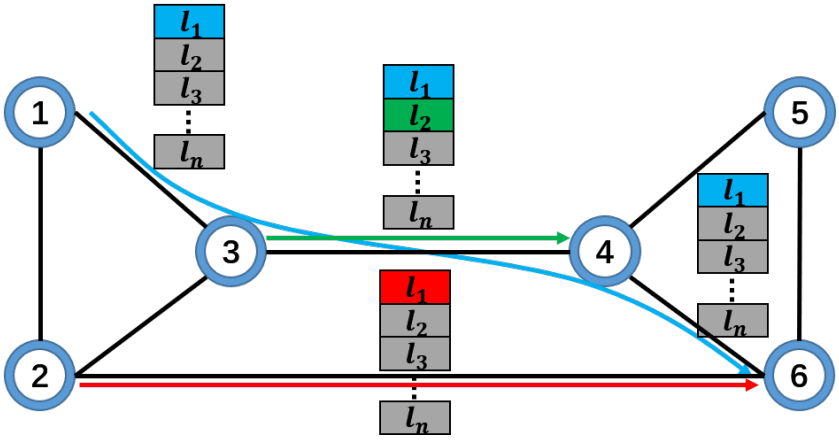

(b) SL continuity and non-overlapping in RSCSA problem

Figure 5.1: Comparison between the RWA problem and the RSCSA problem.

minimizing the number of SLs that are used/required in the SCN (l_{max}; $l_{max} \rightarrow \lambda_{max}$). In this case, if we were able to optimally solve the simplified RSCSA problem, we would also obtain the optimal solution to the RWA problem. Therefore, since the RWA problem is NP-hard and the original RSCSA problem is more complex than the simplified one, we can conclude that the original RSCSA problem is also NP-hard.

5.3 ILP model for the RSCSA problem

In this section, we introduce our ILP model proposed for the RSCSA problem.

5.3.1 Parameters

V the set of nodes v in the network.

E the set of links e in the network.

NP the set of node pairs np in the network.

R the set of connection requests $r = \langle s_r, d_r, t_r \rangle$, where s_r, d_r, and t_r represent the source node, destination node, and traffic volume [bps], respectively, of connection request r.

R_{np} the set of connection requests between node pair np, which is defined as $R_{np} = \{r \in R | \langle s_r, d_r \rangle = np\}$.

P_r the set of k candidate routing paths for connection request r, which is obtained using the k-shortest-path algorithm proposed in Ref. [6].

P_{np} the set of k candidate routing paths between node pair np, where $P_{np} = P_r$ for each $r \in R_{np}$.

L the set of SLs $l \in L$ (per link) in the network.

L_W the set of SLs with wavelength switching support in the network.

L_{NW} the set of SLs without wavelength switching support in the network.

t_{OC}^p the traffic volume [bps] supported by a single OC on routing path p, which is determined by the highest feasible modulation level of the path according to its path length [km].

F_{GB} the number of FSs occupied by a wavelength switching GB.

F_{OC} the number of FSs occupied per OC.

F_{max} the total number of available FSs on each SL.

f_{max} the maximum index of the FSs on each SL. Note that the indices of the FSs start from 0; therefore, $f_{max} = F_{max} - 1$.

5.3.2 Variables

u^l a binary variable that is equal to 1 if SL l is used and to 0 otherwise.

x_r^{pl} a binary variable that is equal to 1 if lightpath $\langle p, l \rangle$ is assigned to serve connection request r and to 0 otherwise.

o_r^{pl} an integer variable that indicates the number of OCs that are assigned to lightpath $\langle p, l \rangle$ to serve connection request r.

α_r^{pl} an integer variable that indicates the starting index of the FSs assigned to lightpath $\langle p, l \rangle$ to serve connection request r.

β_r^{pl} an integer variable that indicates the ending index of the FSs assigned to lightpath $\langle p, l \rangle$ to serve connection request r.

$\theta_{rr'}^{pp'l}$ a binary variable that is equal to 1 if β_r^{pl} is smaller than $\alpha_{r'}^{p'l}$ and to 0 otherwise.

5.3.3 Objectives

$$\text{Main objective:} \quad \textit{Minimize} \quad \sum_{l \in L} u^l \tag{5.1}$$

$$\text{Minor objective:} \quad \textit{Minimize} \quad \sum_{l \in L_W} u^l \tag{5.2}$$

As we mentioned above, the static RSCSA problem is a multiobjective problem. The main objective, shown in Eq. (5.1), is to minimize the number of SLs that are used/required in the network, while the minor objective, shown in Eq. (5.2), is to minimize the number of SLs with wavelength switching support that is used/required.

5.3.4 Constraints

$$\sum_{p \in P_r} \sum_{l \in L} t_{OC}^{p} \cdot o_r^{pl} \geq t_r \quad \forall r \in R \tag{5.3}$$

For a connection request r, multiple lightpaths $\langle p, l \rangle$ can be established to serve it. Constraint (5.3) ensures that the sum of the traffic volumes carried by the established lightpaths (i.e., the left-hand side) is no smaller than the required traffic volume for connection request r (t_r).

$$F_{max} \cdot x_r^{pl} \geq F_{OC} \cdot o_r^{pl} \quad \forall r \in R, p \in P_r, l \in L_{NW} \tag{5.4}$$

Constraint (5.4) ensures that x_r^{pl} is equal to 1 if there is at least one OC assigned to lightpath $\langle p, l \rangle$ to serve connection request r ($o_r^{pl} \geq 1$) and is equal to 0 if no OC has been assigned ($o_r^{pl} = 0$).

$$\beta_r^{pl} = \alpha_r^{pl} + F_{OC} \cdot o_r^{pl} - x_r^{pl} \quad \forall r \in R, p \in P_r, l \in L_W \tag{5.5}$$

Constraint (5.5) ensures the relationship between the starting and ending indices of the assigned FSs.

$$f_{max} \cdot x_r^{pl} \geq \beta_r^{pl} \quad \forall r \in R, p \in P_r, l \in L_W \tag{5.6}$$

Constraint (5.6) ensures that if lightpath $\langle p, l \rangle$ is established to serve connection request r ($x_r^{pl} = 1$), then the ending index of the FSs assigned to the lightpath (β_r^{pl}) is no greater than the maximum index of the FSs (f_{max}).

$$|R| \cdot k \cdot u^l \geq \sum_{r \in R} \sum_{p \in P_r} x_r^{pl} \quad \forall l \in L \tag{5.7}$$

Constraint (5.7) ensures that u^l is equal to 1 if SL l has been assigned to establish at least one lightpath.

$$F_{max} \cdot (1 - x_r^{pl}) \geq F_{OC} \cdot o_{r'}^{p'l}$$
$$\forall r, r' \in R, p \in P_r, p' \in P_{r'}, l \in L_{NW} : p \neq p', p \bigcap p' \neq \emptyset \qquad (5.8)$$

Constraint (5.8) ensures that if lightpath $\langle p, l \rangle$ is established to serve connection request r ($x_r^{pl} = 1$) and SL l belongs to L_{NW}, then SL l cannot be used to establish another lightpath $\langle p', l \rangle$ ($o_{r'}^{p'l} = 0$) that has one or more common links with routing path p ($p \bigcap p' \neq \emptyset$) for connection request r'. Note that this constraint applies only when $p \neq p'$. If this is not the case ($p = p'$), then these two lightpaths can be established on the same routing path p and SL l by composing an SCh of Type II (refer to the following Constraint (5.9)).

$$F_{max} \geq F_{OC} \cdot \sum_{r \in R_{np}} o_r^{pl} \quad \forall np \in NP, p \in P_{np}, l \in L_{NW} \qquad (5.9)$$

Constraint (5.9) indicates that for connection requests with the same source-destination pair ($r \in R_{np}$), they can be transmitted by lightpaths that share a common routing path $p \in P_{np}$ and SL $l \in L_{NW}$, composing an SCh of Type II.

$$\theta_{rr'}^{pp'l} + \theta_{r'r}^{p'pl} = 1$$
$$\forall r, r' \in R, p \in P_r, p' \in P_{r'}, l \in L_W : p \bigcap p' \neq \emptyset \qquad (5.10)$$
$$\alpha_{r'}^{p'l} + F_{max} \cdot (1 - \theta_{rr'}^{pp'l}) \geq \beta_r^{pl} + x_r^{pl}$$
$$\forall r, r' \in R, p \in P_r, p' \in P_{r'}, l \in L_W : p = p', p \bigcap p' \neq \emptyset \qquad (5.11)$$
$$\alpha_{r'}^{p'l} + (F_{max} + F_{GB}) \cdot (1 - \theta_{rr'}^{pp'l}) \geq \beta_r^{pl} + (F_{GB} + 1) \cdot x_r^{pl}$$
$$\forall r, r' \in R, p \in P_r, p' \in P_{r'}, l \in L_W : p \neq p', p \bigcap p' \neq \emptyset \qquad (5.12)$$

Constraints (5.10) ~ (5.12) ensure spectrum contiguity and spectrum nonoverlap – the requirement of spectrum continuity is naturally satisfied – for the lightpaths passing through SLs with wavelength switching support ($l \in L_W$). Since these are general constraints that

have been widely applied in many previous works focusing on the static network optimization problem in optical networks [29], we will not explain them in detail. However, it should be noted that two lightpaths established between the same source-destination pair can be allocated without a wavelength switching GB in the case that their routing paths and SLs are the same (i.e., Constraint (5.11)).

$$F_{max} \cdot u^l \geq \sum_{r \in R} \sum_{p \in P_r : e \in p} F_{OC} \cdot o_r^{pl} \quad \forall e \in E, l \in L \tag{5.13}$$

Constraint (5.13) is a redundant constraint. For each SL l and link e, this constraint stipulates that the total number of FSs assigned to the lightpaths that traverse them should be no greater than F_{max}. As seen from the results of our simulation experiments, this constraint is able to significantly improve the convergence rate of the ILP model.

5.4 Heuristic algorithm for solving the RSCSA problem

In this section, we propose a heuristic algorithm to solve the static RSCSA problem. First, we introduce two tables and a function used in the heuristic algorithm, as follows:

- We define a table $T_{SCh\text{-}II}$. Each entry $\langle np\text{:}\ p,\ l,\ B \rangle$ in this table records an SCh established between node pair np passing through routing path p and SL l, where the spectrum on this SCh is currently not fully used – B represents the remaining available spectrum on this SCh. In the heuristic algorithm, the connection requests are assigned resources one by one. Therefore, the remaining available spectrum on an SCh recorded in $T_{SCh\text{-}II}$ is expected to be assigned to subsequent connection requests with the same source-destination pair (i.e., between the same np) to compose an SCh of Type II.

- We also define a table $T_{SCh\text{-}III}$. Each entry $\langle r : t_{rem}^r \rangle$ in this table records the currently unsatisfied traffic volume t_{rem}^r for connection request r. The unsatisfied traffic volumes of the connection requests recorded in $T_{SCh\text{-}III}$ are expected to be served by SChs of Type III.

- We define a function named *First-Fit SL Allocation (FF-SLA)*. This function takes a routing path p as input and determines the available SL with the lowest index along p (denoted by l_{FF}^p). In this paper, we assume that the indices of SLs without wavelength switching support (i.e., $l \in L_{NW}$) are lower than those of SLs with wavelength switching support (i.e., $l \in L_W$). The output of this function is $\langle p, l_{FF}^p \rangle$.

The heuristic algorithm is divided into three parts, and we will explain each of them individually. To facilitate readers' understanding, we present a simple illustration from Fig. 5.2 to Fig. 5.10. We consider a 6-node network with 4 SLs (per link), of which only one, SL-4, supports wavelength switching. For simplicity, we assume that each SL has 4 THz of available spectrum and supports 8 Tbps of traffic volume regardless of the path length (i.e., without considering adaptive modulation). Then, we consider a set of connection requests $R = \{r_1, r_2, \cdots, r_7\}$. These connection requests belong to different sets R_{np}: $R_{np_{16}} = \{r_1, r_2, r_3\}$, $R_{np_{26}} = \{r_4\}$, $R_{np_{24}} = \{r_5, r_6\}$, and $R_{np_{36}} = \{r_7\}$. The connection requests will be assigned resources one by one following a specified service sequence R_{seq}.

5.4.1 Assignment for SChs of Type I and Type II

Initially, we attempt to assign SChs of Type I and Type II for all connection requests. Fig. 5.2 shows the arrival of the first connection request, $r_1 = \langle 1, 6, 10 \text{ Tbps} \rangle$. According to the output of the *FF-SLA* function, SL-1 and routing path ⟨1-3-4-6⟩, with the shortest distance, are first selected to establish an SCh of Type I with support for 8 Tbps of traffic volume. However, 2 Tbps of the traffic volume of the request still needs to be satisfied. Therefore, by running the *FF-SLA* function again, SL-1 and routing path ⟨1-2-5-6⟩ are additionally selected, and another SCh is established. Since the spectrum available on this SCh is not fully used, the entry $\langle np_{16}$: 1-2-5-6, SL-1, 3 THz⟩ is appended to $T_{SCh\text{-}II}$. The remaining 3 THz of spectrum is expected to be assigned to the subsequent connection requests r_2 and r_3, which belong to the same $R_{np_{16}}$ as r_1, to compose an SCh of Type II. Then, we remove r_1 from $R_{np_{16}}$.

Subsequently, a connection request $r_2 = \langle 1, 6, 6 \text{ Tbps} \rangle$ arrives, as shown in Fig. 5.3. The remaining available spectrum on the SCh recorded in $T_{SCh\text{-}II}$ has the highest priority for assignment to subsequent connection requests. Therefore, we first check whether there is an SCh between np_{16} that is not fully used recorded in $T_{SCh\text{-}II}$. In this case, it is obvious that r_2 can be transmitted using the remaining 3 THz of spectrum on the SCh recorded in $T_{SCh\text{-}II}$ above by composing an SCh of Type II. Since this SCh is fully used after being assigned to r_2, the corresponding entry is removed from $T_{SCh\text{-}II}$. Finally, we remove r_2 from $R_{np_{16}}$.

Then, a connection request $r_3 = \langle 1, 6, 10 \text{ Tbps} \rangle$ arrives, as shown in Fig. 5.4. We call the *FF-SLA* function because there is no SCh between np_{16} recorded in $T_{SCh\text{-}II}$ at this time. Thus, SL-2 and routing path ⟨1-3-4-6⟩ are selected to establish an SCh of Type I. Similar to the case of r_1, 2 Tbps of the traffic volume of the request remains to be satisfied. However, we will not establish another not fully used SCh in this case because if we were to establish such an SCh (represented by the red dotted line), its remaining available spectrum

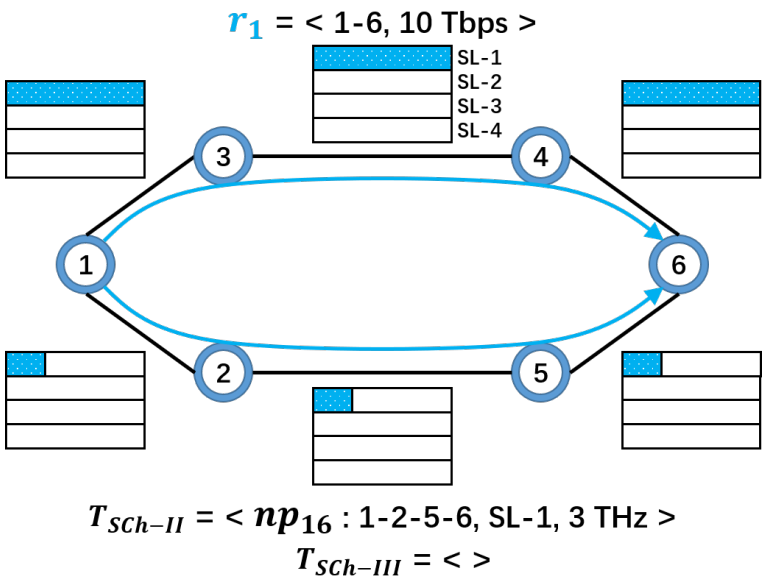

Figure 5.2: Illustration of the proposed heuristic algorithm for the assignment of connection request r_1

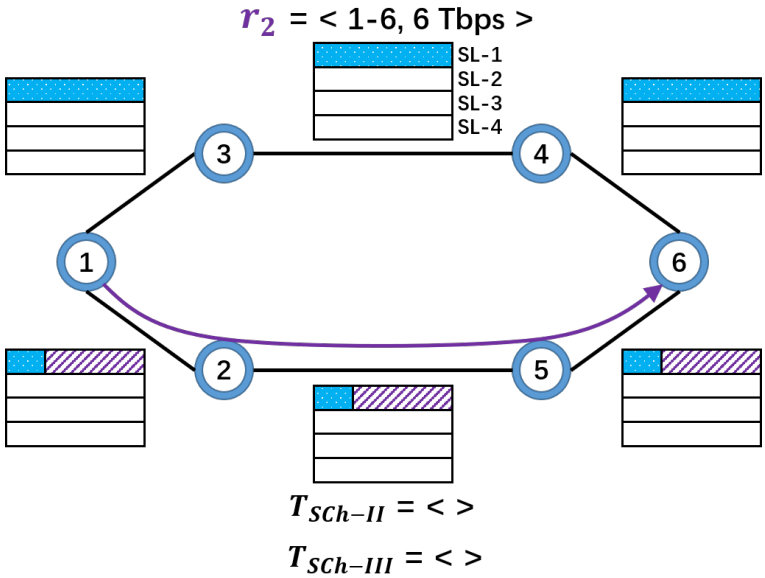

Figure 5.3: Illustration of the proposed heuristic algorithm for the assignment of connection request r_2

would have no chance to be used because no subsequent connection request exists between np_{16}, and this would result in a waste of spectrum on this SCh. Instead, an entry $\langle r_3$: 2 Tbps$\rangle$ is appended to $T_{SCh\text{-}III}$. The unsatisfied 2 Tbps of traffic volume for r_3 is expected to be served by an SCh of Type III – sharing the spectrum with other connection requests between different source-destination pairs.

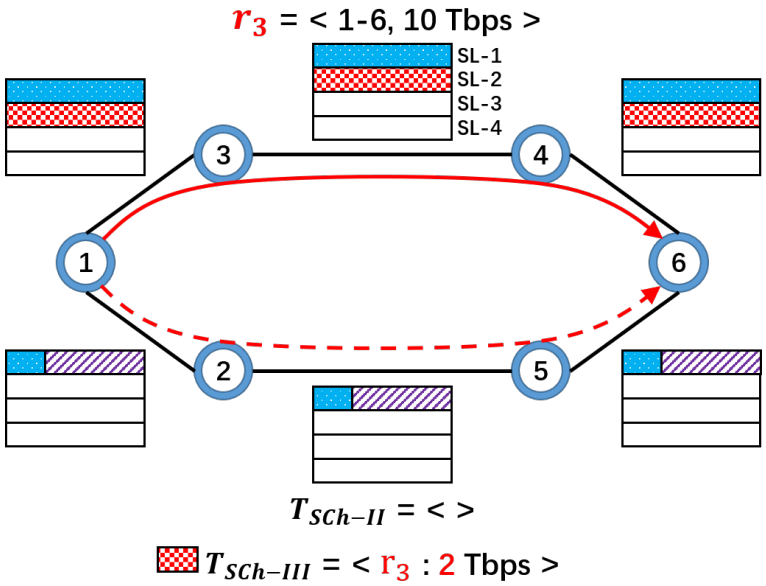

Figure 5.4: Illustration of the proposed heuristic algorithm for the assignment of connection request r_3

The procedures described above will be repeated for the remaining connection request r_4, r_5, r_6, r_7 as shown in Fig. 5.5 ~ Fig. 5.8 in this example. Notably, SChs of Type I and Type II will not result in any spectrum fragmentation and offer wavelength switching GB savings compared to SChs of Type III. Therefore, SChs of Type I and Type II always have a higher priority for establishment than SChs of Type III. Consequently, although it is preferable to use SLs without wavelength switching support (i.e., $l \in L_{NW}$) when establishing SChs of Type I and Type II (this is the reason why lower indices are assigned to the SLs without wavelength switching), SLs with wavelength switching support (i.e., $l \in L_W$) are also allowed to be used if the available SLs without wavelength switching support are inadequate (see, for example, the assignment of r_7 in Fig. 5.8). The pseudocode for this part of the algorithm is shown in Algorithm 1.

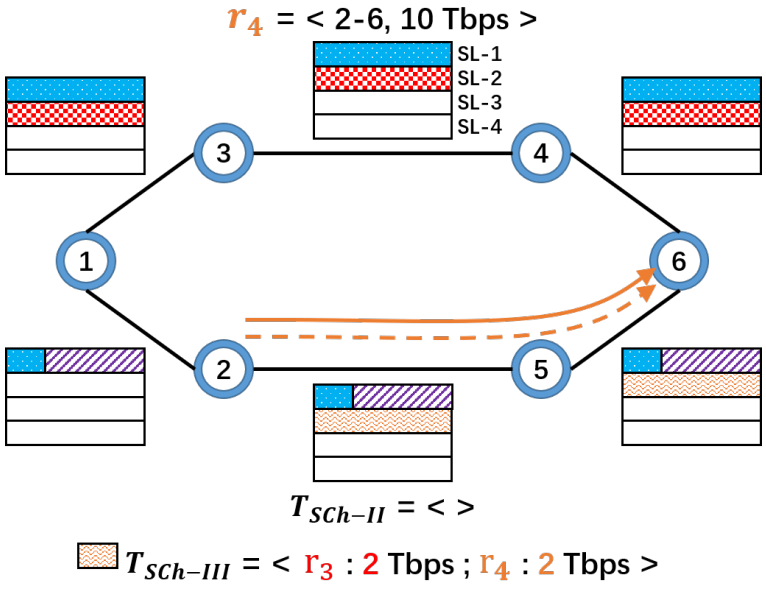

Figure 5.5: Illustration of the proposed heuristic algorithm for the assignment of connection request r_4

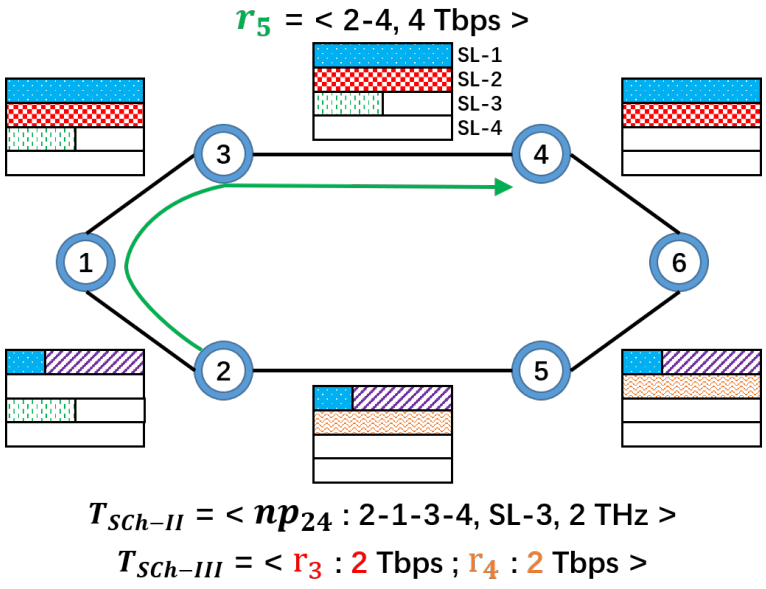

Figure 5.6: Illustration of the proposed heuristic algorithm for the assignment of connection request r_5

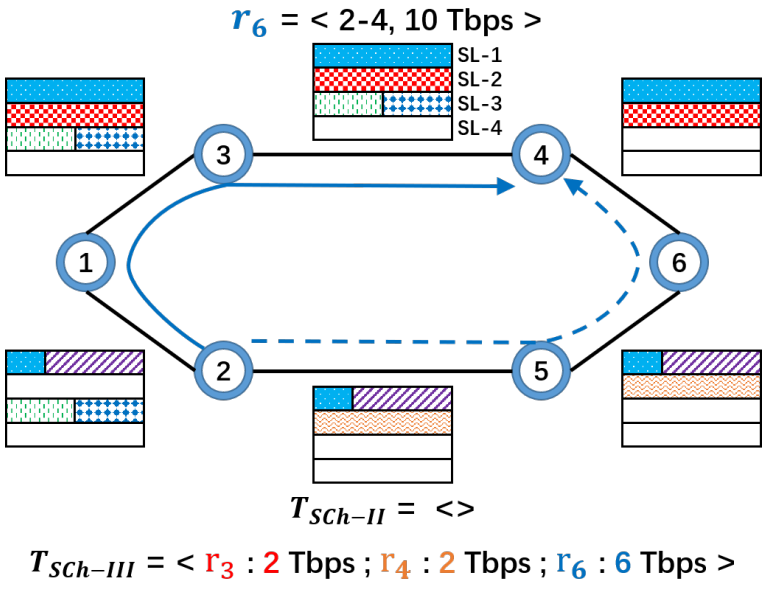

Figure 5.7: Illustration of the proposed heuristic algorithm for the assignment of connection request r_6

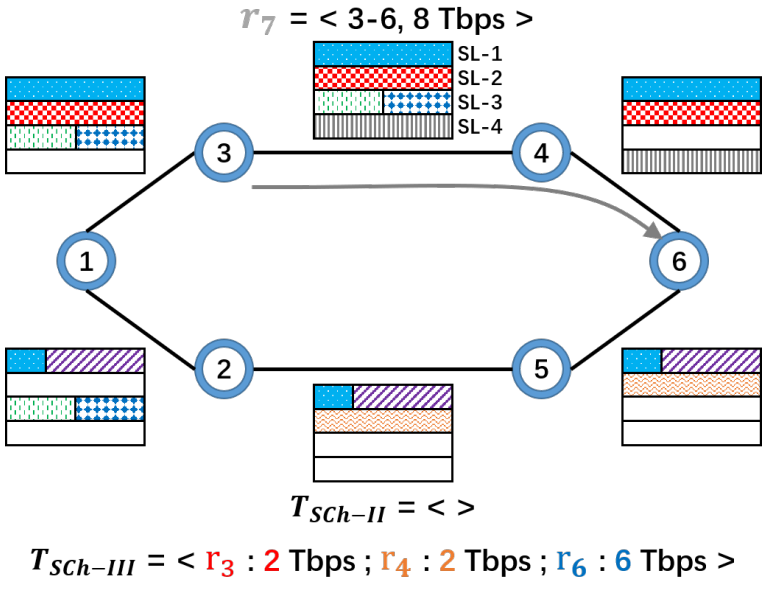

Figure 5.8: Illustration of the proposed heuristic algorithm for the assignment of connection request r_7

Algorithm 1 Assignment for SChs of Type I and Type II

Input: R_{seq}, R_{np} for each $np \in NP$
Output: $T_{SCh\text{-}III}$

1: Create new tables: $T_{SCh\text{-}II}$ and $T_{SCh\text{-}III}$.
2: **for** each $r = \langle s, d, t \rangle \in R_{seq}$ **do**
3: Remove r from $R_{np_{sd}}$.
4: **if** an SCh for $\langle np_{sd}\text{: } p, l, B \rangle$ is recorded in $T_{SCh\text{-}II}$ **then**
5: $t_p \leftarrow$ calculate the supportable traffic volume on the SCh based on the highest feasible modulation format m_p for routing path p and the remaining available spectrum B.
6: **if** $t_p > t$ **then**
7: Assign routing path p, SL l, and the required spectrum to r – create a (not fully used) SCh of Type II.
8: $t \leftarrow 0$
9: $B \leftarrow B$ minus the required spectrum for r.
10: Go to the next connection request (line 2).
11: **else**
12: Assign routing path p, SL l, and the remaining available spectrum B to r – create an SCh of Type II.
13: $t \leftarrow t - t_p$.
14: Remove $\langle np_{sd}\text{: } p, l, B \rangle$ from $T_{SCh\text{-}II}$.
15: **end if**
16: **end if**
17: **while** $t > 0$ **do**
18: $\langle best\text{-}p_r, best\text{-}l_r \rangle \leftarrow$ call the *FF-SLA* function for each candidate path $p_r \in P_r$ and select the one with the smallest $l_{FF}^{p_r}$.
19: $t_{best\text{-}p_r} \leftarrow$ calculate the supportable traffic volume on routing path $best\text{-}p_r$ and SL $best\text{-}l_r$ based on the highest feasible modulation format for $best\text{-}p_r$.
20: **if** $t_{best\text{-}p_r} > t$ **then**
21: **if** $R_{np_{sd}}$ is not an empty set **then**
22: Assign routing path $best\text{-}p_r$, SL $best\text{-}l_r$, and the required spectrum to r – create a (not fully used) SCh.
23: $B_{rem} \leftarrow$ calculate the remaining available spectrum of the SCh.
24: Append $\langle np_{sd}\text{: } best\text{-}p_r, best\text{-}l_r, B_{rem} \rangle$ to $T_{SCh\text{-}II}$.
25: **else**
26: Append $\langle r\text{: } t \rangle$ to $T_{SCh\text{-}III}$.
27: **end if**
28: $t \leftarrow 0$
29: **else**
30: Assign routing path $best\text{-}p_r$, SL $best\text{-}l_r$, and the entire C-band spectrum to r – create an SCh of Type I.
31: $t \leftarrow t - t_{best\text{-}p_r}$.
32: **end if**
33: **end while**
34: **end for**
35: **return** $T_{SCh\text{-}III}$

5.4.2 Reassignment for SChs of Type I and Type II

Using Algorithm 1, we have assigned SChs of Type I and Type II to each connection request and obtained a table containing a set of connection requests with currently unsatisfied traffic volumes (i.e., $T_{SCh\text{-}III}$), which are expected to be served by SChs of Type III. Here, $l^{max}_{NW\text{-}A1}$ denotes the maximum index of the currently used/required SLs without wavelength switching support (i.e., the number of such SLs) in the network after the execution of Algorithm 1. It is obvious that $l^{max}_{NW\text{-}A1}$ SLs without wavelength switching support may not be used on every link. For example, as shown in Fig. 5.8, $l^{max}_{NW\text{-}A1}$ is equal to 3, but only 2 SLs are used on link 2-5. Note that these unused SLs (e.g., SL-3 on link 2-5) cannot be used to establish SChs of Type III hereafter because they do not support wavelength switching. Therefore, before we assign SChs of Type III to the connection requests recorded in $T_{SCh\text{-}III}$, we will first attempt to assign them one by one – starting from the one with the largest unsatisfied traffic volume – to the unused SLs whose indices are smaller than $l^{max}_{NW\text{-}A1}$. As shown in Fig. 5.9, the connection request r_6 can be successfully assigned to pass through routing path $\langle$2-5-6-4$\rangle$, although this will result in a certain degree of spectrum wastage. Then, we remove $\langle r_6$: 6 Tbps$\rangle$ from $T_{SCh\text{-}III}$. In this way, we can somewhat reduce the number of entries in $T_{SCh\text{-}III}$, thus making it possible to use fewer SLs with wavelength switching support hereafter. Such an assignment will not result in any negative effect on the optimization objective(s) because the (main) objective of the RSCSA problem is to minimize the number of SLs that are used/required in the network, not to minimize their sum over all links.

The pseudocode for this part of the algorithm is shown in Algorithm 2. The inputs to Algorithm 2 are $T_{SCh\text{-}III}$ and $l^{max}_{NW\text{-}A1}$, which are obtained after the execution of Algorithm 1. The output of Algorithm 2 is the modified $T_{SCh\text{-}III}$, in which the number of entries may be reduced.

5.4.3 Assignment for SChs of Type III

Finally, we begin to assign resources to the unsatisfied connection requests that are still recorded in $T_{SCh\text{-}III}$ after Algorithm 2 has been executed. Similar to the approach that has been widely applied to the previous RSA and RSSA problems, each connection request will be assigned using the *First-Fit Spectrum Allocation (FF-SA)* function [6], as shown in Fig. 5.10. The pseudocode for this part of the algorithm is shown in Algorithm 3, where l^{min}_{W} and l^{max}_{W} represent the minimum and maximum indices, respectively, of SLs with wavelength switching support (i.e., $l \in L_W$). As stated before, the indices of the SLs with wavelength switching support are lower than those of the SLs without wavelength

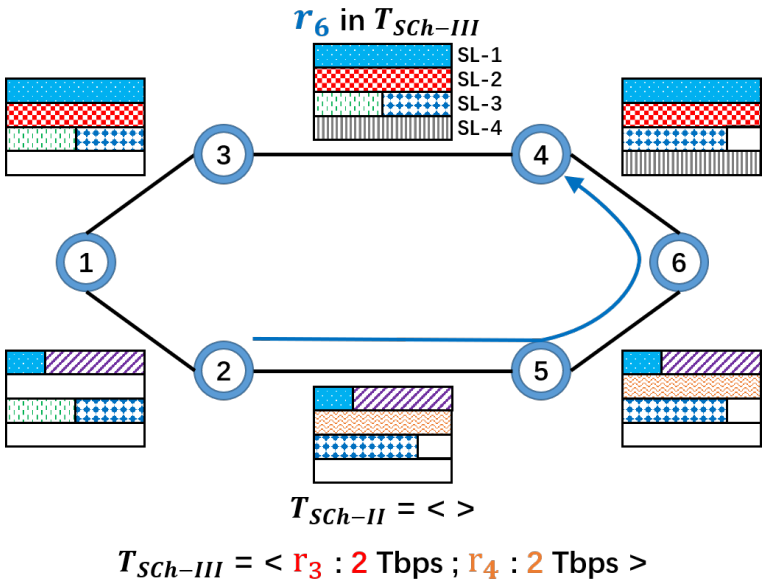

Figure 5.9: Illustration of the proposed heuristic algorithm for the assignment of connection request r_8

Algorithm 2 Reassignment for SChs of Type I and Type II

Input: $T_{SCh\text{-}III}$, $l^{max}_{NW\text{-}A1}$
Output: $T_{SCh\text{-}III}$

1: Sort $T_{SCh\text{-}III}$ by t^r_{rem}, from largest to smallest.
2: **for** each $\langle r : t^r_{rem} \rangle$ in $T_{SCh\text{-}III}$ **do**
3: **while** TRUE **do**
4: $\langle best\text{-}p_r, best\text{-}l_r \rangle \leftarrow$ call the *FF-SLA* function for each candidate path $p_r \in P_r$, and select the one with the smallest $l^{p_r}_{FF}$.
5: **if** $best\text{-}l_r \leq l^{max}_{NW-A1}$ **then**
6: $t_{best\text{-}p_r} \leftarrow$ calculate the supportable traffic volume on routing path $best\text{-}p_r$ and SL $best\text{-}l_r$ based on the highest feasible modulation format for $best\text{-}p_r$.
7: **if** $t_{best\text{-}p_r} > t^r_{rem}$ **then**
8: Assign routing path $best\text{-}p_r$, SL $best\text{-}l_r$, and the required spectrum to r – create a (not fully used) SCh of Type I.
9: Remove $\langle r : t^r_{rem} \rangle$ from $T_{SCh\text{-}III}$.
10: **break while** - go to the next connection request (line 2).
11: **else**
12: Assign routing path $best\text{-}p_r$, SL $best\text{-}l_r$, and the entire C-band spectrum to r – create an SCh of Type I.
13: $t^r_{rem} \leftarrow t^r_{rem} - t_{best\text{-}p_r}$.
14: **end if**
15: **else**
16: **break while** - go to the next connection request (line 2).
17: **end if**
18: **end while**
19: **end for**

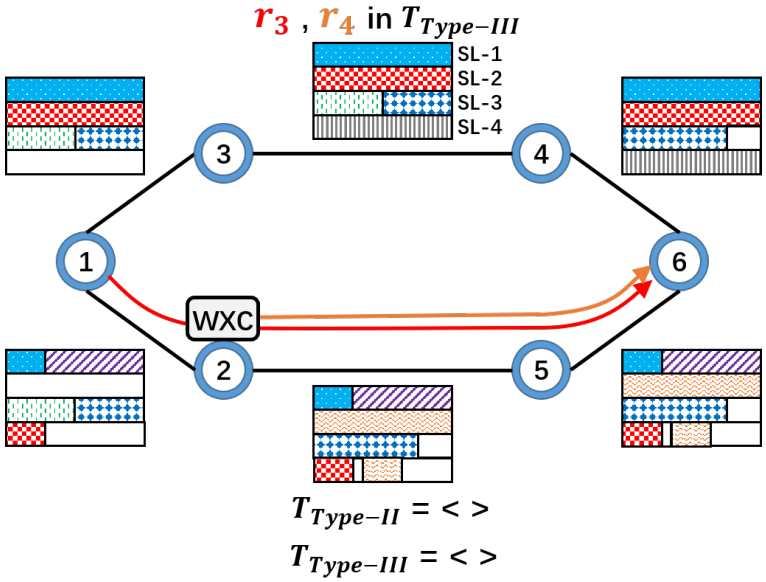

Figure 5.10: Illustration of the proposed heuristic algorithm for the assignment of connection request r_9

Algorithm 3 Assignment for SChs of Type III

Input: $T_{SCh\text{-}III}$
Output: $T_{SCh\text{-}III}$
1: $l_W^{current} \leftarrow l_W^{min}$
2: Sort $T_{SCh\text{-}III}$ by t_{rem}^r, from largest to smallest.
3: **while** $l_W^{current} \leq l_W^{max}$ **and** $T_{SCh\text{-}III}$ is not empty **do**
4: **for** each $\langle r : t_{rem}^r \rangle$ in $T_{SCh\text{-}III}$ **do**
5: *best-*$p_r \leftarrow$ apply the *FF-SA* function [6] for each candidate path $p_r \in P_r$ on SL $l_W^{current}$ and select the one with the lowest ending index of FSs.
6: **if** *best-*$p_r \neq$ None **then**
7: Assign routing path *best-*p_r, $l_W^{current}$, and the required FSs as obtained by the *FF-SA* function to r.
8: Remove $\langle r : t_{rem}^r \rangle$ from $T_{SCh\text{-}III}$.
9: **end if**
10: **end for**
11: $l_W^{current} \leftarrow l_W^{current} + 1$
12: **end while**
13: **if** $T_{SCh\text{-}III}$ is not empty **then**
14: Call Algorithm 2 again while allowing *best-*$l_r > l_{NW\text{-}A1}^{max}$ in line 5.
15: **end if**

switching support (i.e., $l \in L_{NW}$). Therefore, l_W^{min} and l_W^{max} are actually equal to $|L_{NW}| + 1$ and $|L|$, respectively.

Notably, we may not be able to successfully serve all unsatisfied connection requests recorded in $T_{SCh\text{-}III}$ if the available SLs with wavelength switching support are inadequate. In this case, we will call Algorithm 2 again, now allowing the use of SLs with indices greater than $l_{NW\text{-}A1}^{max}$ (i.e., removing line 5 and the corresponding lines 15 ~ 17 from Algorithm 2).

5.5 Simulations and performance evaluations

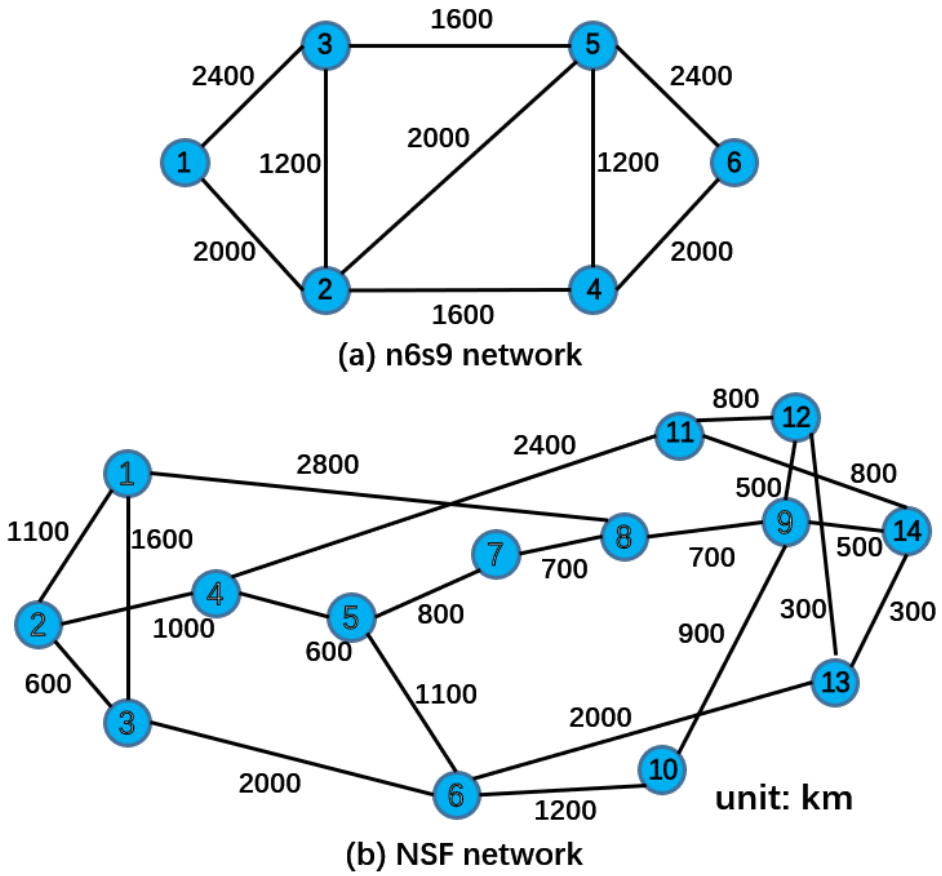

Figure 5.11: Network topologies: (a) the simple 6-node, 18-directed-link n6s9 network; (b) the realistic 14-node, 42-directed-link NSF network.

In this section, we evaluate the performance of the proposed ILP model and heuristic algorithm based on two network topologies: i) the simple 6-node, 18-directed-link n6s9 network, as shown in Fig. 5.11. (a), and ii) the realistic 14-node, 42-directed-link NSF

network, as shown in Fig. 5.11. (b) [146]. We consider that the networks are connected by a bundle of weakly coupled 4-core MCFs, as proposed in Ref. [114], for the following reasons:

- Full compatibility with conventional SMF systems while maintaining a 125 μm cladding diameter.
- Ultralow inter-core crosstalk, enabling ultralong-haul all-optical transmission without the need for costly and complex MIMO DSPs.
- Significant cost savings when combined with the application of cladding-pumped multi-core erbium-doped fiber amplifiers (MC-EDFAs) [42, 147].

The physical features of the considered 4-core MCFs are listed in Table 5.1, where k, r, β and Λ represent the coupling coefficient, bend radius, propagation constant, and core pitch, respectively. Note that other SDM fibers with different physical features, whose physical entities are single-mode cores, can be employed as well. These physical features of the SDM fibers will be used hereafter to calculate the transmission reaches for various modulation formats; note that the application of different SDM fibers may lead to different transmission reaches.

Table 5.1: Physical features of the 4-core MCFs considered in the simulation experiments.

Fiber type	k	Λ [m]	β [1/m]	r [m]
4-core MCF [114]	5.0×10^{-4}	3.9×10^{-5}	4×10^{6}	5×10^{-2}

We assume that the total spectrum per core of a 4-core MCF is 4 THz (C-band), that is, 320 FSs conforming to the ITU-T 12.5 GHz grid [93]. Each subtransceiver operates at a fixed baud rate of 32 Gbaud, supporting an OC that occupies 37.5 GHz (i.e., 3 FSs) [32]. In addition, a spectrum occupation of 12.5 GHz (i.e., 1 FS) is assumed for each wavelength switching GB. We consider four modulation formats in the simulation experiments, namely, (DP) BPSK, QPSK, 8-QAM, and 16-QAM, which support bit rates of 50, 100, 150, and 200 Gbps per OC, respectively.

Regarding the transmission reaches of the considered modulation formats, we consider them to be mainly bounded by two factors: i) the optical signal-to-noise ratio (OSNR) and ii) the inter-core crosstalk (XT) of the MCFs. According to Ref. [32], in coherent systems, the bounds on the transmission reaches due to the OSNR for different modulation formats can be estimated using the Gaussian noise model of nonlinear interference. Moreover, according to Refs. [148] and [50], the statistical mean XT of an MCF after L km transmission can be calculated as follows:

$$XT(L) = \frac{n - n \cdot exp\{-(n+1)2hL\}}{1 + n \cdot exp\{-(n+1)2hL\}} \quad \text{where } h = \frac{2k^2 r}{\beta \Lambda} \tag{5.14}$$

In Eq. (5.14), n represents the number of cores adjacent to the target core. According to Ref. [58], the XT thresholds (XT_{th}^{m}) for BPSK, QPSK, 8-QAM, and 16-QAM are -14, -18.5, -21, and -25 dB, respectively. We consider that a -2 dB margin (XT_{marg}) is required for the XT fluctuation [31]. Therefore, for a given modulation format m, the bound on the transmission reach due to the XT (L_{XT}^{m}) can be calculated as follows:

$$L_{XT}^{m} = \max\{L \in \mathbb{Z}^{+} \mid XT(L) \leq XT_{th}^{m} + XT_{marg}\} \tag{5.15}$$

Consequently, as shown in Table 5.2, the final transmission reaches of the 4-core MCFs considered in the simulation experiments for BPSK, QPSK, 8-QAM, and 16-QAM are all bounded by the OSNR and are 6300, 3500, 1200, and 600 km, respectively.

Table 5.2: Transmission reach bounds due to the OSNR and XT for 4-core MCFs under different modulation formats m.

Limiting factor	Transmission reach [km]			
	BPSK	QPSK	8-QAM	16-QAM
OSNR [32]	6300	3500	1200	600
XT	38945	13872	7808	3111

Moreover, three candidate shortest routing paths ($k = 3$) are considered for each connection request. To compare the network performance of SDM-based EONs and SCNs, we consider three different OXCs, as follows:

- The first is the conventional OXC applied in SDM-based EONs, which is implemented using stacked WXCs as the basic solution to achieve SDM. In such an OXC, wavelength switching is supported on each SL – i.e., $L_W = L$ and $L_{NW} = \emptyset$.
- The second is an HOXC (i.e., SXC+WXC) proposed for SCNs, which is implemented using CSSs as shown in Fig. 2.11. We assume that in such an HOXC, one-ninth of the SLs support wavelength switching, in accordance with the assumptions proposed in Ref. [28]. That is, $|L_W| = \lceil \frac{|L|}{9} \rceil$ and $L_{NW} = L - L_W$.

- The last is an OXC that does not support wavelength switching on any of its SLs. In such an OXC, only SXCs are deployed at intermediate nodes – i.e., $L_W = \emptyset$ and $L_{NW} = L$.

Finally, all simulation experiments were performed in a Microsoft Windows 10 environment using a computer with an AMD Ryzen 6-core 3.6 GHz CPU and 16 GB of memory.

5.5.1 Simulation experiments involving the simple n6s9 network

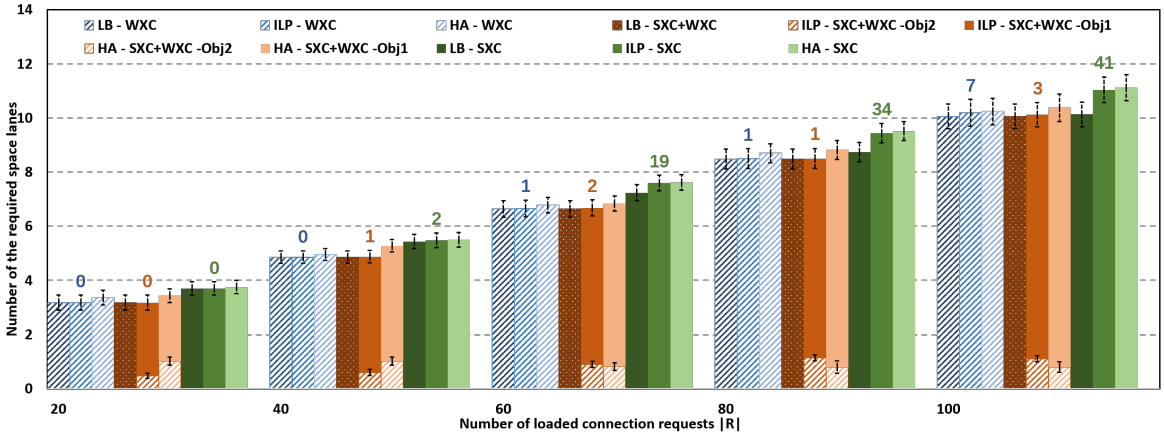

Figure 5.12: Simulation results for the simple 6-node, 18-link n6s9 network.

In these simulation experiments, we considered the simple, small-scale n6s9 network with 20 SLs (i.e., one bundle of five 4-core MCFs per link). Therefore, in the HOXC case, the set of SLs with wavelength switching support, L_W, was $\{18, 19, 20\}$. We considered different numbers of connection requests ranging from 20 to 100 (in increments of 20), representing different traffic loads. Specifically, the total average traffic volumes with which the network was loaded ranged from 0.11 to 0.55 Pbps. For each traffic load, we randomly generated 50 different traffic matrices R. Considering that current traffic volumes are expected to increase by 10× in the future (by 2024) [12,28], for each unidirectional connection request in R, the traffic volume was randomly selected from among traffic profiles of $\{1$ Tbps, 4 Tbps, 10 Tbps$\}$ with probabilities of $\{0.3, 0.3, 0.4\}$ [34, 115, 141, 149, 150].

To solve the ILP model, we used the optimization software *GUROBI v8.0.1* [151]. Since the RSCSA problem is an NP-hard problem, as proven in Chapter 1, it may not be possible to completely solve the ILP model within a reasonable amount of time for certain input matrices and/or traffic loads. Therefore, we bounded the running time of the ILP model

to 1 hour for the main objective and 300 seconds for the minor objective. Moreover, the solutions given by the heuristic algorithm were input into the ILP model as initial solutions to improve the convergence rate.

The simulation results, including the average values of the objective(s) and the 95% confidence intervals (*T-distribution*), are shown in Fig. 5.12. The abbreviations 'LB', 'ILP', and 'HA' in Fig. 5.12 represent the lower bound of the RSCSA problem given by the '*Best-Bound*' of *GUROBI*, the optimal or current feasible solution obtained by solving the ILP model with a 1-hour running time limit, and the solution obtained using the heuristic algorithm with 1000 iterations of R_{seq}, respectively. The abbreviations 'WXC', 'SXC+WXC', and 'SXC' represent the three OXCs introduced above, that is, the OXC with full wavelength switching support (i.e., $L_W = L$) for SDM-based EONs, the HOXC with partial wavelength switching support (i.e., $|L_W| = 3$) for SCNs, and the OXC without wavelength switching support (i.e., $L_W = \emptyset$), respectively. Moreover, the number over the data bar represents the number of input matrices R for which the corresponding ILP models did not yield optimal solutions within 1 hour.

From Fig. 5.12, we can see that even though only approximately one-ninth of the SLs support wavelength switching in the HOXC case, the results of 'ILP - SXC+WXC' and 'ILP - WXC' are the same, while negligible gaps (within 2.4%) exist between the results of 'HA - SXC+WXC' and 'HA - WXC'. Moreover, as we can see from the results of 'ILP - SXC+WXC - Obj2' and 'HA - SXC+WXC - Obj2', the average numbers of used/required SLs with wavelength switching support for the solutions obtained using both the ILP model and the heuristic algorithm are less than 1.2 for all traffic loads in the HOXC case. These observations indicate that the conventional OXC with full wavelength switching support offers no remarkable advantages for future connection requests with large traffic volumes (e.g., several or dozens of Tbps) – or, equivalently, for multiple connection requests between the same source-destination pair with smaller traffic volumes typical of current network traffic that are groomed into a single connection request with a larger traffic volume. Moreover, according to the cost assessments presented in Refs. [113] and [28], for the network with 20 SLs considered in these simulation experiments, the cost of either a full-size CSS-based HOXC or a sub-CSS-based HOXC (see Fig. 2.11. (a)) designed for SCNs is only 25% of that of a conventional OXC with full wavelength switching support designed for SDM-based EONs. Therefore, full wavelength switching support may no longer be necessary for the future massive SDM era.

In contrast, relatively large gaps, ranging from 8% to 14%, can be observed between the results for OXCs without wavelength switching support (i.e., 'SXC') and those for the above two (H)OXC cases with full/partial wavelength switching support. These findings in-

dicate that completely removing wavelength switching support from the intermediate nodes will result in some loss of network performance. However, a low cost savings (compared with the great cost savings between 'WXC' and 'SXC+WXC') can be achieved, as well. The trade-off decision should be made by the network operators.

Moreover, we can observe that the 'ILP' and 'HA' results are very similar in all cases. For the two (H)OXC cases with full/partial wavelength switching support (i.e., 'WXC' and 'SXC+WXC'), the ILP model can be completely solved within 1 hour for all or the majority of the input matrices R, depending on the traffic loads, and the results of both 'ILP' and 'HA' are close to the lower bounds of the problem. For the OXC case without wavelength switching support (i.e., 'SXC'), the ILP model becomes difficult to solve within 1 hour if the traffic load is heavy. In this case, the gaps between the 'HA' results and the lower bounds range from 1.1% to 8.8%, while those between the 'ILP' results and the lower bounds range from 0.7% to 8.2%, which are considered acceptable.

Table 5.3: Average running times of the proposed heuristic algorithm with 1000 iterations for the simple n6s9 network

OXC Architecture	Traffic load $\|R\|$				
	20	40	60	80	100
WXC	11.95	14.03	15.81	17.06	18.49
SXC+WXC	3.98	4.09	4.44	4.20	4.64
SXC	0.67	1.05	1.43	1.79	2.17

Table 5.3 lists the average running times (in seconds) of the heuristic algorithm with 1000 iterations (on a single thread) for the simple n6s9 network. We can see that the running times of the heuristic algorithm in the conventional OXC case with full wavelength switching are much longer than those in the HOXC case with partial wavelength switching, and the shortest running times are incurred in the OXC case without wavelength switching. The reason for this observation is that finding a set of continuous and contiguous FSs with the lowest ending index along a routing path by means of the *FF-SA* function is much more difficult than finding a feasible SL with the lowest index along a routing path by means of the *FF-SLA* function. Therefore, in the conventional OXC case with full wavelength switching, the *FF-SA* function will be called more times – for each SL with wavelength switching support until all connection requests have been served – by the heuristic algorithm, resulting in a longer running time. In contrast, in the OXC case without wavelength switching, the heuristic algorithm will not call the *FF-SA* function even once, since there are no SLs that support wavelength switching, resulting in the shortest running time.

In summary, the simulation results show that the proposed ILP model (with a 1-hour

running time limit) and heuristic algorithm both work well for small-scale problem instances, for which the optimal solutions or solutions close to the lower bounds can be obtained.

5.5.2 Simulation experiments involving the realistic NSF network

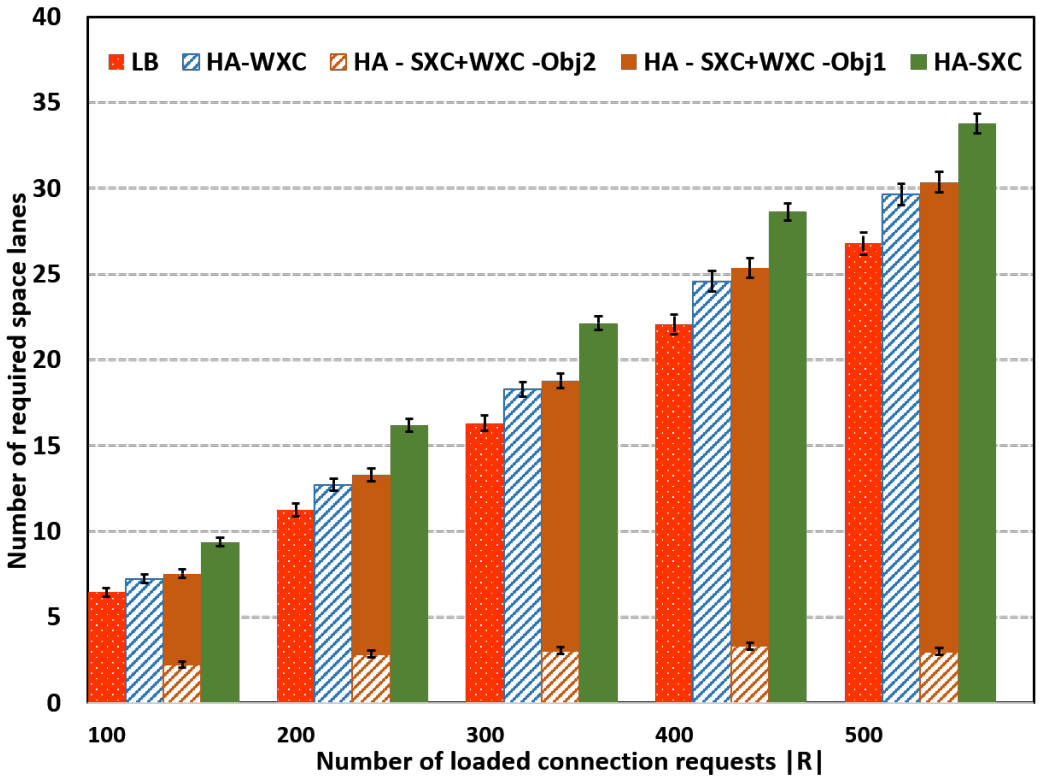

Figure 5.13: Simulation results for the 14-node, 42-link NSF network.

In these simulation experiments, we considered the realistic large-scale NSF network with 40 SLs (i.e., one bundle of five 4-core MCFs per link). Considering that one-ninth of the SLs support wavelength switching [28], the set L_W was $\{36, 37, \cdots, 40\}$ in this case. Moreover, we also considered heavier traffic loads – ranging from 100 to 500 (in increments of 100) connection requests – and 50 different traffic matrices R for each traffic load. In this case, the total average traffic volumes with which the network was loaded ranged from 0.55 to 2.75 Pbps. In such large-scale instances, acceptable solutions become difficult to obtain within a reasonable amount of time by solving the ILP model. Therefore, we relaxed the original ILP model by removing Constraints (5.4) ~ (5.12) and the minor objective to obtain the lower bounds for the RSCSA problem, which we then used as the benchmarks to evaluate the performance of the heuristic algorithm. This relaxation

Table 5.4: Average running times of the proposed heuristic algorithm with 1000 iterations for the realistic NSF network

OXC Architecture	Traffic load $\|R\|$				
	100	200	300	400	500
WXC	87.59	117.44	131.90	151.45	163.48
SXC+WXC	50.13	75.13	78.98	84.17	86.13
SXC	4.92	9.80	15.09	21.21	27.10

means that i) wavelength switching is allowed on all SLs, ii) lightpaths can be established without wavelength switching GBs, and iii) the spectrum contiguity constraint is relaxed. Consequently, in this case, the lower bound obtained by solving the relaxed ILP model is not only the lower bound of the RSCSA problem in an SCN but also the lower bound of the RSSA problem in an SDM-based EON – if we transform the objective of the RSSA problem into the minimization of the number of SLs, as opposed to the number of FSs, that are used/required in the network.

The corresponding simulation results are shown in Fig. 5.13. We can observe that the results in Fig. 5.13 are similar to those presented in Fig. 5.12. First, the gaps between the results of 'HA - SXC+WXC' and 'HA - WXC' are negligible, ranging from 2.3% to 4.2%. This means that the conventional OXC with full wavelength switching support is not a preferred solution for future Pbps-level optical networks because of the significantly higher cost – for the network with 40 SLs considered here, the conventional OXC configuration is 5.8 times as costly as the full-size CSS-based HOXC configuration and 4.2 times as costly as the sub-CSS-based HOXC configuration [28, 113] – for similar performance. By contrast, we can see that the gaps between the results of 'HA - SXC+WXC' and 'HA - SXC' are relatively significant, ranging from 10.1% to 19.6% for different traffic loads. Therefore, the network operators are required to make a decision concerning the balance between the additional cost and better performance.

Moreover, the results of 'HA - WXC' are close to the lower bounds obtained by solving the relaxed ILP model (i.e., 'LB'). The gaps between them range from 9.6% to 11.4%. Compared to the results shown in Fig. 5.12, these gaps are relatively large because the lower bounds for these simulation experiments are not strict – they are obtained by solving the relaxed ILP model, in which almost all of the constraints of the original ILP model have been removed. In addition, it should be noted that it is unfair to evaluate the performance of the heuristic algorithm by comparing the results of 'HA - SXC+WXC' or 'HA - SXC' against these lower bounds because wavelength switching is allowed on all SLs in the relaxed ILP model.

Finally, Table 5.4 lists the average running times (in seconds) of the heuristic algorithm for the realistic NSF network, from which it can again be observed that the results are similar to those in Table 5.3. The heuristic algorithm can yield reasonable solutions within an acceptable running time. Thus, we can see that the proposed heuristic algorithm is also efficient for solving realistic large-scale problem instances.

Chapter 6

Conclusion and Future Work

This Ph.D. thesis has addressed the network optimization problems in face of future-oriented optical networks (SDM-based EONs and SCNs). The conclusion of this thesis are per chapter summarized as follows:

- In Chapter 1, we introduced the evolution history of optical network architectures. we also made a detailed statement on the resource allocation problem corresponding to each network architecture. From WDM optical networks to EONs and further to SDM-based EONs, to conform with the new network features introduced by each evolution, the resource problem has accordingly evolved from RWA to RSA and then to RSSA. By reviewing previous works, we clarified our contribution to the research field of network planning in SDM-based EONs and SCNs.

- In Chapter 2, we discussed the corresponding network features brought by the evolution of the network architecture. For each network architecture, from WDM optical networks to EONs and further to SDM-based EONs, and recently proposed SCNs, we discussed the related technologies in detail.

- In Chapter 3, we focused on the static routing, space, and spectrum assignment (RSSA) problem. Aiming at minimizing the maximum index of required FSs in the network, we propose a novel channel-based ILP model for the problem in consideration of all the SDM technologies introduced in Chapter 1. Moreover, we also proposed a relaxed ILP model for the RSSA problem whose results can be used as the initial solutions in the optimization of the channel-based model and as the benchmarks for comparison with the channel-based model. For the static scenarios, only the ILP model proposed in previous work [47] can cope with the joint optimization of the RSSA problem which considered all the switching paradigms and SLC technology. Therefore, we did simulation experiments for the previous and our model. The

numerical results verified the overwhelming performance of our model compared to the previous one. Considering the advantages of the model, the availability of our model in the large-scale instances, and the application of the pre-computed channels approach in dynamic scenarios are also worth being looked forward to.

- In Chapter 4, we comprehensively evaluated the device costs, power consumption, and network performance of SDM transmission systems based on the application of various highly interrelated transmission technologies. We find that the applications of i) Spa & Spe SpCh with different spatial spans, ii) ROADMs with different spatial switching granularity, iii) ROADMs with or without SLC support, and iv) the number of SpCh transceivers installed at each intermediate node (ROADM) greatly influence the results. We find that trade-off relationships exist between network performance and device cost/power consumption. Network operators should select among the different available transmission systems depending on which objectives are more important to them. If the network operators focus on the improvement of the network performance, the installation of a sufficient number of SpCh transceivers as needed, the application of SpCh with the smallest spatial span, and the ROADM with the smallest spatial switching granularity and SLC support are recommended. In contrast, the transmission system with a moderate spatial span and spatial switching granularity combined with the installation of an appropriate number of SpCh transceivers at intermediate nodes is recommended to achieve higher cost and power efficiency. Finally, we find that joint DSP technology can enable remarkable cost savings for SDM transmission, and thus, the development of such technology is worthy of further exploration.

- In Chapter 5, for the recent proposed SCNs, we reviewed the key features of SCNs from the networking perspective and described how these features are related to the resource allocation problem. we define the resource allocation problem in SCNs as routing, spatial channel, and spectrum assignment (RSCSA) problem and proved its NP-hardness. We proposed two approaches for solving it: an ILP model for small-scale problem instances and a heuristic algorithm with higher scalability. Simulation results show that the ILP model (with a 1-hour running time limit) and the heuristic algorithm both work well for small-scale problem instances, for which the optimal solutions or solutions close to the lower bounds can be obtained. In addition, the heuristic algorithm is also efficient for solving realistic large-scale problem instances. Moreover, the results show that compared to conventional OXCs with full wavelength switching implemented by means of stacked WXCs, which are typically

used in SDM-based EONs, the CSS-based HOXCs designed for SCNs can enable great cost savings while providing similar network performance, and consequently, these HOXCs are expected to be a promising solution for the future massive SDM era.

However, a lot of important challenges still remain for the future-oriented optical network planning problem that should be addressed. As we introduced in Chapter 1, SCN architecture is proposed considering the network traffic by 2024 which can achieve Pbps level optical networks. Since it is a new optical network architecture, there exist a lot of works for its implementation. For example, the RSCSA problem with SLC support implemented by the MS-based HOXCs architecture. Moreover, from the perspective of network operators, a dedicated algorithm for the dynamic RSCSA problem should be developed, and alternative network architectures, such as Architecture-on-Demand, which suffers from similar restrictions to SCNs, deserve more discussions. Finally, a comprehensive evaluation in consideration of device cost, power consumption, and network performance requires investigation as further work.

Bibliography

[1] I. Chlamtac, A. Ganz, and G. Karmi, "Lightpath communications: An approach to high bandwidth optical wan's," *IEEE transactions on communications*, vol. 40, no. 7, pp. 1171–1182, 1992.

[2] H. Zang, J. P. Jue, B. Mukherjee, *et al.*, "A review of routing and wavelength assignment approaches for wavelength-routed optical wdm networks," *Optical networks magazine*, vol. 1, no. 1, pp. 47–60, 2000.

[3] G. Xiao and Y.-W. Leung, "Algorithms for allocating wavelength converters in all-optical networks," *IEEE/ACM Transactions on networking*, vol. 7, no. 4, pp. 545–557, 1999.

[4] Cisco, "White paper: Cisco VNI Forecast and Methodology, 2017-2022," Available: http://www.cisco.com, 2017.

[5] M. Jinno, H. Takara, B. Kozicki, Y. Tsukishima, Y. Sone, and S. Matsuoka, "Spectrum-efficient and scalable elastic optical path network: architecture, benefits, and enabling technologies," *IEEE communications magazine*, vol. 47, no. 11, pp. 66–73, 2009.

[6] K. Christodoulopoulos, I. Tomkos, and E. A. Varvarigos, "Elastic bandwidth allocation in flexible ofdm-based optical networks," *Journal of Lightwave Technology*, vol. 29, no. 9, pp. 1354–1366, 2011.

[7] M. Klinkowski and K. Walkowiak, "Routing and spectrum assignment in spectrum sliced elastic optical path network," *IEEE Communications Letters*, vol. 15, no. 8, pp. 884–886, 2011.

[8] M. Jinno, B. Kozicki, H. Takara, A. Watanabe, Y. Sone, T. Tanaka, and A. Hirano, "Distance-adaptive spectrum resource allocation in spectrum-sliced elastic optical path network [topics in optical communications]," *IEEE Communications Magazine*, vol. 48, no. 8, pp. 138–145, 2010.

[9] Y. Yin, M. Zhang, Z. Zhu, and S. Yoo, "Fragmentation-aware routing, modulation and spectrum assignment algorithms in elastic optical networks," in *Optical Fiber Communication Conference*, pp. OW3A–5, Optical Society of America, 2013.

[10] C. Wang, G. Shen, and S. K. Bose, "Distance adaptive dynamic routing and spectrum allocation in elastic optical networks with shared backup path protection," *Journal of Lightwave Technology*, vol. 33, no. 14, pp. 2955–2964, 2015.

[11] L. Gong and Z. Zhu, "Virtual optical network embedding (vone) over elastic optical networks," *Journal of Lightwave Technology*, vol. 32, no. 3, pp. 450–460, 2013.

[12] P. J. Winzer and D. T. Neilson, "From scaling disparities to integrated parallelism: A decathlon for a decade," *Journal of Lightwave Technology*, vol. 35, no. 5, pp. 1099–1115, 2017.

[13] G. M. Saridis, D. Alexandropoulos, G. Zervas, and D. Simeonidou, "Survey and evaluation of space division multiplexing: From technologies to optical networks," *IEEE Communications Surveys & Tutorials*, vol. 17, no. 4, pp. 2136–2156, 2015.

[14] P. J. Winzer, "Spatial multiplexing: The next frontier in network capacity scaling," in *IET Conference Proceedings*, The Institution of Engineering & Technology, 2013.

[15] B. Li, L. Gan, S. Fu, Z. Xu, M. Tang, W. Tong, and P. P. Shum, "The role of effective area in the design of weakly coupled mcf: Optimization guidance and osnr improvement," *IEEE Journal of Selected Topics in Quantum Electronics*, vol. 22, no. 2, pp. 81–87, 2015.

[16] T. Hayashi, T. Taru, O. Shimakawa, T. Sasaki, and E. Sasaoka, "Characterization of crosstalk in ultra-low-crosstalk multi-core fiber," *Journal of Lightwave Technology*, vol. 30, no. 4, pp. 583–589, 2011.

[17] J. Sakaguchi, B. J. Puttnam, W. Klaus, Y. Awaji, N. Wada, A. Kanno, T. Kawanishi, K. Imamura, H. Inaba, K. Mukasa, *et al.*, "305 tb/s space division multiplexed transmission using homogeneous 19-core fiber," *Journal of Lightwave Technology*, vol. 31, no. 4, pp. 554–562, 2012.

[18] R. Ryf, A. Sierra, R.-J. Essiambre, A. Gnauck, S. Randel, M. Esmaeelpour, S. Mumtaz, P. Winzer, R. Delbue, P. Pupalaikis, *et al.*, "Coherent 1200-km 6× 6 mimo mode-multiplexed transmission over 3-core microstructured fiber," in *European Conference and Exposition on Optical Communications*, pp. Th–13, Optical Society of America, 2011.

[19] R. Ryf, R. Essiambre, A. Gnauck, S. Randel, M. A. Mestre, C. Schmidt, P. Winzer, R. Delbue, P. Pupalaikis, A. Sureka, *et al.*, "Space-division multiplexed transmission over 4200 km 3-core microstructured fiber," in *National Fiber Optic Engineers Conference*, pp. PDP5C–2, Optical Society of America, 2012.

[20] R. Ryf, N. Fontaine, B. Guan, R.-J. Essiambre, S. Randel, A. Gnauck, S. Chandrasekhar, A. Adamiecki, G. Raybon, B. Ercan, *et al.*, "1705-km transmission over coupled-core fibre supporting 6 spatial modes," in *2014 The European Conference on Optical Communication (ECOC)*, pp. 1–3, IEEE, 2014.

[21] R. Ryf, N. Fontaine, B. Guan, B. Huang, M. Esmaeelpour, S. Randel, A. Gnauck, S. Chandrasekhar, A. Adamiecki, G. Raybon, *et al.*, "305-km combined wavelength and mode-multiplexed transmission over conventional graded-index multimode fibre," in *2014 The European Conference on Optical Communication (ECOC)*, pp. 1–3, IEEE, 2014.

[22] N. K. Fontaine, R. Ryf, H. Chen, A. V. Benitez, J. A. Lopez, R. A. Correa, B. Guan, B. Ercan, R. P. Scott, S. B. Yoo, *et al.*, "30× 30 mimo transmission over 15 spatial modes," in *Optical Fiber Communication Conference*, pp. Th5C–1, Optical Society of America, 2015.

[23] R. Ryf, S. Randel, A. H. Gnauck, C. Bolle, A. Sierra, S. Mumtaz, M. Esmaeelpour, E. C. Burrows, R.-J. Essiambre, P. J. Winzer, *et al.*, "Mode-division multiplexing over 96 km of few-mode fiber using coherent 6 *times* 6 mimo processing," *Journal of Lightwave technology*, vol. 30, no. 4, pp. 521–531, 2011.

[24] S. Randel, R. Ryf, A. Sierra, P. J. Winzer, A. H. Gnauck, C. A. Bolle, R.-J. Essiambre, D. W. Peckham, A. McCurdy, and R. Lingle, "6× 56-gb/s mode-division multiplexed transmission over 33-km few-mode fiber enabled by 6× 6 mimo equalization," *Optics Express*, vol. 19, no. 17, pp. 16697–16707, 2011.

[25] T. Hayashi, T. Nagashima, K. Yonezawa, Y. Wakayama, D. Soma, K. Igarashi, T. Tsuritani, and T. Sasaki, "6-mode 19-core fiber for weakly-coupled mode-multiplexed transmission over uncoupled cores," in *Optical Fiber Communication Conference*, pp. W1F–4, Optical Society of America, 2016.

[26] R. Van Uden, R. A. Correa, E. A. Lopez, F. Huijskens, C. Xia, G. Li, A. Schülzgen, H. De Waardt, A. Koonen, and C. Okonkwo, "Ultra-high-density spatial division multiplexing with a few-mode multicore fibre," *Nature Photonics*, vol. 8, no. 11, p. 865, 2014.

[27] S. Randel, P. J. Winzer, M. Montoliu, and R. Ryf, "Complexity analysis of adaptive frequency-domain equalization for mimo-sdm transmission," in *39th European Conference and Exhibition on Optical Communication (ECOC 2013)*, pp. 1–3, IET, 2013.

[28] M. Jinno, "Spatial channel network (scn): Opportunities and challenges of introducing spatial bypass toward the massive sdm era," *Journal of Optical Communications and Networking*, vol. 11, no. 3, pp. 1–14, 2019.

[29] M. Klinkowski, P. Lechowicz, and K. Walkowiak, "Survey of resource allocation schemes and algorithms in spectrally-spatially flexible optical networking," *Optical Switching and Networking*, vol. 27, pp. 58–78, 2018.

[30] M. Klinkowski and K. Walkowiak, "An efficient optimization framework for solving rssa problems in spectrally and spatially flexible optical networks," *IEEE/ACM Transactions on Networking*, vol. 27, no. 4, pp. 1474–1486, 2019.

[31] H. Tode and Y. Hirota, "Routing, spectrum, and core and/or mode assignment on space-division multiplexing optical networks," *Journal of Optical Communications and Networking*, vol. 9, no. 1, pp. A99–A113, 2017.

[32] P. S. Khodashenas, J. M. Rivas-Moscoso, D. Siracusa, F. Pederzolli, B. Shariati, D. Klonidis, E. Salvadori, and I. Tomkos, "Comparison of spectral and spatial superchannel allocation schemes for sdm networks," *Journal of Lightwave Technology*, vol. 34, no. 11, pp. 2710–2716, 2016.

[33] B. Shariati, J. M. Rivas-Moscoso, M. Dan, S. Ben-Ezra, D. Klonidis, L. Velasco, and I. Tomkos, "Impact of spatial and spectral granularity on the performance of sdm networks based on spatial superchannel switching," *Journal of Lightwave Technology*, vol. PP, no. 99, pp. 1–1, 2017.

[34] R. Rumipamba-Zambrano, F.-J. Moreno-Muro, J. Perelló, P. Pavón-Mariño, and S. Spadaro, "Space continuity constraint in dynamic flex-grid/sdm optical core networks: An evaluation with spatial and spectral super-channels," *Computer Communications*, vol. 126, pp. 38–49, 2018.

[35] B. Shariati, D. Klonidis, D. Siracusa, F. Pederzolli, J. Rivas-Moscoso, L. Velasco, and I. Tomkos, "Impact of traffic profile on the performance of spatial superchannel switching in sdm networks," in *ECOC 2016; 42nd European Conference on Optical Communication*, pp. 1–3, VDE, 2016.

[36] H. Tode and Y. Hirota, "Routing, spectrum and core assignment for space division multiplexing elastic optical networks," in *2014 16th International Telecommunications Network Strategy and Planning Symposium (Networks)*, pp. 1–7, IEEE, 2014.

[37] Y. Hirota, Y. Hatada, T. Watanabe, and H. Tode, "Dynamic spectrum allocation based on connection alignment for elastic optical networks," in *2015 10th Asia-Pacific Symposium on Information and Telecommunication Technologies (APSITT)*, pp. 1–3, IEEE, 2015.

[38] D. Siracusa, F. Pederzolli, P. Khodashenas, J. Rivas-Moscoso, D. Klonidis, E. Salvadori, and I. Tomkos, "Spectral vs. spatial super-channel allocation in sdm networks under independent and joint switching paradigms," in *2015 European Conference on Optical Communication (ECOC)*, pp. 1–3, IEEE, 2015.

[39] B. Shariati, P. S. Khodashenas, J. M. Rivas-Moscoso, S. Ben-Ezra, D. Klonidis, F. Jiménez, L. Velasco, and I. Tomkos, "Evaluation of the impact of different sdm switching strategies in a network planning scenario," in *Optical Fiber Communication Conference*, pp. Tu2H–4, Optical Society of America, 2016.

[40] F. Pederzolli, D. Siracusa, J. M. Rivas-Moscoso, B. Shariati, E. Salvadori, and I. Tomkos, "Spatial group sharing for sdm optical networks with joint switching," in *2016 International Conference on Optical Network Design and Modeling (ONDM)*, pp. 1–6, IEEE, 2016.

[41] B. Shariati, D. Klonidis, J. M. Rivas-Moscoso, and I. Tomkos, "Evaluation of the impact of spatial and spectral granularities on the performance of spatial superchannel switching schemes," in *2016 18th International Conference on Transparent Optical Networks (ICTON)*, pp. 1–4, IEEE, 2016.

[42] J. Rivas-Moscoso, B. Shariati, A. Mastropaolo, D. Klonidis, and I. Tomkos, "Cost benefit quantification of sdm network implementations based on spatially integrated network elements," in *ECOC 2016; 42nd European Conference on Optical Communication*, pp. 1–3, VDE, 2016.

[43] F. Pederzolli, D. Siracusa, B. Shariati, J. M. Rivas-Moscoso, E. Salvadori, and I. Tomkos, "Improving performance of spatially joint-switched space division multiplexing optical networks via spatial group sharing," *IEEE/OSA Journal of Optical Communications and Networking*, vol. 9, no. 3, pp. B1–B11, 2017.

[44] N.-P. Diamantopoulos, B. Shariati, and I. Tomkos, "On the power consumption of mimo processing and its impact on the performance of sdm networks," in *2017 Optical Fiber Communications Conference and Exhibition (OFC)*, pp. 1–3, IEEE, 2017.

[45] R. Rumipamba-Zambrano, J. Perelló, J. M. Gené, and S. Spadaro, "Capacity quantification of joint-switching-enabled flex-grid/sdm optical backbone networks," in *2017 Optical Fiber Communications Conference and Exhibition (OFC)*, pp. 1–3, IEEE, 2017.

[46] D. Siracusa, F. Pederzolli, D. Klonidisz, V. Lopezy, and E. Salvadori, "Resource allocation policies in sdm optical networks," in *2015 International Conference on Optical Network Design and Modeling (ONDM)*, pp. 168–173, IEEE, 2015.

[47] M. Yang, C. Zhang, Q. Wu, W. Zheng, and Y. Zhang, "Comparison of switching policies in terms of switching cost and network performance in static sdm-eons," *Optical Switching and Networking*, p. 100573, 2020.

[48] K. Morita and K. Hirata, "Dynamic spectrum allocation method for reducing crosstalk in multi-core fiber networks," in *2017 International Conference on Information Networking (ICOIN)*, pp. 686–688, IEEE, 2017.

[49] Y. Tan, R. Zhu, H. Yang, Y. Zhao, J. Zhang, Z. Liu, Q. Qu, and Z. Zhou, "Crosstalk-aware provisioning strategy with Dedicated Path Protection for elastic multi-core fiber networks," in *Optical Communications and Networks (ICOCN), 2016 15th International Conference on*, pp. 1–3, IEEE, 2016.

[50] Y. Zhao and J. Zhang, "Crosstalk-aware cross-core virtual concatenation in spatial division multiplexing elastic optical networks," *Electronics Letters*, vol. 52, no. 20, pp. 1701–1703, 2016.

[51] S. Fujii, Y. Hirota, H. Tode, and K. Murakami, "On-demand spectrum and core allocation for multi-core fibers in elastic optical network," in *Optical Fiber Communication Conference*, pp. OTh4B–4, Optical Society of America, 2013.

[52] S. Fujii, Y. Hirota, and H. Tode, "Dynamic resource allocation with virtual grid for space division multiplexed elastic optical network," in *39th European Conference and Exhibition on Optical Communication (ECOC 2013)*, pp. 1–3, IET, 2013.

[53] A. Muhammad, G. Zervas, D. Simeonidou, and R. Forchheimer, "Routing, spectrum and core allocation in flexgrid sdm networks with multi-core fibers," in *2014 Inter-*

national Conference on Optical Network Design and Modeling, pp. 192–197, IEEE, 2014.

[54] S. Fujii, Y. Hirota, H. Tode, and K. Murakami, "On-demand spectrum and core allocation for reducing crosstalk in multicore fibers in elastic optical networks," *J. Opt. Commun. Netw.*, vol. 6, pp. 1059–1071, Dec 2014.

[55] S. Fujii, Y. Hirota, T. Watanabe, and H. Tode, "Dynamic spectrum and core allocation with spectrum region reducing costs of building modules in aod nodes," in *2014 16th International Telecommunications Network Strategy and Planning Symposium (Networks)*, pp. 1–6, IEEE, 2014.

[56] A. Muhammad, G. Zervas, G. Saridis, E. H. Salas, D. Simeonidou, and R. Forchheimer, "Flexible and synthetic sdm networks with multi-core-fibers implemented by programmable roadms," in *2014 The European Conference on Optical Communication (ECOC)*, pp. 1–3, IEEE, 2014.

[57] Y. Li, N. Hua, and X. Zheng, "Routing, wavelength and core allocation planning for multi-core fiber networks with mimo-based crosstalk suppression," in *2015 Opto-Electronics and Communications Conference (OECC)*, pp. 1–3, IEEE, 2015.

[58] A. Muhammad, G. Zervas, and R. Forchheimer, "Resource allocation for space-division multiplexing: optical white box versus optical black box networking," *Journal of Lightwave Technology*, vol. 33, no. 23, pp. 4928–4941, 2015.

[59] P. M. Moura and N. L. da Fonseca, "Routing, core and spectrum assignment based on connected component labelling for sdm optical networks," in *2016 IEEE International Conference on Communications (ICC)*, pp. 1–6, IEEE, 2016.

[60] L. Zhang, N. Ansari, and A. Khreishah, "Anycast planning in space division multiplexing elastic optical networks with multi-core fibers," *IEEE Communications Letters*, vol. 20, no. 10, pp. 1983–1986, 2016.

[61] R. Zhu, Y. Zhao, H. Yang, Y. Tan, H. Chen, J. Zhang, and J. P. Jue, "Dynamic virtual optical network embedding in spectral and spatial domains over elastic optical networks with multicore fibers," *Optical Engineering*, vol. 55, no. 8, p. 086108, 2016.

[62] R. Zhu, Y. Zhao, J. Zhang, H. Yang, Y. Tan, and J. P. Jue, "Multi-dimensional resource virtualization in spectral and spatial domains for inter-datacenter optical networks," in *2016 Optical Fiber Communications Conference and Exhibition (OFC)*, pp. 1–3, IEEE, 2016.

[63] H. Tode and Y. Hirota, "Routing, spectrum and core assignment on sdm optical networks," in *2016 Optical Fiber Communications Conference and Exhibition (OFC)*, pp. 1–3, IEEE, 2016.

[64] Y. Li, Y. Li, N. Hua, and X. Zheng, "Shared backup path protection in multi-core fiber networks with mimo-based crosstalk suppression," in *Optical Fiber Communication Conference*, pp. Tu2H–7, Optical Society of America, 2016.

[65] R. Rumipamba-Zambrano, J. Perelló, A. Pagès, J. M. Gené, and S. Spadaro, "Influence of the spatial super channel guard-band width on the performance of dynamic flex-grid/sdm optical core networks," in *2016 18th International Conference on Transparent Optical Networks (ICTON)*, pp. 1–4, IEEE, 2016.

[66] R. Zhu, Y. Zhao, H. Yang, Y. Tan, X. Yu, G. Gao, J. Zhang, N. Wang, and J. P. Jue, "Crosstalk-aware virtual optical network embedding (vone) in spatial division multiplexing enabled elastic optical networks with multi-core fibers," in *ECOC 2016; 42nd European Conference on Optical Communication*, pp. 1–3, VDE, 2016.

[67] A. Muhammad, M. Furdek, G. Zervas, and L. Wosinska, "Filterless networks based on optical white boxes and sdm," in *ECOC 2016; 42nd European Conference on Optical Communication*, pp. 1–3, VDE, 2016.

[68] M. N. Dharmaweera, L. Yan, M. Karlsson, and E. Agrell, "Nonlinear-impairments- and crosstalk-aware resource allocation schemes for multicore-fiber-based flexgrid networks," in *ECOC 2016; 42nd European Conference on Optical Communication*, pp. 1–3, VDE, 2016.

[69] Z. Shi, Y. Zhao, X. Yu, Y. Li, J. Zhang, C. Liu, G. Zhang, and Z. Liu, "Contaminated area-based rsca algorithm for super-channel in flex-grid enabled sdm networks," in *Asia Communications and Photonics Conference*, pp. ATh2E–4, Optical Society of America, 2016.

[70] Q. Yao, H. Yang, Y. Zhao, R. Zhu, J. Zhang, and J. Wu, "Crosstalk-aware routing, spectrum, and core assignment in elastic optical networks with multi-core fibers," in *Asia Communications and Photonics Conference 2016*, p. ATh2C.1, Optical Society of America, 2016.

[71] Y. Tan, H. Yang, R. Zhu, Y. Zhao, J. Zhang, Z. Liu, Q. Ou, and Z. Zhou, "Distance adaptive routing, core and spectrum allocation in space division multiplexing

optical networks with multi-core fibers," in *Asia Communications and Photonics Conference*, pp. AF2A–159, Optical Society of America, 2016.

[72] Y. Zhao, R. Tian, X. Yu, J. Zhang, and J. Zhang, "An auxiliary graph based dynamic traffic grooming algorithm in spatial division multiplexing enabled elastic optical networks with multi-core fibers," *Optical Fiber Technology*, vol. 34, pp. 52–58, 2017.

[73] C. Rottondi, P. Boffi, P. Martelli, M. Tornatore, and A. Pattavina, "Optimal resource allocation in distance-adaptive few-modes backbone networks with flexible grid," in *Asia Communications and Photonics Conference*, pp. AS4H–2, Optical Society of America, 2015.

[74] H. Huang, S. Huang, S. Yin, M. Zhang, J. Zhang, and W. Gu, "Virtual network provisioning over space division multiplexed optical networks using few-mode fibers," *IEEE/OSA Journal of Optical Communications and Networking*, vol. 8, no. 10, pp. 726–733, 2016.

[75] C. Rottondi, P. Boffi, P. Martelli, and M. Tornatore, "Routing, modulation format, baud rate and spectrum allocation in optical metro rings with flexible grid and few-mode transmission," *Journal of Lightwave Technology*, vol. 35, no. 1, pp. 61–70, 2016.

[76] Y. Yang, X. Chen, H. Yan, B. Hua, J. Li, Y. Hao, Z. Chen, and Y. He, "A scattered-spectrum-scan routing and spectrum allocati2020on scheme for spatial-division-multiplexing optical networks based on blocking oxcs," in *Asia Communications and Photonics Conference*, pp. ATh2E–2, Optical Society of America, 2016.

[77] Y. Li, N. Hua, and X. Zheng, "A capacity analysis for space division multiplexing optical networks with mimo equalization," in *Optical Fiber Communication Conference*, pp. Th2A–15, Optical Society of America, 2017.

[78] K. Walkowiak, P. Lechowicz, M. Klinkowski, and A. Sen, "Ilp modeling of flex-grid sdm optical networks," in *2016 17th International Telecommunications Network Strategy and Planning Symposium (Networks)*, pp. 121–126, IEEE, 2016.

[79] J. Perelló, J. M. Gené, A. Pagès, J. A. Lazaro, and S. Spadaro, "Flex-grid/sdm backbone network design with inter-core xt-limited transmission reach," *IEEE/OSA Journal of Optical Communications and Networking*, vol. 8, no. 8, pp. 540–552, 2016.

[80] C. Rottondi, P. Boffi, P. Martelli, and M. Tornatore, "Routing, modulation format, baud rate and spectrum allocation in optical metro rings with flexible grid and few-mode transmission," *Journal of Lightwave Technology*, vol. 35, no. 1, pp. 61–70, 2017.

[81] Y. Zhang, L. Yan, H. Wang, and W. Gu, "Routing, wavelength and mode assignment algorithm for space division multiplexing transmission network," in *2012 Second International Conference on Instrumentation, Measurement, Computer, Communication and Control*, pp. 1383–1385, IEEE, 2012.

[82] M. Jinno, "Spatial channel network (scn) architecture employing growable and reliable spatial channel cross-connects toward massive sdm era," in *2018 Photonics in Switching and Computing (PSC)*, pp. 1–3, IEEE, 2018.

[83] M. Jinno, "Opportunities, challenges, and solutions for spatial channel networks (scns) toward the sdm abundant era," in *2019 24th OptoElectronics and Communications Conference (OECC) and 2019 International Conference on Photonics in Switching and Computing (PSC)*, pp. 1–3, IEEE, 2019.

[84] M. Jinno, "Spatial channel cross-connect architectures for spatial channel networks," *IEEE Journal of Selected Topics in Quantum Electronics*, vol. 26, no. 4, pp. 1–16, 2020.

[85] M. Jinno and T. Kodama, "Spatial channel network (scn): Introducing spatial bypass toward the sdm era," in *Optical Fiber Communication Conference*, pp. M2G–1, Optical Society of America, 2020.

[86] M. Jinno, T. Kodama, and T. Ishikawa, "Feasibility demonstration of spatial channel networking using sdm/wdm hierarchical approach for peta-b/s optical transport," *Journal of Lightwave Technology*, vol. 38, no. 9, pp. 2577–2586, 2020.

[87] "Transatlantic communications cable." Available: https://en.wikipedia.org/wiki.

[88] the Fiber Optic Association, "Optical fiber." Available: https://www.thefoa.org.

[89] S. Arnon, J. Barry, G. Karagiannidis, R. Schober, and M. Uysal, *Advanced optical wireless communication systems*. Cambridge university press, 2012.

[90] R. Ramaswami, K. Sivarajan, and G. Sasaki, *Optical networks: a practical perspective*. Morgan Kaufmann, 2009.

[91] G. Shen and M. Zukerman, "Spectrum-efficient and agile co-ofdm optical transport networks: architecture, design, and operation," *IEEE Communications Magazine*, vol. 50, no. 5, pp. 82–89, 2012.

[92] B. Zhu, L. Leng, A. Gnauck, M. Pedersen, D. Peckham, L. Nelson, S. Stulz, S. Kado, L. Gruner-Nielsen, R. Lingle, *et al.*, "Transmission of 3.2 tb/s (80× 42.7 gb/s) over 5200 km of ultrawave^{TM} fiber with 100-km dispersion-managed spans using rz-dpsk format," in *2002 28TH European Conference on Optical Communication*, vol. 5, pp. 1–2, IEEE, 2002.

[93] ITU-T, "Extension of rec. g.694.1," Dec 2011.

[94] P. Schindler, R. Schmogrow, S. Wolf, B. Baeuerle, B. Nebendahl, C. Koos, W. Freude, and J. Leuthold, "Full flex-grid asynchronous multiplexing demonstrated with nyquist pulse-shaping," *Optics Express*, vol. 22, no. 9, pp. 10923–10937, 2014.

[95] D. Klonidis, F. Cugini, O. Gerstel, M. Jinno, V. Lopez, E. Palkopoulou, M. Sekiya, D. Siracusa, G. Thouénon, and C. Betoule, "Spectrally and spatially flexible optical network planning and operations," *IEEE Communications Magazine*, vol. 53, no. 2, pp. 69–78, 2015.

[96] D. Richardson, J. Fini, and L. E. Nelson, "Space-division multiplexing in optical fibres," *Nature Photonics*, vol. 7, no. 5, p. 354, 2013.

[97] P. J. Winzer, "Spatial multiplexing in fiber optics: The 10x scaling of metro/core capacities," *Bell Labs Technical Journal*, vol. 19, pp. 22–30, 2014.

[98] S. Ö. Arık, K.-P. Ho, and J. M. Kahn, "Optical network scaling: roles of spectral and spatial aggregation," *Optics express*, vol. 22, no. 24, pp. 29868–29887, 2014.

[99] P. S. Khodashenas, J. M. Rivas-Moscoso, B. Shariati, D. M. Marom, D. Klonidis, and I. Tomkos, "Investigation of spectrum granularity for performance optimization of flexible nyquist-wdm-based optical networks," *Journal of Lightwave Technology*, vol. 33, no. 23, pp. 4767–4774, 2015.

[100] M. Yang, Q. Wu, and Y. Zhang, "Joint assignment of spatial granularity, routing, modulation, and spectrum in sdm-eons: Minimizing the network capex considering spectrum, wss, and laser resources," *Journal of Lightwave Technology*, vol. 36, no. 18, pp. 4153–4166, 2018.

[101] M. Jinno, "Elastic optical networking: Roles and benefits in beyond 100-gb/s era," *Journal of Lightwave Technology*, vol. 35, no. 5, pp. 1116–1124, 2017.

[102] K. Nakajima, P. Sillard, D. Richardson, M.-J. Li, R.-J. Essiambre, and S. Matsuo, "Transmission media for an sdm-based optical communication system," *IEEE Communications Magazine*, vol. 53, no. 2, pp. 44–51, 2015.

[103] J. M. Rivas-Moscoso, B. Shariati, D. M. Marom, D. Klonidis, and I. Tomkos, "Comparison of cd (c) roadm architectures for space division multiplexed networks," in *Optical Fiber Communication Conference*, pp. Th2A–45, Optical Society of America, 2017.

[104] R. Rumipamba-Zambrano, F.-J. Moreno-Muro, P. Pavón-Marino, J. Perelló, S. Spadaro, and J. Solé-Pareta, "Assessment of flex-grid/mcf optical networks with roadm limited core switching capability," in *2017 International Conference on Optical Network Design and Modeling (ONDM)*, pp. 1–6, IEEE, 2017.

[105] F.-J. Moreno-Muro, R. Rumipamba-Zambrano, P. Pavón-Marino, J. Perelló, J. M. Gené, and S. Spadaro, "Evaluation of core-continuity-constrained roadms for flex-grid/mcf optical networks," *IEEE/OSA Journal of Optical Communications and Networking*, vol. 9, no. 11, pp. 1041–1050, 2017.

[106] P. J. Winzer, "Scaling optical fiber networks: Challenges and solutions," *Optics and Photonics News*, vol. 26, no. 3, pp. 28–35, 2015.

[107] K. Harada, K. Shimizu, T. Kudou, and T. Ozeki, "Hierarchical optical path cross-connect systems for large scale wdm networks," in *Optical Fiber Communication Conference*, p. WM55, Optical Society of America, 1999.

[108] A. A. Saleh and J. M. Simmons, "Architectural principles of optical regional and metropolitan access networks," *Journal of Lightwave Technology*, vol. 17, no. 12, p. 2431, 1999.

[109] X. Cao, V. Anand, and C. Qiao, "Framework for waveband switching in multigranular optical networks: part i-multigranular cross-connect architectures," *Journal of Optical Networking*, vol. 5, no. 12, pp. 1043–1055, 2006.

[110] K. Ishii, H. Hasegawa, K.-i. Sato, M. Okuno, S. Kamei, and H. Takahashi, "An ultra-compact waveband cross-connect switch module to create cost-effective multi-degree reconfigurable optical node," in *2009 35th European Conference on Optical Communication*, pp. 1–2, IEEE, 2009.

[111] M. Jinno, K. Yamashita, and Y. Asano, "Architecture and feasibility demonstration of core selective switch (css) for spatial channel network (scn)," in *2019 24th Opto-Electronics and Communications Conference (OECC) and 2019 International Conference on Photonics in Switching and Computing (PSC)*, pp. 1–3, IEEE, 2019.

[112] S. Sohma, T. Watanabe, N. Ooba, M. Itoh, T. Shibata, and H. Takahashi, "Silica-based plc type 32 x 32 optical matrix switch," in *2006 European Conference on Optical Communications*, pp. 1–2, IEEE, 2006.

[113] Y. Asano and M. Jinno, "Cost comparison of hierarchical optical cross-connect architectures for spatial channel networks (scns)," in *2018 Asia Communications and Photonics Conference (ACP)*, pp. 1–3, IEEE, 2018.

[114] T. Matsui, T. Sakamoto, Y. Goto, K. Saito, K. Nakajima, F. Yamamoto, and T. Kurashima, "Design of 125 μm cladding multi-core fiber with full-band compatibility to conventional single-mode fiber," in *2015 European Conference on Optical Communication (ECOC)*, pp. 1–3, IEEE, 2015.

[115] S. Talebi and G. N. Rouskas, "On distance-adaptive routing and spectrum assignment in mesh elastic optical networks," *IEEE/OSA Journal of Optical Communications and Networking*, vol. 9, no. 5, pp. 456–465, 2017.

[116] A. Bocoi, M. Schuster, F. Rambach, M. Kiese, C.-A. Bunge, and B. Spinnler, "Reach-dependent capacity in optical networks enabled by ofdm," in *2009 Conference on Optical Fiber Communication-incudes post deadline papers*, pp. 1–3, IEEE, 2009.

[117] M. Klinkowski and K. Walkowiak, "On performance gains of flexible regeneration and modulation conversion in translucent elastic optical networks with superchannel transmission," *Journal of lightwave technology*, vol. 34, no. 23, pp. 5485–5495, 2016.

[118] M. Klinkowski and K. Walkowiak, "A heuristic algorithm for routing, spectrum, transceiver and regeneration allocation problem in elastic optical networks," in *2016 18th International Conference on Transparent Optical Networks (ICTON)*, pp. 1–4, IEEE, 2016.

[119] Online, "Gurobi v9.0.1." Available: http://www.gurobi.com, 2020.

[120] J. M. Rivas-Moscoso, S. Ben-Ezra, P. S. Khodashenas, D. M. Marom, D. Klonidis, P. Zakynthinos, and I. Tomkos, "Cost and power consumption model for flexible super-channel transmission with all-optical sub-channel add/drop capability," in *2015 17th International Conference on Transparent Optical Networks (ICTON)*, pp. 1–4, IEEE, 2015.

[121] R. Rudnick, A. Tolmachev, D. Sinefeld, O. Golani, S. Ben-Ezra, M. Nazarathy, and D. Marom, "Sub-banded/single-sub-carrier drop-demux and flexible spectral shaping with a fine resolution photonic processor," in *Optical Communication (ECOC), 2014 European Conference on*, pp. 1–3, IEEE, 2014.

[122] S. Randel, "Space-division multiplexed transmission," pp. 1–60, 2013.

[123] C. Laperle and M. O'Sullivan, "Advances in high-speed dacs, adcs, and dsp for optical coherent transceivers," *Journal of Lightwave Technology*, vol. 32, no. 4, pp. 629–643, 2014.

[124] D. M. Marom, P. D. Colbourne, A. D'errico, N. K. Fontaine, Y. Ikuma, R. Proietti, L. Zong, J. M. Rivas-Moscoso, and I. Tomkos, "Survey of photonic switching architectures and technologies in support of spatially and spectrally flexible optical networking," *IEEE/OSA Journal of Optical Communications and Networking*, vol. 9, no. 1, pp. 1–26, 2017.

[125] M. Feuer, L. Nelson, X. Zhou, S. Woodward, R. Isaac, B. Zhu, T. Taunay, M. Fishteyn, J. Fini, and M. Yan, "Demonstration of joint dsp receivers for spatial superchannels," in *Photonics Society Summer Topical Meeting Series, 2012 IEEE*, pp. 183–184, IEEE, 2012.

[126] R. Uden, van, *MIMO digital signal processing for optical spatial division multiplexed transmission systems*. PhD thesis, 2014.

[127] R.-J. Essiambre, R. Ryf, N. Fontaine, and S. Randel, "Breakthroughs in photonics 2012: Space-division multiplexing in multimode and multicore fibers for high-capacity optical communication," *IEEE Photonics Journal*, vol. 5, no. 2, pp. 0701307–0701307, 2013.

[128] B. Shariati, P. S. Khodashenas, J. M. R. Moscoso, S. Ben-Ezra, D. Klonidis, F. Jiménez, L. Velasco, and I. Tomkos, "Evaluation of the impact of different sdm switching strategies in a network planning scenario," in *Optical Fiber Communication Conference*, pp. Tu2H–4, Optical Society of America, 2016.

[129] R. G. van Uden, C. M. Okonkwo, V. A. Sleiffer, M. Kuschnerov, H. de Waardt, and A. Koonen, "Single dpll joint carrier phase compensation for few-mode fiber transmission," *IEEE Photonics Technology Letters*, vol. 25, no. 14, pp. 1381–1384, 2013.

[130] P. Papanikolaou, P. Soumplis, K. Manousakis, G. Papadimitriou, G. Ellinas, K. Christodoulopoulos, and E. Varvarigos, "Minimizing energy and cost in fixed-grid and flex-grid networks," *Journal of Optical Communications and Networking*, vol. 7, no. 4, pp. 337–351, 2015.

[131] M. Garrich, N. Amaya, G. S. Zervas, J. R. Oliveira, P. Giaccone, A. Bianco, D. Simeonidou, and J. C. R. Oliveira, "Architecture on demand design for high-capacity optical sdm/tdm/fdm switching," *Journal of Optical Communications and Networking*, vol. 7, no. 1, pp. 21–35, 2015.

[132] H. Takara, A. Sano, T. Kobayashi, H. Kubota, H. Kawakami, A. Matsuura, Y. Miyamoto, Y. Abe, H. Ono, K. Shikama, *et al.*, "1.01-pb/s (12 sdm/222 wdm/456 gb/s) crosstalk-managed transmission with 91.4-b/s/hz aggregate spectral efficiency," in *European Conference and Exhibition on Optical Communication*, pp. Th–3, Optical Society of America, 2012.

[133] L. Nelson, M. Feuer, K. Abedin, X. Zhou, T. Taunay, J. Fini, B. Zhu, R. Isaac, R. Harel, G. Cohen, *et al.*, "Spatial superchannel routing in a two-span roadm system for space division multiplexing," *Journal of Lightwave Technology*, vol. 32, no. 4, pp. 783–789, 2014.

[134] A. Singla, A. Singh, K. Ramachandran, L. Xu, and Y. Zhang, "Proteus: a topology malleable data center network," in *Proceedings of the 9th ACM SIGCOMM Workshop on Hot Topics in Networks*, p. 8, ACM, 2010.

[135] C. Kachris and I. Tomkos, "Power consumption evaluation of all-optical data center networks," *Cluster Computing*, vol. 16, no. 3, pp. 611–623, 2013.

[136] M. Filer and S. Tibuleac, "N-degree roadm architecture comparison: Broadcast-and-select versus route-and-select in 120 gb/s dp-qpsk transmission systems," in *OFC 2014*, pp. 1–3, IEEE, 2014.

[137] K. Manousakis and G. Ellinas, "Crosstalk-aware routing spectrum assignment and wss placement in flexible grid optical networks," *Journal of Lightwave Technology*, vol. 35, no. 9, pp. 1477–1489, 2017.

[138] A. S. Wright and W. G. Durtler, "Experimental performance of an adaptive digital linearized power amplifier," in *Microwave Symposium Digest, 1992., IEEE MTT-S International*, pp. 1105–1108, IEEE, 1992.

[139] W. Van Heddeghem, F. Idzikowski, W. Vereecken, D. Colle, M. Pickavet, and P. Demeester, "Power consumption modeling in optical multilayer networks," *Photonic Network Communications*, vol. 24, no. 2, pp. 86–102, 2012.

[140] A. Klekamp, O. Rival, A. Morea, R. Dischler, and F. Buchali, "Transparent wdm network with bitrate tunable optical ofdm transponders," in *2010 Conference on Optical Fiber Communication (OFC/NFOEC), collocated National Fiber Optic Engineers Conference*, pp. 1–3, IEEE, 2010.

[141] R. Rumipamba-Zambrano, J. Perelló, J. M. Gené, and S. Spadaro, "On the scalability of dynamic flex-grid/sdm optical core networks," *Computer Networks*, vol. 142, pp. 208 – 222, 2018.

[142] R. Rumipamba-Zambrano, J. Perelló, J. M. Gené, and S. Spadaro, "Cost-effective spatial super-channel allocation in flex-grid/mcf optical core networks," *Optical Switching and Networking*, vol. 27, pp. 93–101, 2018.

[143] R. D. Rumipamba Zambrano, "Contributions to network planning and operation of flex-grid/sdm optical core networks," 2019.

[144] J. Y. Zhang, O. W. Yang, J. Wu, and M. Savoie, "Optimization of semi-dynamic lightpath rearrangements in a wdm network," *IEEE Journal on Selected Areas in Communications*, vol. 25, no. 9, pp. 3–17, 2007.

[145] N. Wauters and P. Demeester, "Design of the optical path layer in multiwavelength cross-connected networks," *IEEE Journal on Selected Areas in Communications*, vol. 14, no. 5, pp. 881–892, 1996.

[146] M. Yang, Y. Zhang, and Q. Wu, "Routing, spectrum, and core assignment in sdm-eons with mcf: node-arc ilp/milp methods and an efficient xt-aware heuristic algorithm," *Journal of Optical Communications and Networking*, vol. 10, no. 3, pp. 195–208, 2018.

[147] K. Abedin, T. Taunay, M. Fishteyn, D. DiGiovanni, V. Supradeepa, J. Fini, M. Yan, B. Zhu, E. Monberg, and F. Dimarcello, "Cladding-pumped erbium-doped multicore fiber amplifier," *Optics express*, vol. 20, no. 18, pp. 20191–20200, 2012.

[148] H. Yuan, M. Furdek, A. Muhammad, A. Saljoghei, L. Wosinska, and G. Zervas, "Space-division multiplexing in data center networks: on multi-core fiber solutions and crosstalk-suppressed resource allocation," *Journal of Optical Communications and Networking*, vol. 10, no. 4, pp. 272–288, 2018.

[149] A. C. Jatoba-Neto, D. A. Mello, C. E. Rothenberg, S. Ö. Arik, and J. M. Kahn, "Scaling sdm optical networks using full-spectrum spatial switching," *IEEE/OSA Journal of Optical Communications and Networking*, vol. 10, no. 12, pp. 991–1004, 2018.

[150] P. M. Moura and N. L. Da Fonseca, "Routing, core, modulation level, and spectrum assignment based on image processing algorithms," *IEEE/OSA Journal of Optical Communications and Networking*, vol. 10, no. 12, pp. 947–958, 2018.

[151] Online, "Gurobi v8.0.1." Available: http://www.gurobi.com, 2018.